농학박사학위논문

*Streptomyces microflavus*와 *Juniperus chinensis* 유래 대사산물의 항균 활성 및 작용 기전 연구

Studies on the Antibacterial Activity and Mode of Action of Metabolites from *Streptomyces microflavus* and *Juniperus chinensis*

2022년 8월

서울대학교 대학원
농생명공학부 응용생명화학전공
조 은 지

A Dissertation for the Degree of Doctor of Philosophy

Studies on the Antibacterial Activity and Mode of Action of Metabolites from *Streptomyces microflavus* and *Juniperus chinensis*

August 2022

Eunji Cho

Applied Life Chemistry Major

Department of Agricultural Biotechnology
Seoul National University

*Streptomyces microflavus*와 *Juniperus chinensis* 유래 대사산물의 항균 활성 및 작용 기전 연구

Studies on the Antibacterial Activity and Mode of Action of Metabolites from *Streptomyces microflavus* and *Juniperus chinensis*

지도교수 오 기 봉

이 논문을 농학박사학위논문으로 제출함
2022년 7월

서울대학교 대학원
농생명공학부 응용생명화학전공

조 은 지

조은지의 박사학위논문을 인준함
2022년 7월

위 원 장 이 상 기 (인)

부 위 원 장 오 기 봉 (인)

위 원 신 종 헌 (인)

위 원 권 용 훈 (인)

위 원 이 희 승 (인)

Studies on the Antibacterial Activity and Mode of Action of Metabolites from *Streptomyces microflavus* and *Juniperus chinensis*

Advisor: Ki-bong Oh

A Dissertation Submitted in Partial Fulfillment
of the Requirement for the Degree of

DOCTOR OF PHILOSOPHY

to the Faculty of
Applied Life Chemistry Major,
Department of Agricultural Biotechnology

at

SEOUL NATIONAL UNIVERSITY

by

Eunji Cho

Date Approved

_____

Sangkee Rhee

Ki-Bong Oh

Jongheon Shin

Yonghoon Kwon

Hyi-Seung Lee

Abstract

Natural products from marine-derived microorganisms and terrestrial plant are worth researching on drug discovery because of chemical structural diversity and broad spectrum of bioactivities. In this study, the antibacterial activities of metabolites isolated from marine actinomycete *Streptomyces microflavus* and traditional medical folk plant *Juniperus chinensis* were evaluated and their mechanisms of action were investigated.

Part I deals with the antibiotic compounds, isolated from a marine-derived actinomycete *Streptomyces* sp. MBTI36. This strain was identified as *Streptomyces microflavus* through 16S rDNA sequencing analysis. A new chromomycin A_9 (**1**), along with chromomycin Ap (**2**), chromomycin A_2 (**3**), and chromomycin A_3 (**4**), were isolated from the culture of MBTI36, for which the structures were determined using extensive spectroscopic methods as well as comparisons with the previously reported data. Compounds **1**–**4** showed potent antibacterial activities against gram-positive bacteria including MRSA strains. In a passage experiment, minimum inhibitory concentration (MIC) values for compounds **1**–**4** showed no more than a 4-fold increase from the starting MIC value, indicating that no resistance has been recorded during the 21 passages. Transcriptome analysis revealed that chromomycin widely inhibits gene expressions related with various metabolic processes including purine and pyrimidine biosynthesis pathway.

In part II, six compounds (**5–10**) were isolated from a Korean folk medical plant *Juniperus chinensis* based on activity-guided separation, and their structures were determined by combined spectroscopic analyses. A novel compound designated 3',3"-dihydroxy-(−)-matairesinol (**5**) was identified, which exhibited potent inhibitory activity toward *Streptococcus mutans*-derived SrtA (IC_{50} = 16.1 μM) without affecting microbial viability (MIC value > 300 μM), whereas (−)-matairesinol (**6**) could not inhibit SrtA at all. Other compounds (**7**–**10**) displayed

weak to moderate inhibitory activities toward SrtA. Inhibition of *S. mutans* aggregation, adhesion, and biofilm formation on solid surfaces, including artificial resin teeth, were associated with SrtA activity. The onset and magnitude of inhibition of adherence and biofilm formation in *S. mutans* treated with compound **5** at 4× the SrtA IC_{50} were comparable to the behaviors of the untreated *srtA*-deletion mutant.

Through the above results, this study presents the natural products that have the potential to inhibit pathogenic bacteria effectively with their underlying mechanism of action.

Key words: antibiotics, antibiotic resistance, anti-infectious drugs, chromomycins, marine-derived actinomycete, sortase A inhibitor, *Juniperus chinensis, Streptomyces microflavus*

Student number: 2015-21798

Contents

Part II. Inhibition of *Streptococcus mutans* adhesion and biofilm formation with small-molecule inhibitors of sortase A from *Juniperus chinensis*

List of Tables

List of Figures

List of Abbreviations

AMR	Antimicrobial resistance
ATCC	American type culture collection
BHI	Brain heart infusion
BLAST	Basic local alignment search tool
cDNA	Complementary DNA
CFU	Colony-forming units
CLSI	Clinical and laboratory standards institute
COSY	Correlation spectroscopy
DEG	Differentially expressed gene
DMSO	Dimethyl sulfoxide
DNA	Deoxyribonucleic acid
E. coli	*Escherichia coli*
ESI	Electrospray ionization
FAB	Fast atom bombardment
FPKM	Fragments per kilobase of exon per million
HMBC	Heteronuclear multiple bond correlation
HMQC	Heteronuclear multiple quantum coherence
HPLC	High-performance liquid chromatography
HR	High-resolution
HSQC	Heteronuclear single quantum coherence
IC_{50}	Half-maximal inhibitory concentration
IR	Infrared
KPB	Potassium phosphate buffer
m/z	Mass-to-charge ratio
MDR	Multi-drug resistance

MHB	Mueller hinton broth
MIC	Minimum inhibitory concentration
MRSA	Methicillin-resistant *Staphylococcus aureus*
MSSA	Methicillin-sensitive *Staphylococcus aureus*
MS	Mass spectrometry
NCBI	National center for biotechnology information
NCTC	The national collection of type cultures
NMR	Nuclear magnetic resonance
NOESY	Nuclear overhauser effect spectroscopy
NP	Natural product
OD	Optical density
PBP	Penicillin binding protein
PCR	Polymerase chain reaction
PDR	Pan-drug resistance
rDNA	Ribosomal DNA
RNA	Ribonucleic acid
RPMI	Roswell park memorial institute
S. aureus	*Staphylococcus aureus*
S. mutans	*Streptococcus mutans*
s-HAs	Saliva-coated hydroxyapatite beads
TOCSY	Total correlation spectroscopy
t_R	Retention time
UV	Ultraviolet
WT	Wild type
XDR	Extensive drug resistance

Part I.

Antimicrobial Activity of Chromomycins from Marine-Derived *Streptomyces microflavus*

Introduction

Appearance of antibiotic resistance

Antibiotics have contributed to saving a great number of people as a powerful weapon against pathogenic microorganisms. Since the discovery of penicillin, first antibiotic, a lot of antibiotics have been discovered and used. Antibiotics having various structures, for example macrolide, aminoglycoside, beta-lactam, etc., inhibit the growth of target microorganisms in the way of suppress pathways related bacterial reproduction or killing the pathogens directly (Zaman et al., 2017; Hutchings et al., 2019).

The arrival of antibiotics accompanies the appearance of antimicrobial resistance (AMR). Since the report about sulfonamide-resistant *Streptococcus pyogenes* in 1930s (Levy, 1982), resistant pathogens withstanding clinical drugs appeared one by one. Nowadays, AMR becomes a growing threat to global health (Kupferschmidt, 2016). It was reported that annually about 2.8 million people are infected and 35,000 people even die by resistance bacteria in USA (Control and Prevention, 2019), and over 25,000 death are caused in Europe, too (Laxminarayan, 2014). AMR can occur against either one or multiple antibiotics. In case of multiple resistance, following terms can be used: MDR (multi-drug resistance, non-susceptibility to agents in three or more antimicrobial classes), XDR (extreme-drug resistance, non-susceptibility to at least one agent in all except for a few antimicrobial classes) and PDR (pan-drug resistance, non-susceptibility to all commercially available antimicrobial agents) (Magiorakos et al., 2012).

Methicillin-resistance *Staphylococcus aureus* (MRSA) is one of the most representative antibiotic-resistant pathogens and there are many studies on various type of MRSA. Every MRSA acquires methicillin-resistance through mobile genetic

elements, staphylococcal cassette chromosome *mec* (SCC*mec*) which codes resistance genes including *mecA,* penicillin binding protein 2a (PBP2a) (Katayama et al., 2000). PBP2a which is presumed to be originated *Staphylococcus sciuri* (Stapleton and Taylor, 2002), has structural difference with original PBP causing decrease the affinity to beta-lactam antibiotics, so results resistance against that class agents (Otero et al., 2013). MRSA still continues to infect people throughout the world and the effectiveness of vancomycin is getting weaker (Katayama et al., 2016). The development of novel antimicrobial agents is an urgent issue to restrain antibiotic-resistant bacteria (Holmes et al., 2016; Hutchings et al., 2019).

Natural products and marine actinomycetes

Natural products (NPs) are discovered from diverse living organisms, such as microorganisms, plants, and animals. These chemicals are reported to have various bioactivities, such as anticancer, antibacterial/antifungal/antiviral, antidiabetic activities and so on. Due to these bioactivities, NPs are considered as the most important source of drug discovery. According to research reporting new drugs from 2015 to 2019, 4.6% of newly approved drugs were originated from NP, but 44.6% of drugs come from semi-synthetic variant of NPs or synthetic drugs using/mimicking pharmacophore of NPs (Newman and Cragg, 2020).

Actinomycetes are high-GC-contents gram-positive bacteria, which show fungi-like features, producing hyphae and spores though there are many differences in details. Soil actinomycetes were reported to produce diverse bioactive secondary metabolites through grand-scale screening in 1950s, providing the majority of antibiotics. Especially, many antibiotics were isolated from *Streptomyces* genus, for example, streptomycin from *S. griseus* in 1944, chloramphenicol from *S. venezuelae* in 1949, tetracycline from *S. aureofaciens* in 1950, vancomycin from *S. orientalis* in 1959, daptomycin from *S. roseosporus* in 2003 and platensimycin from *S. platensis*

in 2006 (Procópio et al., 2012).

Overlapping the appearance of AMR, the needs for novel antibiotic lead compounds are growing but the number of newly discovered antibiotics keeps to decline after the 2000s (Bérdy, 2012). To discover novel antibiotics, various approaches have been pursued. Because NPs have kept a key post in pharmaceutical market in the last few decades, some researchers have been interested in NPs from marine as unusual circumstances. Deep sea environment provides different habitation condition for microorganisms, such as minimal light, high water pressure, high salinity, extremely high/low temperature, and low concentration of oxygen (Subramani and Aalbersberg, 2012). It would be expected that the unique environment of deep sea confers uncommon features on marine microorganisms to produce new bioactive NPs comparing terrestrial bacteria. (Ramesh and Mathivanan, 2009; Subramani and Aalbersberg, 2012; Kamjam et al., 2017). Therefore, marine actinomycetes can be an influential source of structurally unique NPs with diverse biological activities, including antibacterial and anticancer (Carroll et al., 2019).

Aurelioic acid and chromomycins

Compounds of aureolic acid family have the structure of aromatic polyketides glycosylated with two oligosaccharide chains (Figure **1.1**). Members of aureolic acid include mithramycin (Grundy et al., 1953; Sensi et al.; 1958; Rao et al.; 1962), olivomycin (Brazhnikova et al., 1962), durhamycin (Jayasuriya et al., 2002), chromomycin and so on, which are with potent antitumor and antibacterial activities (Lombó et al., 2006). These compounds show deep yellow color with intense fluorescence under ultraviolet (UV) light and are classified by types of 2,6-dideoxysugar: D-olivose, D-oliose, D-mycarose, L-chromose B, and *O*-methylated/*O*-acetylated derivatives, and their combinations on oligosaccharide chains. Aureolic acids are also known as minor groove binders that interact with the

high-GC-content region of double helix DNA, as dimer form with the Mg^{2+} ion in a non-intercalative way. The interaction with double stranded DNA can cause DNA damage (Chatterjee et al., 2001), inhibition of DNA-dependent RNA synthesis (Bianchi et al., 1999; Remsing et al., 2003) or DNA gyrase inhibition (Simon et al., 1994; Lombó et al., 2006).

Chromomycins, firstly isolated from *Streptomyces griseus* No. (Sato et al., 1960), are found in diverse strains of genus *Streptomyces* living in terrestrial or marine habitats. These compounds belong to the aureolic acid family, possessing core of tricyclic aglycone with two aliphatic side chains and two sugar side chains. Disaccharide chain consists of two D-olioses and a trisaccharide chain is composed of two D-olivoses and one L-chromose. The acetyl/methyl substituents on sugars of chromomycin make sugar chains more rigid so the interaction between compounds and DNA stable (Chakrabarti et al., 2000). Various derivatives of chromomycins are found and identified, including chromomycin A_2, A_3 (Miyamoto et al., 1967; Toume et al., 2014), A_5 (Pettit et al., 2015), A_6, A_7 and A_8 (Pinto et al., 2019) from extracts of actinomycetes, chromomycin SK, SA, SDK by disruption of genes on chromomycin biosynthesis *cmm* gene cluster (Menéndez et al., 2004). Chromomycins present a wide range of biological activities such as antimicrobial activity against gram-positive bacteria (Ogawa et al., 1998; Lombó et al., 2006), anticancer (Mir et al., 2003; Hu et al., 2011; Pinto et al., 2019), and also, antiviral activities (Bianchi et al., 1997). Like other aureolic acid family members, chromomycins interact with the DNA, causing DNA damages (Barceló et al., 2010; Zihlif et al., 2010; Murase et al., 2018).

Figure 1.1 Structures of aureolic acid family, mithramycin, olivomycin and durhamycin

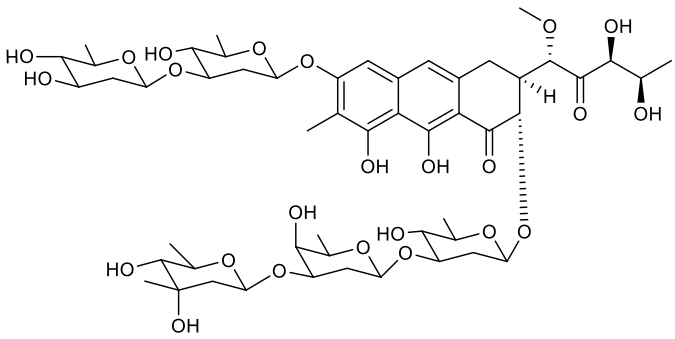

Mithramycin

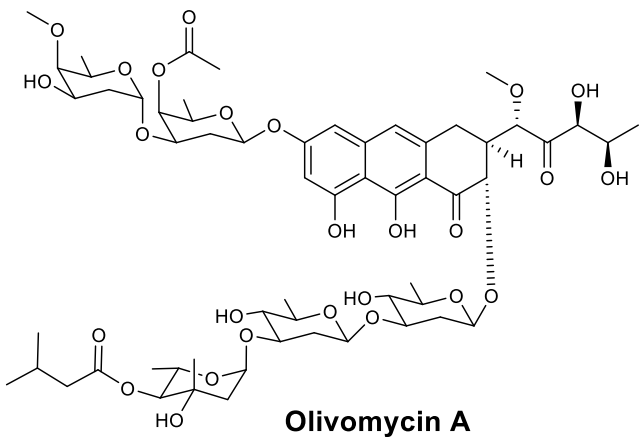

Olivomycin A

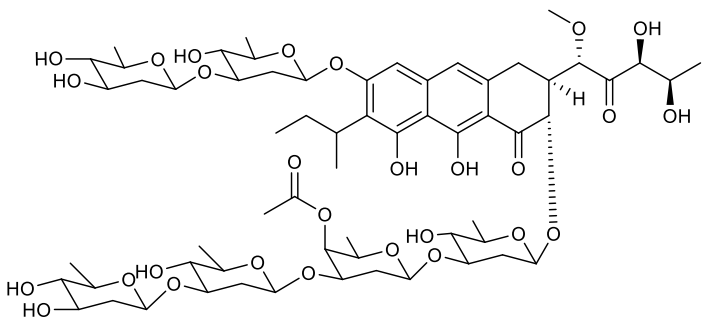

Durhamycin A

Aims

Screening for bioactive secondary metabolites from marine-derived actinobacteria, MBTI36 isolated from marine sediment of Jeju Island, Republic of Korea, was characterized that organic extract of these actinobacteria exhibit showed strong antibacterial activity against *S. aureus* (Minimum inhibitory concentration (MIC) value of 0.5 μg/mL). Based on 16S ribosomal DNA (rDNA) analysis, MBTI36 was identified as *Streptomyces microflavus.* Next, according to antibacterial activity-guided separation, the culture extract of MBTI36 was fractionated by flash-column chromatographic methods and separated furtherly by high-performance liquid chromatography (HPLC). Herein, four compounds were isolated from MBTI36 culture medium, three known chromomycins Ap (**2**), A_2 (**3**), and A_3 (**4**) and new chromomycin derivative, chromomycin A_9 (**1**). The antimicrobial activities of compounds **1**–**4** were evaluated against several gram-positive including MRSA, negative bacteria and fungi.

Materials and Methods

General experimental equipments

Optical rotations were measured using a JASCO P-1020 polarimeter (Jasco, Tokyo, Japan) with a 1 cm cell. UV spectra were acquired using a Hitachi U-3010 spectrophotometer (Tokyo, Japan). Infrared (IR) spectra were recorded on a JASCO 4200 FT-IR spectrometer (Easton, MD, USA) using a ZnSe cell. Nuclear magnetic resonance (NMR) spectra were recorded in $CDCl_3$ with the solvent peaks (δ_H 7.26/ δ_c 77.2) as internal standards on a JEOL JNM 400 MHz NMR spectrometer. High-resolution fast atom bombardment mass spectrometry (HR-FAB-MS) data were obtained at the National Center for Inter-University Research Facilities (NCIRF), Seoul National University, and acquired using a JEOL JMS 700 mass spectrometer (Jeol, Tokyo, Japan) with 6 keV-energy, emission current 5.0 mA, xenon as inert gas, and meta-nitrobenzyl alcohol as the matrix. HPLC separations were performed on a SpectraSYSTEM p2000 equipped with a refractive index detector (SpectraSYSTEM RI-150; Thermo Scientific, Waltham, MA, USA) and a UV-Vis detector (Gilson UV-Vis-151). All solvents used were of spectroscopic grade or were distilled prior to use.

Taxonomic identification of microorganism producing chromomycin

Marine sediment samples were collected from the shoreline of Jeju Island, Republic of Korea. The air-dried sediment (1 g) was mixed with 10 mL of sterilized artificial seawater and shaken at 150 rpm for 30 min at 25°C. The suspension was serially diluted with sterilized artificial seawater and 0.1 mL volumes of 3 appropriate dilutions, based on turbidity, were spread onto actinomycete isolation agar plates supplemented with cycloheximide (100 μg/mL) and artificial seawater. Plates were incubated at 28°C for 2 to 3 weeks. To obtain single strains, colonies were transferred

several times on fresh agar plates by streaking.

The isolated bacterial strain MBTI36 was identified using standard molecular biological protocols including DNA amplification and sequencing of the 16S rDNA region. Briefly, genomic DNA was prepared from MBTI36 mycelium using an i-Genomic BYF DNA Extraction Mini Kit (Intron Biotechnology, Seoul, Republic of Korea) according to the manufacturer's protocol. Polymerase chain reaction (PCR) amplification using the primers 27F (5′-AGAGTTTGATCCTGGCTCAG-3′) and 1429R (5′- GGTTACCTTGTTACGACTT-3′) was performed under the following conditions: pre-denaturation (95°C, 5 min), 30 cycles of denaturation (95°C, 15 s), annealing (50°C, 30 s), extension (72°C, 1 min 30 s), and final extension (72°C, 5 min). The nucleotide sequence was deposited in GenBank under accession number MK396664 and aligned according to nucleotide basic logic alignment search tool (BLAST) of the National Center for Biotechnology Information (NCBI) database. The phylogenetic tree was simulated using a neighbor-joining method (Saitou and Nei, 1987) and evolutionary distances were analysed with the Kimura two-parameter model using MEGA-X (Kumar et al., 2018). The bootstrap was replicated a thousand times.

Cultivation

MBTI36 was sporulated on GTYB (10 g of glucose, 2 g of tryptone, 1 g of yeast extract, and 1 g of beef extract in 1 L of artificial seawater) agar plates (20 g of agar in 1 L) at 28°C for 5 days. Mature spores were inoculated in 25 mL GTYB broth in 100ml baffled flask at 28°C for 24 h on a rotatory shaker. Each seed culture was transferred to 100 mL GTYB broth in 500ml Erlenmeyer flask and incubated at 28°C for 14 days without shaking.

Extraction and isolation

Strain MBTI36 was cultured in GTYB broth at 28°C without shaking. After incubation for 14 days, cultures were collected from 160 flasks (each containing 125 mL of culture broth, total 20 L) and filtered through filter paper. Culture filtrate was then lyophilized and extracted three times with 5 L of MeOH. After removing the solvent under vacuum, the crude extract was redissolved in H_2O and partitioned with *n*-hexane (0.4 g) and EtOAc (1.83 g). Based on the results of the antibacterial activity assay, the latter fraction was separated using semi-preparative reverse-phase HPLC (Agilent C_{18} column, 10 × 250 mm; 2.0 mL/min; H_2O-MeCN, 50:50) eluting compounds **4** (t_R = 15.8 min), **2** (t_R = 22.6 min), **1** (t_R = 23.4 min), and **3** (t_R = 34.5 min) in that order. Further purification for compounds **1** and **2** was accomplished using analytical HPLC (Agilent C_{18} column, 4.6 × 250 mm; 0.7 mL/min; water-acetonitrile, 55:45). The metabolites were isolated in the following amounts: 6.0, 8.7, 14.1, and 130.0 mg of **1**–**4**, respectively.

chromomycin A₉ (**1**): pale yellow, amorphous solid; $[\alpha]_D^{25}$ –18.3 (*c* 0.25, MeOH); UV (MeOH) λ_{max} (log ε) 205 (3.78), 223 (2.14), 282 (1.93), 317 (1.22), 329 (1.19), 430 (1.34) nm; IR (ZnSe) ν_{max} 3408, 2933, 1731, 1722, 1252, 1167, 1068 cm^{-1}; ^{13}C and ^{1}H NMR data, see Table 1; HRFABMS *m/z* 1219.5143 $[M+Na]^+$ (calcd for $C_{58}H_{84}O_{26}Na$, 1219.5149).

Antibacterial activity assays

The antibacterial activity assays were performed according to the Clinical and Laboratory Standards Institute (CLSI) guide methods (CLSI, 2018). Gram-positive bacteria (*S. aureus* ATCC25923, *Enterococcus faecium* ATCC19434, and *Enterococcus faecalis* ATCC19433) and gram-negative bacteria (*Salmonella enterica* ATCC14028, *K. pneumoniae* ATCC10031, and *E. coli* ATCC25922) were used for each quality control strain. The following drug-resistant strains were

obtained from the stock Culture Collection of Antimicrobial Resistant Microorganisms (CCARM; Seoul Women's University) and American Type Culture Collection (ATCC) and used for antibacterial activity assays: MSSA strains were CCARM0027, CCARM0204, CCARM0205, and CCARM3640; MRSA strains were CCARM3089, CCARM3090, CCARM3634, CCARM3635, ATCC43300, ATCC700787, and ATCC700788. Cells were cultured overnight in cation-adjusted Mueller-Hinton broth (MHB; BD Difco, Sparks, MD, USA) at 37°C, collected by centrifugation, and washed twice with sterile distilled water. Each test compound was dissolved in dimethyl sulfoxide (DMSO) and diluted with MHB to prepare serial 2-fold dilutions ranging from 0.008 to 128 μg/mL. The final DMSO concentration was maintained at 1% by adding DMSO to the medium according to CLSI guidelines. In each well of a 96-well plate, 90 μL of MHB containing the test compound was mixed with 10 μL of broth containing approximately 5×10^6 colony-forming units (CFU)/mL of test bacterium (final concentration: 5×10^5 CFU/mL) adjusted to match the turbidity of a 0.5 MacFarland standard at 625 nm wavelength. The plates were incubated for 24 h at 37°C. The MIC was defined as the lowest concentration of test compound that prevented cell growth. Ampicillin (Duchefa, Netherlands), tetracycline, daptomycin, vancomycin, platensimycin, linezolid, and ciprofloxacin (Sigma-Aldrich, St. Louis, MO, USA) were used as reference compounds.

Antifungal activity assays

The antifungal activity assays were performed in accordance with the guidelines in CLSI document M38 (CLSI, 2017). *Candida albicans* ATCC10231 was cultured on potato dextrose agar (PDA) plates. After incubation for 24 h at 28°C, yeast cells were harvested by centrifugation and washed twice with sterile distilled water. Filamentous fungi (*Aspergillus fumigatus* HIC6094, *Trichophyton rubrum* NBRC9185, and *Trichophyton mentagrophytes* IFM40996) were cultured on PDA

plates at 28°C for 5 days. Spores were harvested and washed twice with sterile distilled water. Stock solutions of the compound were prepared in DMSO. Each stock solution was diluted in Roswell Park Memorial Institute (RPMI) 1640 broth (Sigma-Aldrich) at a concentration ranging from 0.008 to 128 μg/mL. The final DMSO concentration was maintained at 1% by adding DMSO to the broth. In each well of a 96-well plate, 90 μL of RPMI 1640 containing the test compound was mixed with 10 μL of broth containing approximately 5×10^5 spores/mL of test fungus (final concentration: 5×10^4 spores /mL) adjusted to match the turbidity of a 0.5 McFarland standard. The plates were incubated for 24 h (for *C. albicans*), 48 h (for *A. fumigatus*), or 96 h (for *T. rubrum* and *T. mentagrophytes*) at 35°C. The MIC value was determined as the lowest concentration of test compound that fully inhibited cell growth. A culture with DMSO (1%) was used as a solvent control, and a culture supplemented with amphotericin B (Sigma-Aldrich) was used as a positive control.

Multi-step resistance development assays

Multi-step resistance development experiments were performed based on methods previously described (Farrell et al., 2011) with minor modifications. The initial inoculum (10^6 CFU/mL) of *S. aureus* ATCC43300, a MRSA strain, was prepared in MHB at 35°C, and adjusted to 0.5 MacFarland standard. A dilution series of 12 concentrations was prepared for ciprofloxacin and compounds **1**–**4** in fresh MHB based on the previous MIC at 2× the required final concentration. Next, 50 μL of bacterial inoculum was added to 50 μL of each compound dilution series in a 96-well plate (final concentration: 5×10^5 CFU/mL) and a control plate (no antimicrobial). The plates were incubated at 35°C for 24 h and the MIC was determined. The cultures were passaged daily for 21 days using 0.5-mL inocula (5×10^5 CFU/mL) from the 96-well plate corresponding to 0.5× the MIC determined

from the previous passage to inoculate a fresh series of compound dilutions and control plates.

RNA sample preparation

S. aureus Newman strain was inoculated overnight in 5ml MHB broth with shaking at 37°C and transferred 1/100 in 50 ml MHB, incubating until OD_{600} reaches 0.3. The culture was portioned into 5 ml aliquots in test tubes, and the compound **4** was added into treated groups to give final concentration 0.1 μM with 1% the solvent DMSO, while negative groups was treated only DMSO solvent. Each culture was furtherly incubated during 40 min at same condition. The concentration of compound **4** was determined in a preliminary test, which can affect the pattern of differential-display reverse transcription-PCR for cDNA but not the expression house-keeping genes (data not shown). The bacterial pellets were acquired by centrifugation (12000 rpm, 1min, 4°C) and stored at -80°C until RNA extraction.

RNA isolation was performed by easy-BLUE total RNA extraction kit (iNtRON Biotechnology) according to manufacturer's instructions. Mechanical disruption of cells was executed by Precellys 24 (bertin Technologies, Montigny le Bretonneux, France) with micro-glass beads (acid washed, ≤106 μm; Sigma). The qualities of total RNA samples were assessed using 2100 Expert Bioanalyzer (Agilent).

RNA-seq and analysis

Libraries were constructed by library kit TruSeq Stranded Total RNA with Ribo-Zero Plus (Illumina), and were sequenced at a high-throughput sequencing facility (DNA link, South Korea) on Illumina Novaseq 6000 platform. Short reads were checked for quality by FastQC and mapped to the reference genome, *S. aureus* NCTC8325 (NCBI Reference Sequence: accession number NC_007795.1) by TopHat (v2.0.13)

(Trapnell et al., 2009). Cuffdiff (v2.2.0) (Trapnell et al., 2013) was used to normalize short reads into fragments per kilobase of transcripts per million mapped reads (FPKM) and to report differentially expressed genes (DEG). Genes which display fold change more than twice and p value < 0.05 were identified as DEGs. Gene ontology (GO) analysis was performed using Amigo2 (Balsa-Canto et al., 2016) and Kyoto encyclopedia of genes and genomes (KEGG) pathway analysis by KEGG database (Kanehisa and Goto, 2000). Analysis was performed on three replicates.

Results

Taxonomy and phylogenetic analysis of MBTI36

The 16S rDNA of strain MBTI36 was amplified using PCR reaction by primers 27F/1429R and sequenced (1389 bp). According to BLAST sequence comparison, strain MBTI36 showed 99.9% identity to *Streptomyces microflavus* NBRC13062 (type strain, GenBank accession number: NR1123524), *S. microflavus* strain DR009 (GenBank accession number: JQ422181), strain PM122 (GenBank accession number: JQ422127), and strain PM100 (GenBank accession number: JQ422182). Thus, this strain was designated as *Streptomyces microflavus* strain MBTI36 (GenBank accession number: MK396664). The phylogenetic tree generated using MEGA-X program, with the neighbor-joining and maximum likelihood method based on the 16S rDNA sequence, revealed the evolutionary relationships of MBTI36 with a group of known *Streptomyces* type strains (Figure 1.1).

Figure 1.2 A neighbor-joining phylogenetic tree of strain MBTI36 based on 16S rDNA sequence.

The phylogenetic tree was constructed using MEGA-X and bootstrap was replicated a thousand times. The Kimura two-parameter model considering transversional and transitional substitution rates was used to measuring distance. Bar indicates 10 nucleotide substitutions per 1000 sites. ^{T}: type strain.

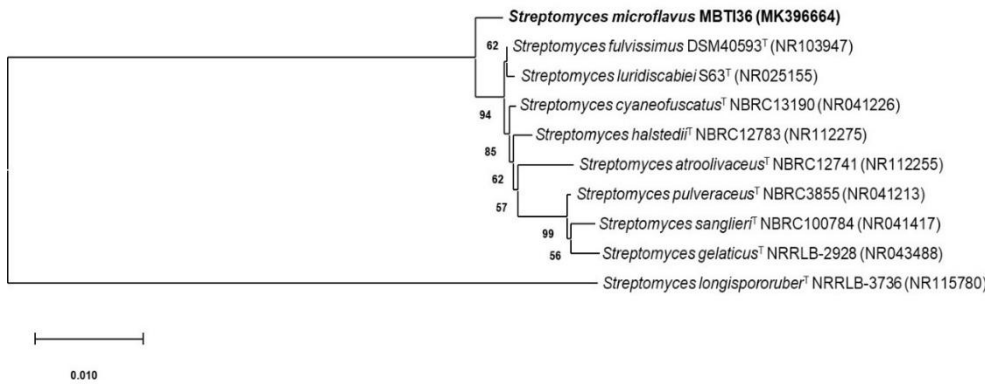
Streptomyces microflavus MBTI36 (MK396664)
62
Streptomyces fulvissimus DSM40593T (NR103947)
Streptomyces luridiscabiei S63T (NR025155)
94
Streptomyces cyaneofuscatus T NBRC13190 (NR041226)
Streptomyces halstedii T NBRC12783 (NR112275)
85
Streptomyces atroolivaceus T NBRC12741 (NR112255)
62
Streptomyces pulveraceus T NBRC3855 (NR041213)
57
Streptomyces sanglieri T NBRC100784 (NR041417)
99
Streptomyces gelaticus T NRRLB-2928 (NR043488)
56
Streptomyces longispororuber T NRRLB-3736 (NR115780)
0.010

Isolation and structural elucidation of compounds 1–4

Strain MBTI36 was cultured in GTYB broth and cultivated 14 days without shaking. The culture filtrate was lyophilized and extracted 3 times with methanol. The crude extract was separated using solvent-partitioning and semi-preparative HPLC. In consequence, four antibiotic compounds were obtained. Based on combined spectroscopic analyses, including ^{1}H, ^{13}C NMR, two-dimensional (2D) NMR spectral analyses including correlation spectroscopy (COSY), heteronuclear multiple quantum coherence (HMQC), and heteronuclear multiple bond correlation (HMBC), and UV data, compounds **2**–**4** were identified as known chromomycins, chromomycin Ap (**2**) (Norio S, 1976), chromomycin A_2 (**3**) (Miyamoto et al., 1967; Yoshimura et al., 1988), and chromomycin A_3 (**4**) (Sato et al., 1960; Toume et al., 2014) (Figure 1.2). The spectroscopic data for these compounds were in good agreement with previous reports.

The molecular formula of compound **1** was determined to be $C_{58}H_{84}O_{26}$ based on HR-FAB-MS analysis ($[M+Na]^+$ *m/z* 1219.5143, calculated for $C_{58}H_{84}O_{26}Na$, 1219.5149) having 17 degrees of unsaturation.

The molecular formula of compound **1** was determined to be $C_{58}H_{84}O_{26}$ based on HR-FAB-MS analysis ($[M+Na]^+$ *m/z* 1219.5143, calcd for $C_{58}H_{84}O_{26}Na$, 1219.5149) having 17 degrees of unsaturation. The ^{13}C NMR data of this compound showed signals of two ketone carbons at δ_C 211.3 and 202.3, which were supported by a strong absorption band at 1722 cm^{-1} in the IR data. Similarly, two additional carbonyl carbons at δ_C 174.6 and 171.7, in conjunction with the absorption band at 1731 cm^{-1} in the IR data, were assigned as ester carbons. The ^{13}C NMR data showed 10 deshielded carbons in the region of δ_C 159.9–101.0 with the corresponding proton signals at δ_H 6.76 and 6.64 in the ^{1}H NMR data (Table 1), indicative of a naphthalene-type aromatic moiety. In addition, more than 20 oxygen-bearing methines and

methylenes were observed, indicating the presence of several sugar units. For these, the five anomeric carbons at δ_C 100.5–95.4 and the corresponding protons at δ_H 5.21–4.60 in the ^{13}C and ^{1}H NMR data, respectively, defined the presence of five sugars. Because these preliminary interpretations accounted for 16 degrees of unsaturation (4 for carbonyls, 7 for naphthalene, and 5 for sugars), compound **1** must possess an additional cycle for the 17 degrees of unsaturation inherent from the mass data. All the structural features coincide well with congener chromomycins Ap (**2**), A_2 (**3**), and A_3 (**4**), indicating **1** to be a new member of this class.

Based on this information, the structure of **1** was determined by comparing the ^{13}C and ^{1}H NMR data with other chromomycins as well as combined 2D NMR analyses (Figure 3, Figures S1–S6). First, the aromatic carbons and protons had almost the same chemical shifts as congeners assigned the *tri*-oxygenated methylnaphthalene moiety (C-4-C-10, C-4a, C-8a, C-9a, and C-10a) in **1**. This interpretation was confirmed based on ^{1}H-^{1}H COSY, HSQC, and HMBC data including the long-range correlations of key protons (H-5, H-10, and 7-H_3) with neighboring carbons. The expansion of this moiety was also determined based on combined COSY (H-2-H-3-H_2-4) and HMBC correlations (H-2/C-1, H_2-4/C-4a, and H-5/C-4) to construct a dihydroxy-3,4-dihydroanthracen-1-one moiety, the common aglycone of the chromomycin class. Then, an additional COSY correlation of H-3 placed a methoxy-bearing methine (C-1') at this position. A COSY-based 2,3-dihydroxypropyl group (C-3'-C-5') was connected at this methine *via* a ketone (C-2') based on HMBC correlations (H-1'/C-2' and H-3'/C-2'), establishing a five-carbon side chain that was previously reported for the chromomycin family.

The ^{13}C and ^{1}H NMR and 2D NMR data for the sugar portion of **1** were also similar to **4**, indicating the same sugars and linkages (Table 1.1). The five sugar units were identified as two D-olioses, two D-olivoses, and one L-chromose, based on the comparison of NMR data with **4** using COSY correlations. Then, the linkage

between the sugars and their connection at the aglycone were certified by 3-bond HMBC correlations of anomeric carbons with protons (Figure 1.3). However, an extra ethyl group was identified based on the COSY and HSQC data (δ_C 27.8, δ_H 2.46; δ_C 9.7, δ_H 1.19), and the attachment at C-A4 of D-oliose (sugar A) *via* a ketone (δ_C 174.6) was also found by HMBC correlations, substituting the 4-*O*-acetyl group of **4** with the 4-*O*-propioyl group in **1**. Accordingly, the structure of compound **1** was determined to be a new chromomycin, chromomycin A_9, possessing a 4-*O*-propioyl-D-oliose moiety.

Table 1.1 ^{13}C and ^{1}H NMR assignments for compound 1 in $CDCl_3$.[a.]

Position	δ_C, type	δ_H (*J* in Hz)	Position	δ_C, type	δ_H (*J* in Hz)
1	202.3, C		4-*O*-methyl-D-oliose (Sugar B)		
2	76.1, CH	4.72, d (11.4)	B1	95.4, CH	5.11, br s
3	44.0, CH	2.60, m	B2	33.7, CH_2	1.76, m; 1.73, m
4	27.1, CH_2	3.10, m	B3	66.0, CH	3.96, m
		2.67, dd (16.6, 3.5)	B4	81.7, CH	3.22, d (2.8)
5	101.0, CH	6.64, s	B5	66.9, CH	3.87, q (6.6)
6	159.9, C		B6	17.4, CH	1.28, d (6.3)
7	111.9, C		B4-OCH_3	62.6, CH_3	3.60, s
8	156.3, C		D-olivose (Sugar C)		
9	165.5, C		C1	100.5, CH	5.10, dd (9.7, 1.3)
10	117.2, CH	6.75, s	C2	37.7, CH_2	2.48, m; 1.70, m
4a	134.8, C		C3	82.5, CH	3.61, m
8a	108.3, C		C4	75.3, CH	3.12, m
9a	108.3, C		C5	72.3, CH	3.38, m
10a	138.6, C		C6	18.2, CH_3	1.35, d (5.6)
7-CH_3	8.4, CH_3	8.40, s	D-olivose (Sugar D)		
8-OH		9.81, s	D1	99.9, CH	4.60, dd (9.6, 1.7)
1’	82.0, CH	4.70, d (1.5)	D2	37.3, CH_2	2.28, m; 1.70, m
2’	211.3, C		D3	80.9, CH	3.50, m
3’	78.3, C	4.22, br s	D4	75.4, CH	3.12, m
4’	68.1, C	4.36, m	D5	72.5, CH	3.30, m
5’	20.8, CH_3	1.37, d (5.6)	D6	18.0, CH_3	1.24, d (6.1)
1’-OCH_3	59.9, CH_3	3.52, s	L-chromose (Sugar E)		
4-*O*-propioyl-D-oliose (Sugar A)			E1	97.3, CH	5.02, dd (3.6, 1.8)
A1	97.6, C	5.21, dd (9.7, 2.0)	E2	43.9, CH_2	2.04, m; 2.00, m
A2	33.2, CH_2	2.19, m; 2.05, m	E3	70.8, C	
A3	70.2, CH	3.98, m	E4	79.9, CH	4.61, d (9.3)
A4	67.2, CH	5.18, d (2.9)	E5	67.2, CH	3.98, m
A5	70.0	3.82, q (6.5)	E6	18.0, CH_3	1.38, d (5.4)
A6	17.0, C	1.28, d (6.3)	E3-CH_3	23.2, CH_3	1.35, s
COCH_2CH_3	174.6, C		*C*OCH_3	171.7, C	
CO*C*H_2CH_3	27.8, CH_2	2.46, q (7.5)	$COCH_3$	21.1, CH_3	2.14, s
$COCH_2$*C*H_3	9.7, CH_3	1.19, t (7.5)			

[a] ^{13}C and ^{1}H NMR data were obtained at 100 and 400 MHz, respectively.

Figure 1.3 The structures of compounds 1–4.

1: Chromomycin A_9, **2**: Chromomycin Ap, **3**: Chromomycin A_2, **4**: Chromomycin A_3

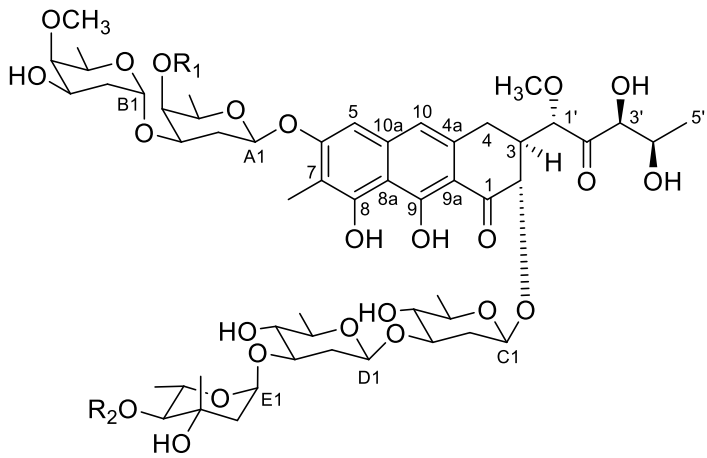

1 R_1=$COCH_2CH_3$ R_2=$COCH_3$
2 R_1=$COCH_3$ R_2=$COCH_2CH_3$
3 R_1=$COCH_3$ R_2=$COCH(CH_3)_2$
4 R_1=$COCH_3$ R_2=$COCH_3$

Figure 1.4 Key correlations of COSY and HMBC experiments for compound 1.

Bold lines represent COSY correlations and arrows display HMBC

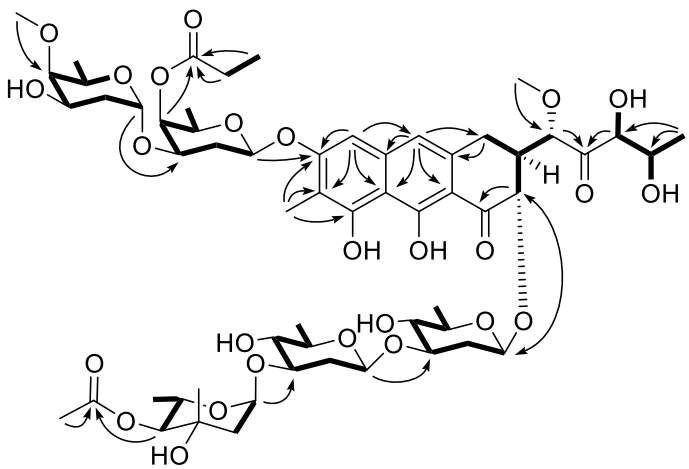
O
HO
O
O
O
O
O
O
O
O
O
H
OH
O
OH
OH
OH
O
HO
HO
O
O
O
O
O
O
HO

Antimicrobial activity of compounds 1–4

The antibacterial activities of compounds **1**–**4** were evaluated against diverse pathogenic bacteria, compared with ampicillin and tetracycline as positive controls. (Table 1.2) Compounds **1**–**4** exhibited outstanding antibacterial activity against the gram-positive strains (*S. aureus* ATCC25923, *E. faecium* ATCC19434, and *E. faecalis* ATCC19433), with MIC values of 0.03–0.5 μg/mL (Table 1.2). These compounds also inhibited the growth of gram-negative bacteria *S. enterica* ATCC14028 (MIC = 0.5–1 μg/mL), however, failed to inhibit the growth of other gram-negative bacteria such as *K. pneumoniae* ATCC10031 and *E. coli* ATCC25922 (MIC > 128 μg/mL).

Given that compounds **1**–**4** showed powerful inhibitory activities against *S. aureus*, further antibacterial activities were evaluated against drug-resistant *S. aureus* strains. These compounds successfully inhibited the growth of all tested methicillin-sensitive *S. aureus* (MSSA) and MRSA strains (Table 1.3). Remarkably, compounds **1**–**4** exhibited broad-spectrum antibiotic effects on MRSA strains, representing MIC values from 0.06 to 0.25 μg/mL. These values are much lower than those of major classes of antibiotics including daptomycin (MIC > 32 μg/mL), vancomycin (MIC = 0.5–2 μg/mL), platensimycin (MIC = 4–8 μg/mL), linezolid (MIC = 1–2 μg/mL), and ciprofloxacin (MIC = 0.13–>32 μg/mL).

The antifungal activities of compounds **1**–**4** were also evaluated against pathogenic fungal strains, *C. albicans* ATCC10231, *A. fumigatus* HIC6094, *T. rubrum* NBRC9185, and *T. mentagrophytes* IFM40996, comparing amphotericin B as a positive control compound. However, these compounds did not show inhibitory activity against the any tested fungi (Table 1.2).

Table 1.2 Results of antimicrobial activity test.

Compound	MIC values (μg/mL)									
	Gram(+) Bacteria			Gram(-) Bacteria			Fungi			
	A	**B**	**C**	**D**	**E**	**F**	**G**	**H**	**I**	**J**
1	0.03	0.5	0.13	0.5	>128	>128	>128	>128	>128	>128
2	0.13	0.5	0.13	1	>128	>128	>128	>128	>128	>128
3	0.06	0.5	0.06	0.5	>128	>128	>128	>128	>128	>128
4	0.13	0.5	0.13	0.5	>128	>128	>128	>128	>128	>128
Ampicillin	0.06	0.5	0.25	0.25	128	32				
Tetracycline	0.06	0.13	0.25	0.25	0.5	0.5				
Amphotericin B							0.5	1	1	1

A: *Staphylococcus aureus* ATCC25923, B: *Enterococcus faecium* ATCC19434, C: *Enterococcus faecalis* ATCC19433, D: *Salmonella enterica* ATCC14028, E: *Klebsiella pneumoniae* ATCC10031, F: *Escherichia coli* ATCC25922, G: *Candida albicans* ATCC10231, H: *Aspergillus fumigatus* HIC6094, I: *Trichophyton rubrum* NBRC9185, J: *Trichophyton mentagrophytes* IFM40996.

Table 1.3 Antibacterial activities of compounds 1–4 against MSSA and MRSA.

Microorganism	MIC values (μg/mL)								
	Dap	**Van**	**Pla**	**Lin**	**Cip**	**1**	**2**	**3**	**4**
CCARM0027 [a]	8	0.5	4	2	0.25	0.13	0.13	0.06	0.13
CCARM0204 [a]	2	0.25	4	1	0.25	0.06	0.06	0.03	0.06
CCARM0205 [a]	1	0.13	2	1	0.25	0.06	0.13	0.06	0.06
CCARM3640 [a]	8	0.25	4	2	0.25	0.13	0.25	0.06	0.13
CCARM3089 [b]	>32	1	8	2	>32	0.13	0.25	0.13	0.13
CCARM3090 [b]	>32	1	8	1	>32	0.13	0.25	0.13	0.13
CCARM3634 [b]	>32	0.5	8	2	>32	0.13	0.13	0.06	0.13
CCARM3635 [b]	>32	1	8	2	>32	0.13	0.06	0.06	0.13
ATCC43300 [b]	>32	1	4	2	0.25	0.13	0.13	0.06	0.13
ATCC700787 [b]	>32	2	8	2	0.13	0.13	0.25	0.25	0.13
ATCC700788 [b]	>32	2	8	2	16	0.13	0.25	0.13	0.13

[a] Methicillin-sensitive *Staphylococcus aureus* (MSSA). [b] Methicillin-resistant *Staphylococcus aureus* (MRSA). Dap : daptomycin, Van : vancomycin, Pla : platensimycin, Lin : Linezolid, Cip : ciprofloxacin.

Multi-step resistance development

To investigate properties of compounds **1**–**4,** the potential for resistance development to test compounds in a *S. aureus* strains was also observed. The representative resistance development profiles for compounds **1**–**4** against *S. aureus* ATCC43300 and ciprofloxacin (used as a comparator antibiotic) are presented in Figure 1.4, and resistance was defined as a > 4-fold increase for the initial MIC (Clark et al., 2009; Kosowska-Shick et al., 2009). In case of ciprofloxacin, the MIC values have kept increasing during 21 days passage experiments showing 128-fold change from the initial MIC value 0.25 μg/mL to a final MIC of 32 μg/mL in *S. aureus* ATCC43300. In contrast, compounds **1**–**4** showed only 2-fold increases in the MIC (**1**,**2** and **4**: from 0.13 to 0.25 μg/mL, **3**: from 0.06 to 0.13 μg/mL) during the observation over 21 passages. During the passage experiment, MIC values for compounds **1**–**4** showed no more than a 4-fold increase from the starting MIC values, indicating that resistance did not develop during the passages.

Figure 1.5 Resistance acquisition during 21 days serial passaging in the presence of chromomycins

Resistance acquisition during 21 days in the presence of sub-MIC (0.5 × the MIC determined from the previous passage) levels of ciprofloxacin, chromomycin A_9 (**1**), Ap (**2**), A_2 (**3**), and A_3 (**4**) for *S. aureus* ATCC43300. The *y* axis is the highest concentration the cells grew in during passaging. For ciprofloxacin, 128 × MIC was the highest concentration tested. The figures are representative of 3 independent experiments.

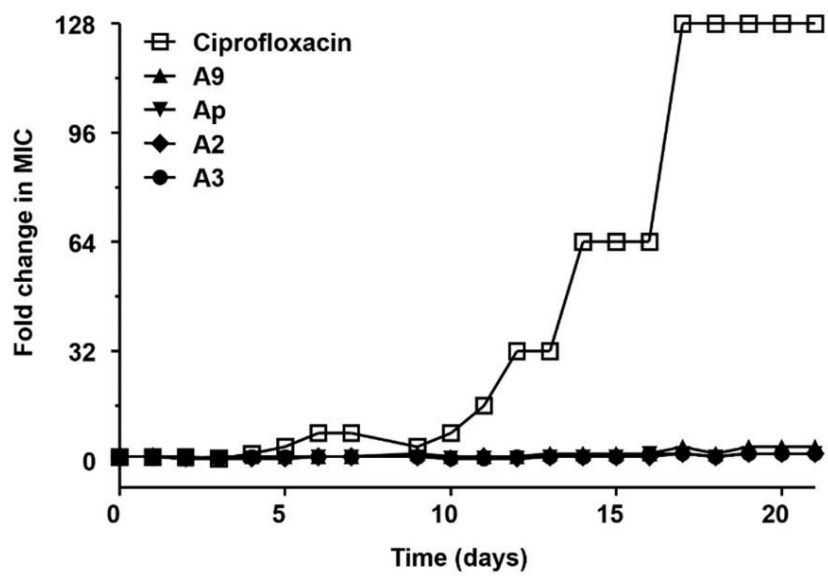
Ciprofloxacin
A9
Ap
A2
A3
Fold change in MIC
128
96
64
32
0
0
5
10
15
20
Time (days)

Results of transcriptome analysis

Through the high-throughput RNA sequencing process, total mapped reads of 46,575,243 on average were obtained from each sample. Among them, 328 DEGs by chromomycin treatment were reported as 48 up-regulated genes and 280 down-regulated genes (Figure 1.6, Table S1). GO enrichment analysis was performed with the DEGs by adjusted EASE score (a modified Fisher exact *p*-value) < 0.05. Up-regulated DEGs were grouped into 18 GO terms which involved cellular process and metabolic process (Table 1.4). Down-regulated DEGs covered much wider range of changes than up-regulated genes. Total 243 GO term was categorized into 170 of biological process, 13 of cellular component and 60 molecular function. The down-regulated GO terms that have threshold EASE score < 0.001 were presented Table 1.5.

According to DEGs and KEGG pathway analysis, it was verified that several biosynthesis pathways are closely corelated with the treatment of chromomycin (Figure 1.6, Table S2). Especially two pathways were significantly inhibited by chromomycin treated groups, purine biosynthesis pathway and pyrimidine biosynthesis pathway. Purine pathway was inhibited in initial steps of biosynthesis (Figure 1.7, Table S1), and the inhibition levels were highly intensive. The $\log_2$(fold change) value of *purH* was -6.36 (absolutely 82-fold down) and that of other genes, *purN*, *purD*, *purM*, *purF*, *purL* and *purQ*, on *pur* operon were -5.8 to -2.8 (absolutely 7- to 56-fold down). Similarly, the $\log_2$ values of genes on *pyr* operon, *pyrP*, *pyrB*, *pyrC*, *carA*, *carB* and *pyrE*, were -4.6 to -2.5 (absolutely 5.7- to 24-fold down), which contribute to the initial steps of pyrimidine biosynthesis (Figure 1.8, Table S1).

Table 1.4 Gene ontology distribution for chromomycin treatment (up-regulated)

Category	Term	EASE Score	DEG Count
Biological Process	GO:0009987~cellular process	0.0348518	14
	GO:0008152~metabolic process	0.027349	10
	GO:0044237~cellular metabolic process	0.0428499	10
	GO:0071704~organic substance metabolic process	0.0130835	8
	GO:0051604~protein maturation	0.022742	3
	GO:0046483~heterocycle metabolic process	0.0427185	3
	GO:1901360~organic cyclic compound metabolic process	0.0313162	3
	GO:0016485~protein processing	0.0306397	2
Cellular Component	GO:0030312~external encapsulating structure	0.0002882	4
	GO:0005618~cell wall	0.0020342	4
	GO:0005622~intracellular anatomical structure	0.010557	3
	GO:0005737~cytoplasm	0.0036721	2
Molecular Function	GO:0003824~catalytic activity	0.0020434	10
	GO:0005488~binding	0.0087979	7
	GO:1901363~heterocyclic compound binding	0.0101153	4
	GO:0097159~organic cyclic compound binding	0.0101153	4
	GO:0036094~small molecule binding	0.003317	2
	GO:0043167~ion binding	0.0009208	2

Table 1.5 Gene ontology distribution for chromomycin treatment (down-regulated)

Category	Term	EASE Score	DEG Count
Biological Process	GO:0009987~cellular process	0.0000001	176
	GO:0008152~metabolic process	0.0003908	133
	GO:0071704~organic substance metabolic process	0.0000435	128
	GO:0044237~cellular metabolic process	0.0000640	124
	GO:0044238~primary metabolic process	0.0000760	112
	GO:0006807~nitrogen compound metabolic process	0.0000169	112
	GO:1901564~organonitrogen compound metabolic process	0.0000034	89
	GO:0009058~biosynthetic process	0.0000006	89
	GO:1901576~organic substance biosynthetic process	0.0000005	88
	GO:0044249~cellular biosynthetic process	0.0000006	87
	GO:0044281~small molecule metabolic process	0.0000029	74
	GO:1901566~organonitrogen compound biosynthetic process	0.0000000	72
	GO:0006810~transport	0.0000165	60
	GO:0051234~establishment of localization	0.0000165	60
	GO:0051179~localization	0.0000165	60
	GO:0044271~cellular nitrogen compound biosynthetic process	0.0000726	52
	GO:0055085~transmembrane transport	0.0001118	50
	GO:0006796~phosphate-containing compound metabolic process	0.0004481	47
	GO:0018130~heterocycle biosynthetic process	0.0000059	45
	GO:1901362~organic cyclic compound biosynthetic process	0.0000250	45
	GO:0006082~organic acid metabolic process	0.0005331	42
	GO:0019637~organophosphate metabolic process	0.0000176	39
	GO:0043436~oxoacid metabolic process	0.0006231	39
	GO:0019438~aromatic compound biosynthetic process	0.0003089	38
	GO:0090407~organophosphate biosynthetic process	0.0000004	35
	GO:1901137~carbohydrate derivative biosynthetic process	0.0000470	33
	GO:0006811~ion transport	0.0000389	33
	GO:0034654~nucleobase-containing compound biosynthetic process	0.0000868	32
	GO:0055086~nucleobase-containing small molecule metabolic process	0.0002444	31
	GO:0006753~nucleoside phosphate metabolic process	0.0000374	29
	GO:0009117~nucleotide metabolic process	0.0000159	29
	GO:0006812~cation transport	0.0000329	28
	GO:0006520~cellular amino acid metabolic process	0.0005292	28
	GO:0009259~ribonucleotide metabolic process	0.0000017	26
	GO:0019693~ribose phosphate metabolic process	0.0000031	26
	GO:1901293~nucleoside phosphate biosynthetic process	0.0000023	25
	GO:0009165~nucleotide biosynthetic process	0.0000012	25
	GO:0009260~ribonucleotide biosynthetic process	0.0000003	23

Biological Process	GO:0046390~ribose phosphate biosynthetic process	0.0000006	23
	GO:0008652~cellular amino acid biosynthetic process	0.0001543	22
	GO:1901605~alpha-amino acid metabolic process	0.0005252	22
	GO:0072521~purine-containing compound metabolic process	0.0002157	20
	GO:0006163~purine nucleotide metabolic process	0.0001227	20
	GO:0009123~nucleoside monophosphate metabolic process	0.0000017	20
	GO:0009124~nucleoside monophosphate biosynthetic process	0.0000005	20
	GO:0009150~purine ribonucleotide metabolic process	0.0001429	19
	GO:0009161~ribonucleoside monophosphate metabolic process	0.0000003	19
	GO:0009156~ribonucleoside monophosphate biosynthetic process	0.0000002	19
	GO:1901607~alpha-amino acid biosynthetic process	0.0008181	18
	GO:0098655~cation transmembrane transport	0.0002654	17
	GO:0009152~purine ribonucleotide biosynthetic process	0.0000124	17
	GO:0006164~purine nucleotide biosynthetic process	0.0000207	17
	GO:0072522~purine-containing compound biosynthetic process	0.0000207	17
	GO:0000041~transition metal ion transport	0.0009599	15
	GO:0098662~inorganic cation transmembrane transport	0.0003232	14
	GO:0098660~inorganic ion transmembrane transport	0.0009529	14
	GO:0009167~purine ribonucleoside monophosphate metabolic process	0.0000150	13
	GO:0009126~purine nucleoside monophosphate metabolic process	0.0000150	13
	GO:0009168~purine ribonucleoside monophosphate biosynthetic process	0.0000100	13
	GO:0009127~purine nucleoside monophosphate biosynthetic process	0.0000100	13
	GO:0046040~IMP metabolic process	0.0000045	12
	GO:0006189~'de novo' IMP biosynthetic process	0.0000074	11
	GO:0006188~IMP biosynthetic process	0.0000124	11
	GO:0043545~molybdopterin cofactor metabolic process	0.0007321	7
	GO:0051189~prosthetic group metabolic process	0.0007321	7
	GO:0006777~Mo-molybdopterin cofactor biosynthetic process	0.0007321	7
	GO:0019720~Mo-molybdopterin cofactor metabolic process	0.0007321	7
Molecular Function	GO:0003824~catalytic activity	0.0004834	142
	GO:0036094~small molecule binding	0.0003097	69
	GO:0000166~nucleotide binding	0.0003974	62
	GO:1901265~nucleoside phosphate binding	0.0003974	62
	GO:0022857~transmembrane transporter activity	0.0000939	47
	GO:0005215~transporter activity	0.0000939	47
	GO:0022804~active transmembrane transporter activity	0.0007836	25
	GO:0015297~antiporter activity	0.0001143	12
	GO:0016854~racemase and epimerase activity	0.0009174	8

Figure 1.6 Scatter plot comparing gene expression in *S. aureus* Newman with and without chromomycin

The $\log_2$ values of gene expression levels with chromomycin (Y-axis) have been plotted against the $\log_2$ values without chromomycin (X-axis). DEGs were identified with cut-off of $|\log_2(\text{fold change}) \geq 1|$. The red dots represent up-expressed genes and the blue dots represent down-expressed genes.

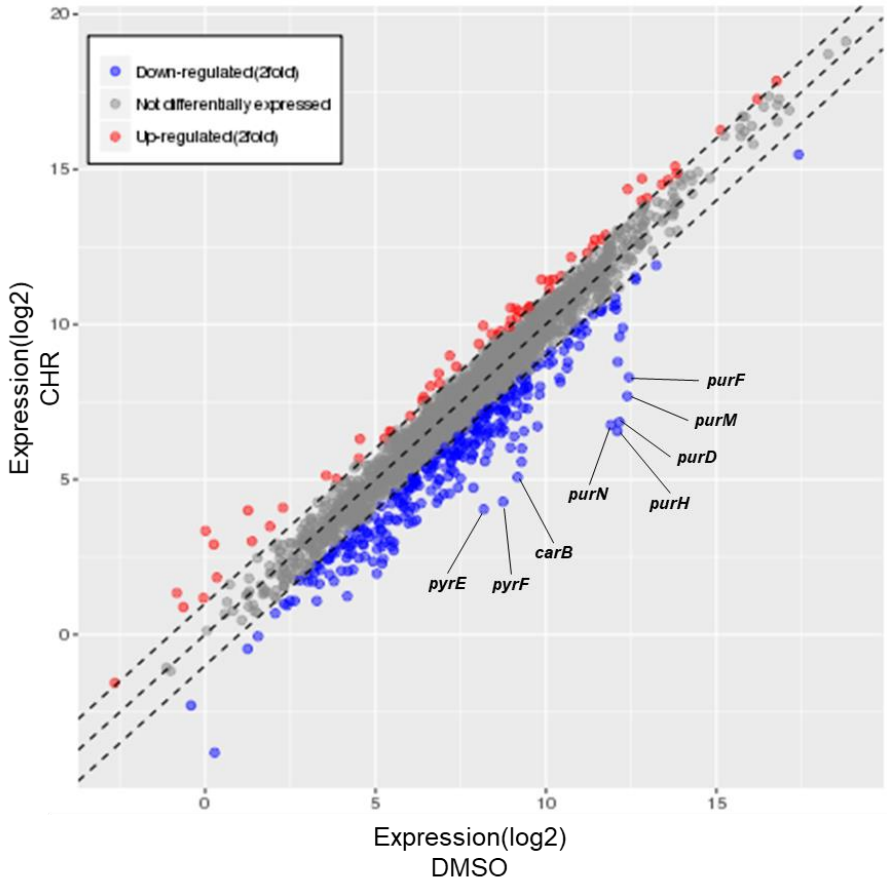
Down-regulated(2fold)
Not differentially expressed
Up-regulated(2fold)
Expression(log2)
CHR
Expression(log2)
DMSO
purF
purM
purD
purN
purH
carB
pyrE
pyrF
0
5
10
15
20

Figure 1.7 KEGG pathway of "purine metabolism"

Blue highlighted genes represent down-regulated DEGs of chromomycin. (Kanehisa and Goto, 2000)

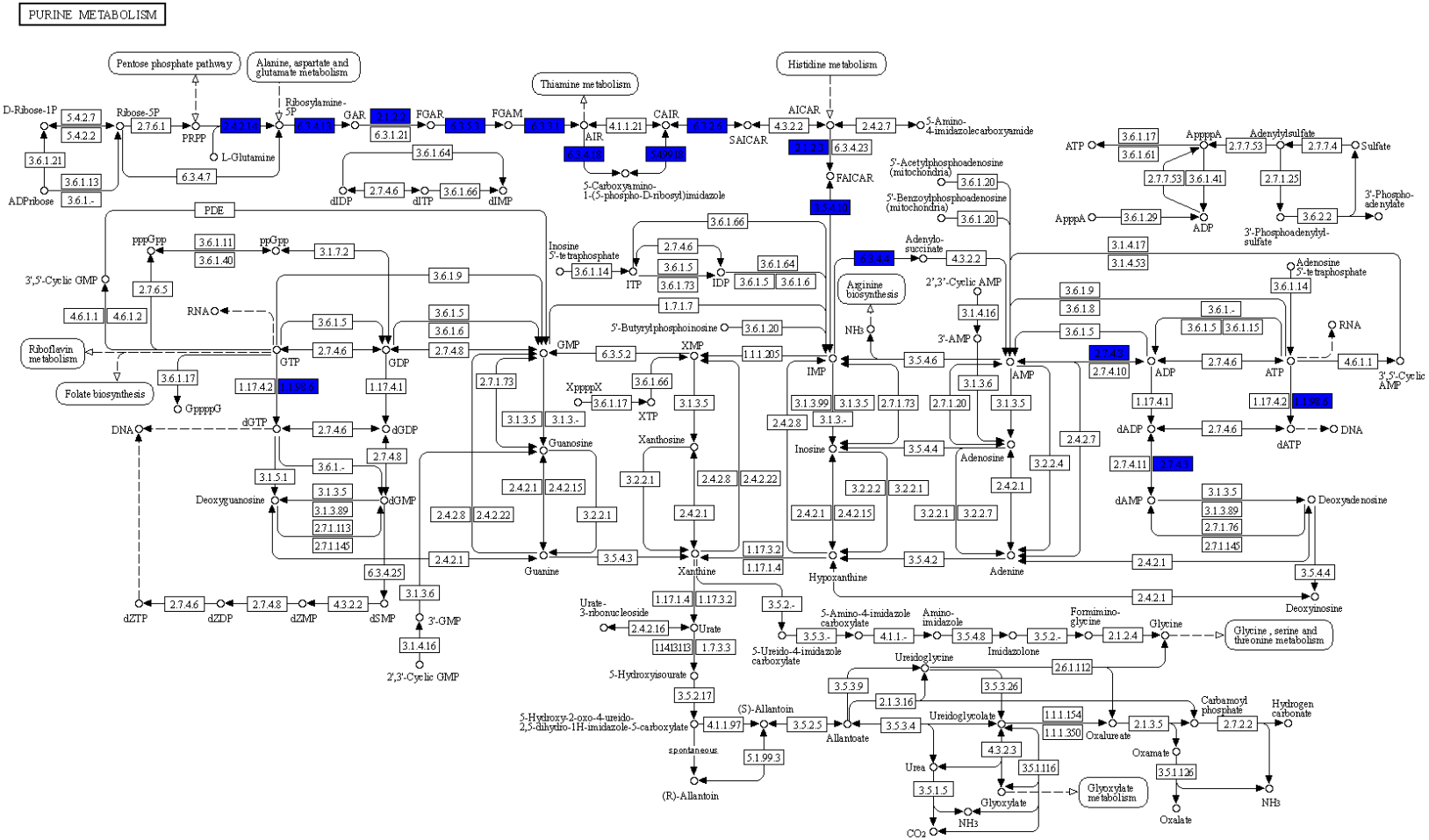

Figure 1.8 KEGG pathway of "pyrimidine metabolism"

Blue highlighted genes represent down-regulated DEGs of chromomycin. (Kanehisa and Goto, 2000)

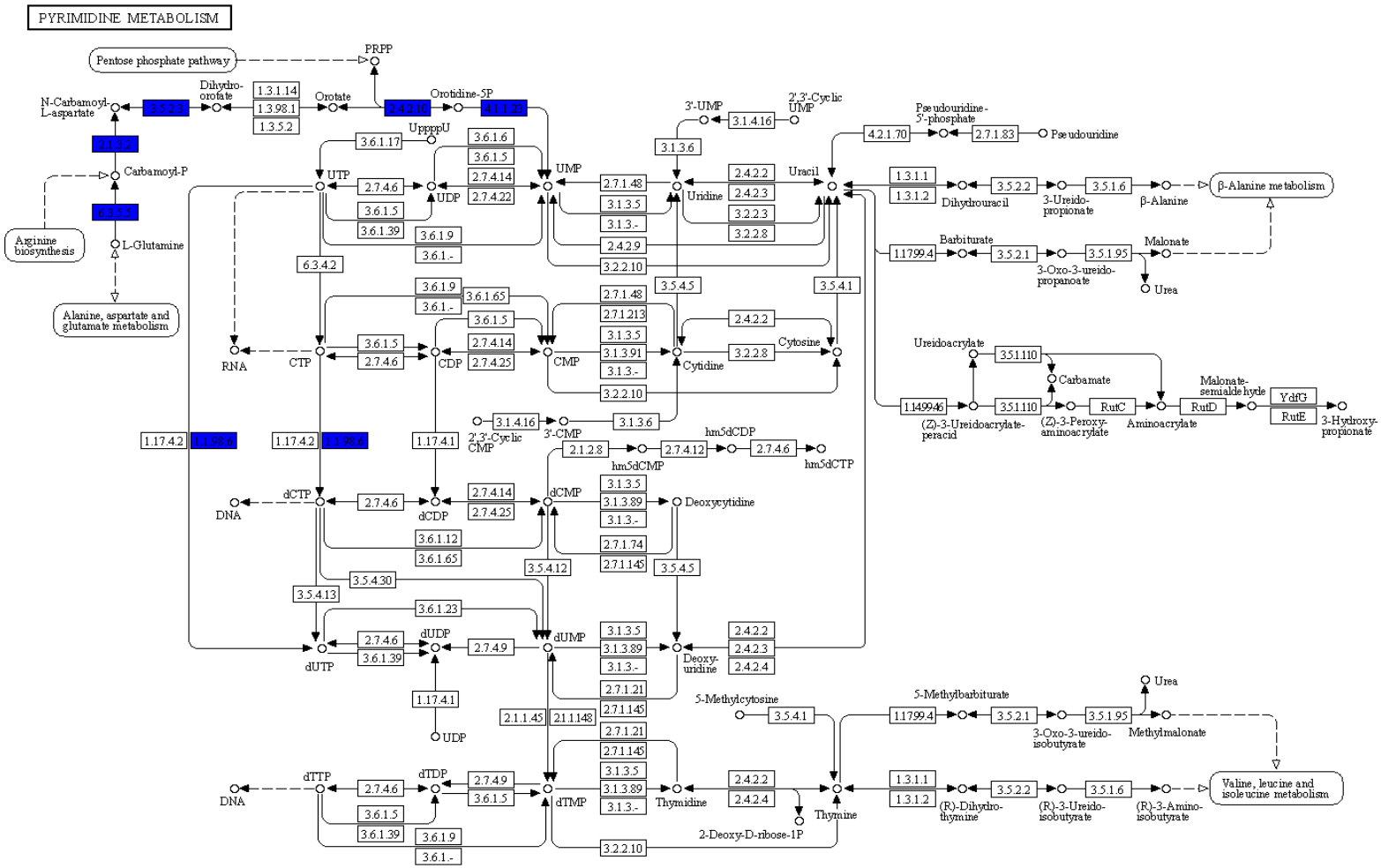
PYRIMIDINE METABOLISM
Pentose phosphate pathway
PRPP
N-Carbamoyl-L-aspartate
Dihydro-orotate
Orotate
Orotidine-5P
UMP
UDP
UTP
CTP
CDP
CMP
Carbamoyl-P
L-Glutamine
Arginine biosynthesis
Alanine, aspartate and glutamate metabolism
RNA
Uridine
Uracil
Cytidine
Cytosine
3'-UMP
2',3'-Cyclic UMP
3'-CMP
2',3'-Cyclic CMP
Pseudouridine-5'-phosphate
Pseudouridine
Dihydrouracil
3-Ureido-propionate
β-Alanine
β-Alanine metabolism
Barbiturate
3-Oxo-3-ureido-propanoate
Malonate
Urea
Ureidoacrylate
Carbamate
(Z)-3-Ureidoacrylate-peracid
(Z)-3-Peroxy-aminoacrylate
Aminoacrylate
Malonate-semialdehyde
3-Hydroxy-propionate
YdfG
RutE
RutC
RutD
hm5dCDP
hm5dCMP
hm5dCTP
dCTP
dCDP
dCMP
DNA
Deoxycytidine
dUTP
dUDP
dUMP
Deoxy-uridine
5-Methylcytosine
5-Methylbarbiturate
3-Oxo-3-ureido-isobutyrate
Methylmalonate
dTTP
dTDP
dTMP
Thymidine
Thymine
2-Deoxy-D-ribose-1P
(R)-Dihydro-thymine
(R)-3-Ureido-isobutyrate
(R)-3-Amino-isobutyrate
Valine, leucine and isoleucine metabolism

Discussion

Chromomycins are glycosylated polyketides, which are members of the aureolic acid family, exhibiting various bioactivity spectrums: antimicrobial and anticancer activity that are produced by terrestrial and marine *Streptomycete* species. In this study, a chemical investigation of a liquid culture extract of the marine-derived actinomycete *S. microflavus* strain MBTI36 led to the isolation of four chromomycin derivatives (**1**–**4**). The elucidation of structures for compounds **2**–**4** were based on spectroscopic data and comparisons with the reported data (Sato et al., 1960; Miyamoto et al., 1967; Yoshimura et al., 1988; Toume et al., 2014), and were identified as chromomycin Ap (**2**), chromomycin A_2 (**3**), and chromomycin A_3 (**4**), respectively. The ^{13}C and ^{1}H NMR spectroscopic data of compound **1** were similar to congener compounds **2**–**4**, indicating **1** as a new member of this class. Similar to compound **4,** the linkage among the sugar moieties and their attachments to the aglycone were the same; however, the COSY and HSQC data showed an ethyl group in compound **1**. The attachment of this group at C-A4 of D-oliose (sugar A) *via* a ketone was also found based on a series of HMBC correlations, replacing the 4-*O*-acetyl substituent of **4** with the 4-*O*-propioyl group in **1**. Thus, the structure of compound **1** was designed to be a new chromomycin A_9 possessing a 4-*O*-propioyl-D-oliose moiety.

Chromomycins, typically represented chromomycin A_3 (**4**), were previously isolated from *Streptomycete* species including *S. griseus* and *S. cavourensis* (Sato et al., 1960; Lombó et al., 2006) and showed antibacterial activity against gram-positive bacteria such as *Bacillus subtilis*, *Staphylococcus aureus*, and *Enterococcus hirae* (Ogawa et al., 1998). In the study, the isolated compounds **1**–**4** displayed the potent antibacterial activity against gram-positive pathogenic strains such as *S. aureus*, *E. faecium*, and *E. faecalis*, with MIC values of 0.03–0.5 μg/mL.

These compounds also displayed inhibitory activities against MRSA strains (MIC values of 0.06–0.25 μg/mL), which are more potent than other major antibiotics including vancomycin and linezolid. The development potential for antibiotic resistance to compounds **1**–**4** in the MRSA strain *S. aureus* ATCC43300 was also investigated. As shown in Table 3, ciprofloxacin which is one of fluoroquinolones class antibiotics showed potent antibacterial activities against MRSA strains *S. aureus* ATCC43300 and ATCC700787. However, through multi-step (21-passage) resistance development studies in the presence of sub-inhibitory concentrations (0.5 × MIC) of ciprofloxacin , a continuous increase in MIC value for this comparator antibiotic against *S. aureus* ATCC43300 during the 21 days passage experiment was observed (Figure 1.4). According to a previously reported study, topoisomerase IV is the primary target of fluoroquinolones in *S. aureus,* showing the higher sensitivity of topoisomerase IV relative to DNA gyrase to these agents (Ng et al., 1996). Furthermore, resistance from an altered DNA gyrase requires resistant topoisomerase IV for expression (Ferrero et al., 1995, Ng et al., 1996). On the other hand, MIC values for compounds **1**–**4** showed no more than a 4-fold increase from the starting MIC value during the passage experiment, indicating resistance did not evolve.

RNA-seq data and transcriptome analysis revealed that the treatment of chromomcyin at 0.1 μM during 40 mins brought out widespread gene expression change in *S. aureus*. Especially, chromomycin treated group had problems to express genes related to various metabolic biological process and only comparatively few numbers of genes were upregulated. The DEGs showed the most drastic change were *pur* operon and *pyr* operon genes (Figure 1.6, Table S2). These genes had the tendency to be more down-expressed as go further downstream of operon. Considering general bacteria have polycistronic mRNA, this result suggests that chromomycin punctuates the transcription of the entire mRNA expressions of these

two operons. Because *pur* genes and *pyr* genes play in the upstream of purine or pyrimidine biosynthesis pathway as essential genes for growth of *S. aureus* (Forsyth et al., 2002), the severe down-expressions of these genes can be fatal to bacterial viability. Moreover, according to KEGG pathway database, this pathway can affect to another pathway, folate biosynthesis (Kanehisa et al., 2017), which were also listed in KEGG pathway of chromomycin DEGs.

Members of the aureolic acid family of antibiotics including chromomycins were isolated in the present study and reported to exhibit antimicrobial activities against gram-positive bacteria, while there were inactive against gram-negative bacteria due to the difficulty of permeability to bacterial cell. That is why the main pharmacological interest has focused on in their antitumor activity (Lombó et al., 2006). Reportedly by several previous studies, the antitumor activities and mode of action of aureolic acid family antibiotics was shown to be partly come from non-intercalating interaction between GC-rich-regions in the minor groove of the DNA double helix and dimeric complexes of the antibiotics with Mg^{2+} ion. (Barceló et al., 2010; Zihlif et al., 2010; Murase et al., 2018). A suggested mode of action involves the binding of chromomycin A_3 to DNA as a Mg^{2+} dimer, which cross-links the two strands, thus blocking the processes of replication and mainly transcription of DNA and resulting in cytotoxic activity. Therefore, modifications of the side chain can potentially be exploited for the modulation of biological activity of chromomycin compounds.

Part II.

Inhibition of *Streptococcus mutans* adhesion and biofilm formation with small-molecule inhibitors of sortase A from *Juniperus chinensis*

Introduction

Anti-infective target

Due to the appearance of AMR in worldwide, various strategy and efforts are attempting in biological and pharmaceutical fields. In an effort to overcome the crisis of AMR, anti-infection targeting drugs have emerged as a solution (Rasko and Sperandio, 2010). Unlike antimicrobial drugs directly interrupting survival or growth, the drugs disturbing the virulence of pathogens should introduce weaker selective pressure towards microorganisms, therefore, less evolving resistance strains (Maura et al., 2016).

Anti-infective therapy generally uses a strategy to block or interrupt virulence factors, which are directly involved in the pathogenesis pathways for pathogens. So anti-infective drugs are developing, for example, to block adherence or invasion or pathogen toward host cell surface, to interrupt biofilm formation or quorum sensing process and to inhibit the biosynthesis or secretion of toxins (Rasko and Sperandio, 2010).

Sortase A as an anti-infective target against gram-positive bacteria

Gram-positive pathogenic bacteria have many surface proteins playing a key role in bacterial adherence and host invasion, which are closely related with virulence and pathogenesis. Sortase A (SrtA), a transpeptidase found in broad range of gram-positive pathogens including streptococci, staphylococci and enterococci (Dramsi et al., 2005), controls anchoring of surface proteins in the peptidoglycan cell walls of gram-positive bacteria. SrtA recognizes the LPXTG motif in substrates, which is a part of cell wall sorting signal on the C-terminal tail. Then SrtA severs the amide bond between threonine and glycine residues by nucleophilic attack with highly

conserved cysteine residue, and form a covalent bond between the substrate proteins and bacterial cell wall via thioacyl bond (Hendrickx et al., 2011). Because numerous gram-positive bacteria possess genes encoding SrtA and surface proteins with sorting signals recognized by SrtA, the SrtA-mediated anchoring system is considered a universal mechanism.

Knockout mutants of *srtA* fail to display surface proteins with the LPXTG motif, which leads to diminished infectiousness without impacting bacterial viability. *S. aureus srtA* mutants were not able to display surface proteins such as Spa (protein A), FnbA (fibronectin-binding protein), ClfA (clumping factor) proteins, and showed impaired infections in mice (Mazmanian et al., 2000). Due to these properties, SrtA is closely associated with the pathogenicity of gram-positive pathogens and is considered a desirable anti-infective drug target (Cossart and Jonquières, 2000). Because SrtA affects the action of multiple surface proteins, it is expected that SrtA inhibitors could concurrently disrupt multiple targets.

A cariogenic pathogen, *Streptococcus mutans*

Streptococcus mutans is a facultative aerobic gram-positive bacterium and an important cariogenic pathogen. This bacterium inhabits the human oral cavity, causing dental plaque and dental caries (Loesche, 1986). The major virulence factors of *S. mutans* are the capacity to form biofilms attached to the tooth surface, the capacity to produce organic acids (acidogenicity), and viability in low-pH conditions (aciduricity) (Lemos et al., 2013).

Biofilm formation by *S. mutans* proceeds via sucrose-dependent and sucrose-independent pathways, following the steps of adherence, aggregation, microcolony formation, and maturation (Scharnow et al., 2019). Sucrose-independent adhesion is primarily facilitated by antigens I/II (also called as, Pac, SpaP and P1) adhesins, which has a high affinity with human salivary agglutinin

(Ahn et al., 2008), and sucrose-dependent adhesion is known to be mediated by series of glucosyltransferases (Gtfs, including GtfB, GtfC, and GtfD) and glucan-binding proteins (Gbps, including GbpA, GbpB and GbpD) (Krzyściak et al., 2014). In case of GbpC, there is a report that this protein is involved in both sucrose-dependent/independent pathway (Mieher et al., 2018).

Like other gram-positive bacteria, *S. mutans* utilizes SrtA for its sorting system. Through genome sequencing of strain UM159, it was revealed that there are six proteins assumed as SrtA substrates in *S. mutans*, possessing LPXTG motif: antigens I/II, GbpC (glucan-binding protein C), DexA (dextranase), FruA (Fructanase), WapA and WapE (wall-associated protein A and E) (Ajdić et al., 2002). Research using *srtA* knockout mutant strains of *S. mutans* revealed the importance of SrtA in aggregation processes, as failed to sort out substrate protein (Lee and Boran, 2003). The mutants exhibited a lower tendency to colonize surfaces of the oral mucosa or teeth, as well as reduced biofilm accumulation (Lévesque et al., 2005). Considering the close relationship between sorting the surface proteins, biofilm formation and virulence in *S. mutans*, SrtA is a promising anti-virulent target to this pathogen like other gram-positive bacteria.

Juniperus chinensis

Juniperus chinensis (commonly Chinese juniper) is an evergreen coniferous ornamental tree which is widely distributed in East Asia. Chemical investigations of this shrub have shown various compounds, for example, lignans (Fang et al., 1992), diterpenes (Fang et al., 1993; Lee et al., 1995), sesquiterpenes (Fang et al., 1996), and flavonoids (Lim et al., 2002). Compounds isolated from leaves, heartwood, fruits of *J. chinensis* showed various bioactivities such as anti-leukemia (Miyata et al., 1998), anti-fungal (Ohashi et al., 1994), and acaricidal activity (Lee et al., 2009). Also, several compounds have antioxidant activity (Lim et al., 2002), and inhibitory

activities against tyrosinase (Park et al., 2018; Park et al., 2021), protein-tyrosine phosphatase 1B and cholinesterase (Jung et al., 2015). Because of varied bioactivities, this plant has been traditionally used for medical purposes (But et al., 1997). However, no SrtA inhibitor from *J. chinensis* has been reported so far.

Aims

Based on an initial screening of bioactive metabolites that may function as SrtA inhibitors, extracts of 120 commercially available Korean traditional medicines were tested against *S. aureus*- and *S. mutans*-derived SrtA. Some of these extracts showed enzyme inhibitory activity exceeding 40% at 100 μg/mL concentration. The SrtA inhibitory metabolites of these traditional medicines were identified as curcuminoids from *Curcuma longa* (Park et al., 2005), flavonoids from *Sophora flavescens* (Oh et al., 2011), lignans and phenyl propanoids from *Pulsatilla koreana* (Lee et al., 2014), maltol derivatives and flavonol glycosides from *Sophora japonica* (Yang et al., 2015, Yang et al., 2016), flavonoids from *Psoralea corylifolia* (Won et al., 2015) and *Spatholobus suberectus* (Cho et al., 2017, Park et al., 2017), and coumarins from *Poncirus trifoliata* (Park et al., 2020).

In this study, chemical structures were investigated in *J. chinensis* crude extract, which effectively inhibited *S. mutans*-derived SrtA (71.2% inhibition at a concentration of 100 μg/mL). Bioassay-guided fractionation of the extract using various chromatographic methods following combined spectroscopic analysis yielded six compounds (**5–10**) of various skeletal classes including, flavonoid, lignan, and tropolone-bearing sesquiterpene (Figure 2.1). Among these compounds, a novel lignan (**5**) was structurally characterized as a dihydroxy derivative of matairesinol through combined spectroscopic analysis. This study describes the structures of a novel lignan (**5**) and several previously reported compounds (**6**–**10**) isolated from *J. chinensis*. Compound **5** strongly inhibited *S. mutans*-derived SrtA. The inhibition of

S. mutans aggregation, adhesion, and biofilm formation on solid surfaces, including artificial resin teeth, was associated with a SrtA-mediated mechanism. These results suggest that an inhibitor of SrtA may be a useful tool for inhibiting the cariogenic properties of *S. mutans*

Material and Methods

General experimental procedures

Optical rotation was measured with a JASCO P-2000 polarimeter (Easton, MD, USA) with a 1-cm cell. UV spectra were acquired using a Hitachi U-3010 spectrophotometer (Tokyo, Japan). IR spectra were obtained with a JASCO 4200 FT-IR spectrometer (Easton, MD, USA) using a ZnSe cell. High-resolution electrospray ionization mass spectrometry (HR-ESI-MS) data were acquired at the National Instrumentation Center for Environmental Management (Seoul, Korea) using an AB Sciex 5600 QTOF HR-MS instrument (Sciex, MA, USA). Proton and carbon nuclear NMR and 2D NMR spectra were recorded with a Varian Gemini 2000 300 MHz spectrometer (Palo Alto, CA, USA) or Bruker Avance 500 and 600 MHz spectrometers (Berlin, Germany) using MeOH-d_4 with a solvent peak at δ_H 3.31/δ_C 49.0 or DMSO-d_6 with a solvent peak at δ_H 2.50/δ_C 39.50 as internal standards. HPLC separation was conducted on a SpectraSYSTEM p2000 instrument equipped with a refractive index detector (SpectraSYSTEM RI-150) and a UV-Vis detector (UV-Vis-151, Gilson, Middleton, WI, USA). All solvents used were of spectroscopic grade or were distilled prior to use.

Plant material

The dried heartwood of *J. chinensis* was purchased from Kyungdong Oriental Herbal Market in Seoul, Korea, on November 13, 2017. A voucher specimen (specimen number 2017-YH-1) was deposited at the Natural Products Research Institute, College of Pharmacy, Seoul National University, Seoul, Republic of Korea. Taxonomic identification of the specimen was conducted by prof. Y. Suh at Seoul National University.

Extraction and isolation of compounds

The macerated heartwood (5.0 kg) of *J. chinensis* was repeatedly extracted into methanol (5 L × 3) and dichloromethane (5 L × 3) at room temperature. The organic extracts were combined and concentrated in a rotary evaporator. The residue (247.1 g) was fractionated between water and *n*-butanol, and then the latter layer (223.1 g) was partitioned between water–methanol (15:85) and *n*-hexane. The water–methanol portion (117.8 g) was separated into eight fractions through C_{18} reversed-phase vacuum flash chromatography and eluted with sequential mixtures of methanol and water (six fractions across a water–methanol gradient from 50:50 to 0:100) followed by acetone and finally ethyl acetate.

According to the results of ^{1}H NMR analysis, the fractions eluted with water–methanol (50:50) and (40:60) were separated further. The water–methanol (50:50) fraction (32.7 g) was subjected to semi-preparative reversed-phase HPLC (YMC-ODS column, 250 × 10 mm; 2.0 mL/min; water–methanol, 68:32). The peak at t_R = 43.3 min was purified through analytical HPLC (0.7 mL/min; water–acetonitrile gradient from 80:20 to 65:35 over 60 min) to yield compound **5** (t_R = 47.5 min). The fraction (23.4 g) eluted with water–methanol (40:60) was separated through HPLC (1.8 mL/min; water–methanol, 50:50) to obtain compounds **6** (t_R = 33.2 min) and **7** (t_R = 46.5 min). Purification of an additional peak (t_R = 44.7 min) through analytical HPLC (0.7 mL/min; water–acetonitrile, 75:25) produced compounds **8** (t_R = 6.8 min) and **9** (t_R = 60.1 min). The peak at t_R = 70.8 min was purified through analytical HPLC (0.7 mL/min; water–acetonitrile, 70:30) to obtain compound **10** (t_R = 46.3 min). The overall isolated amounts of compounds **5–10** were 13.2, 3.6, 3.3, 4.2, 4.8, and 1.1 mg, respectively.

*3',3''-Dihydroxy-(−)-matairesinol (**5**)*: yellow, amorphous solid; $[\alpha]_D^{25}$ −28.1 (*c* 0.4, MeOH); UV (MeOH) λ_{max} (log ε) 231 (3.36), 272 (2.86) nm; IR (ZnSe) ν_{max} 3276,

1760, 1607, 1515, 1456, 1340, 1204, 1151, 1093, 1022 cm^{-1}; ^{1}H and ^{13}C NMR data, Table 1; HR-ESI-MS *m/z*: 391.1388 $[M+H]^+$ (calculated for $C_{20}H_{23}O_8$, 391.1387).

SrtA inhibition assay

Recombinant SrtA protein was prepared following previously described procedures (Oh et al., 2006, Wang et al., 2015). *S. mutans* OMZ65 isolated from the human oral cavity was provided by Seoul National University School of Dentistry. The *srt*A genes derived from *S. mutans* OMZ65 were expressed in *Escherichia coli* and SrtA was purified through metal chelate affinity chromatography on Ni-nitriloacetic acid (NTA) resin. Each reaction was performed in a total volume of 100 μL, containing 50 mM Tris-HCl, 150 mM NaCl, and 5 mM $CaCl_2$ at pH 7.5, along with 17 μg of purified SrtA and 250 ng of synthetic substrate (Dabcyl-LPETG-Edans). The sample compounds were added to each reaction mixture with the solvent DMSO (final concentration, 1%). After 1 h of incubation at 37°C, the reactions were quantified based on fluorometric intensity (350 nm excitation and 495 nm emission wavelengths) using a microplate reader (FLx800, BioTek Instruments, Winooski, VT, USA). Triphasiol was used as a positive control for the SrtA inhibitor.

Antibacterial activity assay

Antibacterial activities of isolated compounds were determined according to a previously described method (Cho et al., 2020) based on Clinical and Laboratory Standards Institute guidelines (CLSI, 2018). Briefly, 5 mL of *S. mutans* OMZ65 was inoculated into brain heart infusion (BHI) broth, incubated for 16 h at 37°C, and the bacterial density was adjusted based on turbidity to match the 0.5 MacFarland standard at 625 nm. In each well of a 96-well plate, 20 μL of 2-fold diluted test compounds in 10% DMSO was added to 180 μL of cell culture in BHI broth and incubated for 16–20 h at 37°C. The final concentration of cells was approximately 5

$\times 10^5$ CFU/mL. The minimal inhibitory concentration (MIC) values were identified as the lowest concentration that inhibited cell growth. Ampicillin was used as an antibacterial positive control.

Saliva-induced aggregation assay

The effect of SrtA inhibitor on bacterial cell aggregation induced by human saliva was conducted according to a previously documented procedure (Lee and Boran, 2003). *S. mutans* NG8 and *srtA*-mutants were inoculated into Todd Hewitt broth and incubated for 16 h at 37°C, washed twice with KPBS (137 mM NaCl, 2.7 mM KCl, 6.5 mM Na_2HPO_4, 1.5 mM KH_2PO_4, pH 7.2), and resuspended in KPBS to an approximate optical density of 1.0 at 700 nm. Assay mixtures consisted of 400 μL of cells, 100 μL of fresh clarified saliva, and diluted test compounds. The mixtures were gently mixed through inversion and incubated at 37°C for 2 h. Turbidity at 700 nm was recorded every 20 min.

Adherence assay on saliva-coated hydroxyapatite beads

The effect of SrtA inhibition on bacterial adherence was evaluated using saliva-coated hydroxyapatite beads (s-HAs) (Lee et al., 2011). A total of 30 μg of s-HAs (diameter, 80 μm; Bio-Rad, Hercules, CA, USA) were coated with fresh saliva for 1 h at room temperature and rinsed twice with 0.01 M potassium phosphate buffer (KPB; pH 7.0). *S. mutans* NG8 (wild type, WT), *srtA*-deletion mutant (*ΔsrtA*), and *srtA*-complemented mutant (*ΔsrtA* + *srtA*) (Lee and Boran, 2003) were inoculated into 5 mL of BHI broth, incubated for 16 h at 37°C, and diluted to about 10^8 CFU/mL. The cell suspension and s-HAs were mixed with or without compound **5** (final concentration of cells 10^7 CFU/mL with 1% DMSO) and incubated for 90 min at 37°C with weak shaking. After three rounds of washing with KPB, attachment between s-HAs and *S. mutans* cells was disrupted through sonication (50 W, 30 s) in

KPB. Dispersed cells were spread on Mitis-Salivarius agar (Difco, Detroit, MI, USA) plates containing 3.2 mg/mL bacitracin. The number of colonies formed was determined after incubation for 48 h at 37°C.

Biofilm formation assay

The effect of SrtA inhibition on bacterial biofilm formation was investigated using the polystyrene plate and resin teeth model according to a previously described method (Petersen et al., 2004). Wild-type *S. mutans* and *srtA* mutants were inoculated into 5 mL of BHI broth at 37°C. Cultures in BHI broth containing 0.1% sucrose (final concentration 5×10^5 CFU/mL) were incubated with or without test compounds on 96-well polystyrene plates or with resin teeth (Endura, Shofu Inc., Kyoto, Japan) at 37°C for 24 h. Biofilms formed on the plate and resin teeth were washed twice with distilled water and then stained with 0.1% safranin for 30 s. After three further washes, the safranin-bound biofilms on plates were dissolved with 30% acetate and the intensity of absorbance at 530 nm wavelength, indicating safranin, was measured. Biofilms on resin teeth was also washed three times and photographed.

Statistical analysis

Statistical analysis was conducted using GraphPad Prism 9.3.1 software (Graphpad, San Diego, CA, USA). Statistical differences between groups were analyzed with Student's *t*-test or two-way analysis of variance followed Dunnett's test for post-hoc analysis. A p-value < 0.05 was regarded as statistically significant.

Results

Structural characterization of compounds 5–10

The molecular formula of compound **5** was determined to be $C_{20}H_{22}O_8$ through HR-ESI-MS analysis ($[M+H]^+$ *m/z* 391.1388, calculated for $C_{20}H_{23}O_8$, 391.1387). Combining HSQC NMR data, the ^{13}C and ^{1}H NMR features of this compound were identified as a carbonyl carbon (δ_C 178.5), 12 aromatic methines and non-protonated carbons (δ_C/δ_H 148.4–103.8/6.31–6.15), two methoxy groups (δ_C/δ_H 55.7/3.71 and 55.7/3.70), three methylenes (δ_C/δ_H 70.7/4.03 and 3.83, 37.2/2.44 and 2.32, and 33.9/2.74 and 2.69), and two methines (δ_C/δ_H 45.6/2.63 and 40.8/2.39) (Table 2.1). These characteristic features of 18 carbons (excluding the two methoxy groups) including a carbonyl and 12 aromatic carbons, in conjunction with an unsaturation degree of 10 determined from the mass data, strongly indicate that compound **5** is a lactone-bearing lignan compound.

Based on this information, the planar structure of **1** was determined from a combination of ^{1}H-^{1}H coupling constants, ^{1}H correlated spectroscopy, and heteronuclear multiple bond correlation NMR analyses (Figure 2.2). The three key structural motifs were readily identified as 2,3-dimethylene bearing butyrolactone (C-1-C-4, C-7', and C-7") and two 3,4-dihydroxy-5-methoxyphenyl groups (C-1'-C-6' and C-1"-C-6") based on the conspicuous ^{1}H-^{1}H and ^{1}H-^{13}C correlations. Subsequently, the connections of aromatic moieties at the lactone methylenes were assessed using a series of long-range ^{1}H-^{13}C correlations: H-2/C-1', H-3/C-1", H-2'/C-7', H-6'/C-7' H_2-7'/C-2' and C-6', H-2"/C-7", H-6"/C-7", and H_2-7"/C-2" and C-6". Literature review

revealed that the deduced planar structure of **5** was the 3',3"-dihydroxy derivative of matairesinol, a dibenzylic butanolide lignan found in *Cryptomeria japonica* (Imai et al., 2005) or *Forsythia koreana* (Kim et al., 2006).

Compound **5** possessed two stereogenic centers at C-2 and C-3 of the lactone moiety. As extensively described in the literature (Corrie et al., 1970; Lopes et al., 1983), the non-equivalence of H_2-4 (δ_H 4.03 and 3.83) assured the *trans* configuration between C-2 and C-3. Then, the absolute configurations were assigned as 2*R* and 3*R* based on comparison of its specific rotation ($[\alpha]_D^{25}$ −28.1) with those of (−)- and (+)-matairesinol ($[\alpha]_D^{25}$ and −47.2 and +15.2 for the (−) and (+) enantiomers, respectively) (Akiyama et al., 2007, Liu and Tu, 2013). Thus, the structure of compound **5**, designated 3',3"-dihydroxy-(−)-matairesinol, was determined to be a novel 2,3-dibenzyl-4-butanolide lignan.

In addition to compound **5**, five congeners of diverse structural classes were isolated and identified through combined spectroscopic analysis and literature comparison: (−)-matairesinol (**6**), quercetin (**7**) (Güvenalp and Demirezer, 2005), 4,6-dihydroxy-2-methoxyacetophenone (**8**) (Basabe et al., 2010), 5-hydroxyhinokitiol (**9**) (Dixon and Murphy, 1974), and juniperone A (**10**) (Park et al., 2021). Spectroscopic data for these compounds were in accordance with information in the literature.

Figure 2.1 Structures of compounds 5–10 from *Juniperus chinensis*

3',3''-dihydroxy-(−)-matairesinol (**5**), (−)-matairesinol (**6**), quercetin (**7**), 4,6-dihydroxy-2-methoxyacetophenone (**8**), 5-hydroxyhinokitiol (**9**), and juniperone A (**10**).

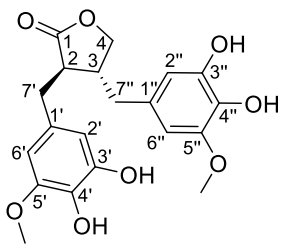
O
O
1
2
3
4
7'
7''
1''
2''
OH
3''
OH
4''
1'
2'
6'
3'
OH
6''
5''
O
5'
4'
O
OH

5

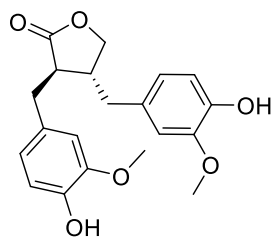
O
O
OH
O
O
OH

6

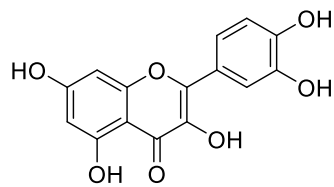
OH
HO
O
OH
OH
OH
OH
O

7

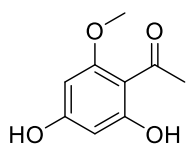
O
O
HO
OH

8

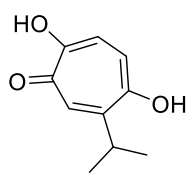
HO
O
OH

9

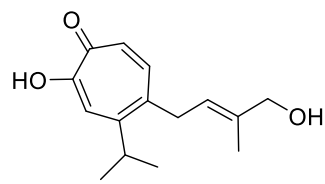
O
HO
OH

10

Figure 2.2 Key correlations found in COSY and HMBC experiments for compound 5.

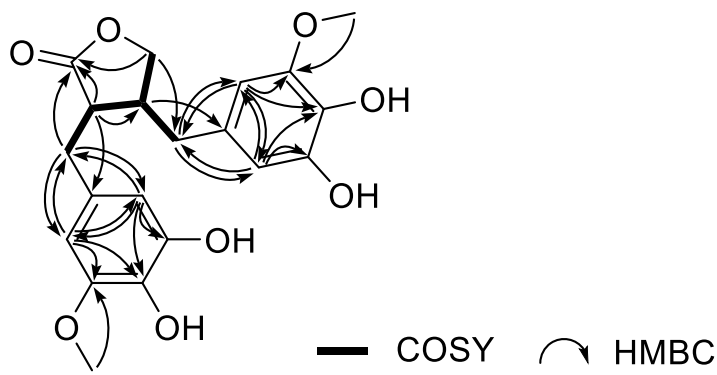

5

Table 2.1 The ^{13}C and ^{1}H NMR data of compound 5

(δ_H and δ_C in ppm).

No.	**5**[a]	
	δ_C type	δ_H (*J* in Hz)
1	178.5, C	
2	45.6, CH	2.63, m
3	40.8, CH	2.39, m
4	70.7, CH_2	4.03, t (8.0)
		3.83, t (8.0)
1'	128.1, C	
2'	104.7, CH	6.26, d (2.0)
3'	148.2, C	
4'	132.4, C	
5'	145.6, C	
6'	109.9, CH	6.31, d (2.0)
7'	33.9, CH_2	2.74, dd (13.5, 5.5)
		2.69, dd (13.5, 6.5)
OCH_3	55.7, CH_3	3.71, s
1"	128.9, C	
2"	103.8, CH	6.15, d (2.0)
3"	148.4, C	
4"	132.6, C	
5"	145.7, C	
6"	109.2, CH	6.17, d (2.0)
7"	37.2, CH_2	2.44, dd (12.5, 9.0)
		2.32, dd (13.0, 5.0)
OCH_3	55.7, CH_3	3.70, s

[a]Data were obtained in DMSO-*d*

SrtA inhibitory activities of compounds 5–10

Recombinant SrtA protein derived from *S. mutans* OMZ65 was expressed in *E. coli* transformant and prepared using Ni-NTA affinity chromatography (Oh et al., 2006; Yang et al., 2015). SrtA enzyme activities were measured through a fluorophotometric method using synthetic peptide substrate. The inhibitory effects, assessed using half-maximal inhibitory concentration (IC_{50}) values, of compounds **5–10** against *S. mutans* SrtA are shown in Table 2, along with that of triphasiol (IC_{50} = 25.3 μM). Triphasiol has been described as a potent inhibitor of *S. aureus* ATCC6537p-derived SrtA (IC_{50} = 34.5 μM) (Park et al., 2020), and it exhibited strong inhibitory activity toward *S. mutans*-derived SrtA. Among the isolated compounds, 3',3''-dihydroxy-(−)-matairesinol (**5**) exhibited outstanding inhibitory activity against *S. mutans* SrtA (IC_{50} = 16.1 μM). Analysis of SrtA inhibition by 3',3''-dihydroxy-(−)-matairesinol (**5**) and (−)-matairesinol (**6**) indicated that the hydroxyl groups at the C-3' and C-3'' sites play important roles. Substitution of the C-3' and C-3'' hydroxyl groups of **1** through dehydroxylation (**6**) led to complete loss of activity (IC_{50} > 300 μM). 5-Hydroxyhinokitiol (**9**) and juniperone A (**10**) showed moderate inhibitory activities, with IC_{50} values of 51.7 and 62.5 μM, respectively, while quercetin (**7**) and 4,6-dihydroxy-2-methoxyacetophenone (**8**) displayed weak inhibitory activities. As SrtA inhibitors may act as anti-infectious agents and disrupt bacterial pathogenicity without impacting bacterial viability (Mazmanian et al., 2000), the MICs of the each of compounds were evaluated to identify possible effects on *S. mutans* aggregation, adhesion, and biofilm formation. As shown in Table 2.2, no compounds evaluated herein except compound **10** (MIC = 256.9 μM) inhibited *S. mutans* OMZ65 growth (all other MICs > 300 μM).

Table 2.2 Inhibitory effects of compounds 5–10 on the activity of SrtA

Enzyme and bacterial growth of *S. mutans* strain OMZ65.

Compound	SrtA IC_{50} (μM)	MIC (μM)*
5	16.1	>300
6	>300	>300
7	185.3	>300
8	151.4	>300
9	51.7	>300
10	62.5	256.9
Triphasiol	25.3	ND**
Ampicillin	ND	0.4

*MIC means minimum inhibitory concentration. ** ND means not determined. Triphasiol and ampicillin were used as a reference inhibitor of SrtA and standard of antibacterial drug, respectively.

Inhibitory effects of compound 5 on saliva-induced cell aggregation

As a combined bioactivity test, saliva-induced aggregation of *S. mutans* was furtherly examined the inhibitory effects of compound **5** (Figure 2.3). The saliva-induced aggregation assay was performed using *S. mutans* strain NG8 (WT) and isogenic *srtA*-knockout mutants. SrtA sequence alignment of NG8 (GenBank accession number: AF542085) showed that it is identical to SrtA of *S. mutans* OMZ65 over its entire length (data not shown). Aggregation levels were measured based on the decline of turbidity at 700 nm. As shown in Figure 2.3A, both the WT and *srtA*-complemented strains started to aggregate dramatically at 20 min and the relative turbidity decreased by 75% at 2 h. By contrast, the *srtA*-deletion mutant showed no aggregation and kept high turbidity. Interestingly, compound **5** markedly reduced the aggregation of NG8 cells in a dose-dependent manner (tested at 0×, 1×, 2× and 4× the SrtA IC_{50}) (Figure 2.3B).

Figure 2.3 Inhibitory effects of compound 5 on saliva-induced aggregation of *Streptococcus mutans* NG8.

Cells with approximate optical density of 1.0 at 700 nm were incubated at 37°C with human saliva for 2 h. **(A)** Saliva-induced aggregation of *S. mutans* NG8 (WT), *srtA*-deletion mutant (*ΔsrtA*), and *srtA*-complemented mutant (*ΔsrtA + srtA*). NG8-buffer refers to the aggregation assay performed with *S. mutans* NG8 in the absence of saliva. **(B)** *S. mutans* NG8 treated with compound **5**. The aggregation assay was performed with *S. mutans* NG8 in the presence of 16.1 μM (1× IC_{50}) 32.2 μM (2× IC_{50}) and 64.4 μM (4× IC_{50}) compound **5**. Each point indicates the mean ± standard deviation of three independent experiments. Results were compared using two-way analysis of variance with the post-hoc Dunnett's test. * $p < 0.05$, ** $p < 0.01$, and *** $p < 0.001$ versus controls.

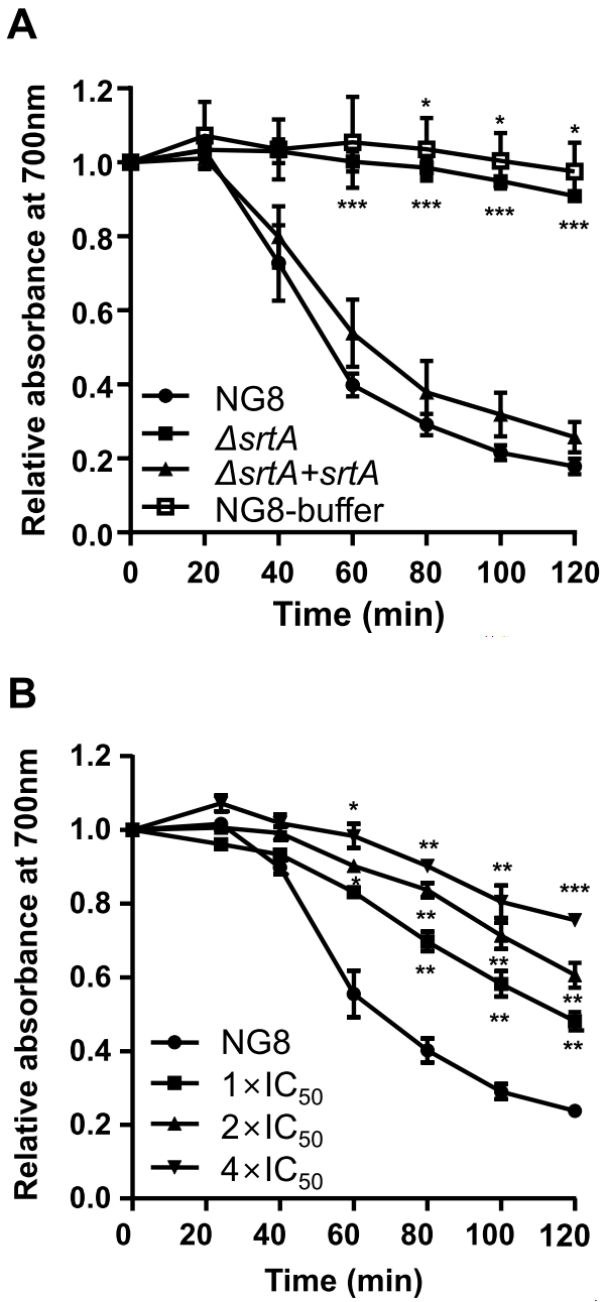
A
Relative absorbance at 700nm
1.2
1.0
0.8
0.6
0.4
0.2
0.0
0
20
40
60
80
100
120
Time (min)
NG8
ΔsrtA
ΔsrtA+srtA
NG8-buffer
B
Relative absorbance at 700nm
Time (min)
NG8
1×IC50
2×IC50
4×IC50

Inhibitory effects of compound 5 on bacterial adherence

In this study, the role of SrtA inhibitors in modulating cell-surface-related properties of *S. mutans* was investigated in terms of adherence. Because SrtA is essential to the display of surface proteins, including adhesins in *S. mutans*, inhibition of SrtA reduces adhesion capability and aggregation of the bacteria. The adherence assay was performed on s-HAs over a concentration range of 1–4 times the IC_{50} value of compound **5**. *S. mutans* NG8 and isogenic *srtA* mutants were attached to s-HAs during 90 min, and the resulting CFUs were counted. The adherence of *S. mutans* in the treatment with 1× IC_{50} (16.1 μM) of compound **5** was not significantly different from that of the control (NG8). However, in the treatment containing 4× the IC_{50} of compound **5** (64.4 μM), bacterial adherence was significantly reduced, showing a decrease of about 60% compared to the control group (Figure 2.4).

Figure 2.4 Inhibitory effects of compound 5 on *Streptococcus mutans* adherence to saliva-coated hydroxyapatite beads (s-HAs).

Attachment of *S. mutans* NG8, *srtA*-deletion mutant (*ΔsrtA*), and *srtA*-complemented mutant (*ΔsrtA+srtA*) was induced for 90 min at 37°C, followed by dispersal via sonication (50 W, 30 s) after three washes, and then colony-forming unit counting on Mitis-Salivarius agar (3.2 mg/mL bacitracin) after incubation for 48 h at 37°C. The concentration of compound **5** ranged from 1× the IC_{50} (16.1 μM) to 4× the IC_{50} (64.4 μM). Data are presented as the mean ± standard deviation of three independent experiments (* $p < 0.05$, ** $p < 0.01$, and *** $p < 0.001$ based on Student's *t*-test).

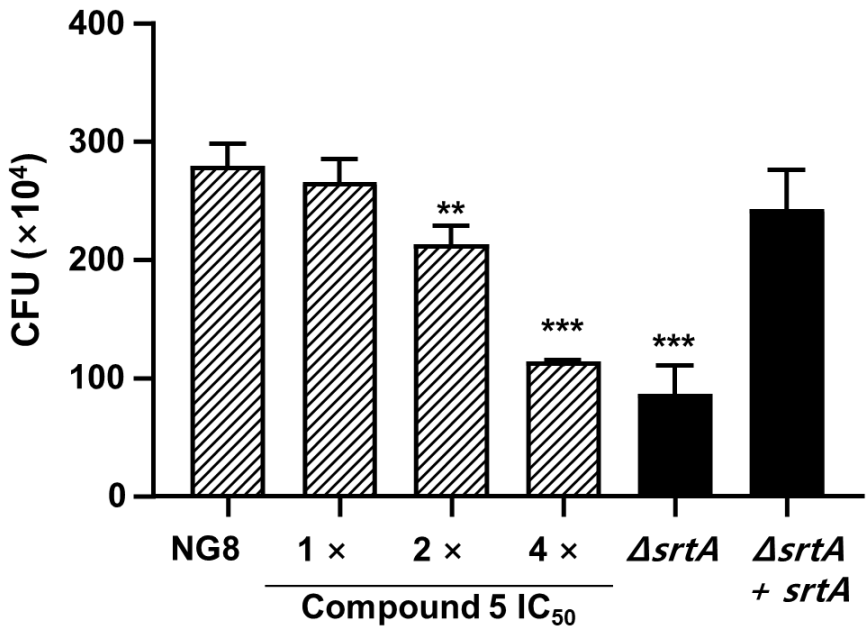
400
300
200
100
0
CFU (×10⁴)
**
***
***
NG8
1 ×
2 ×
4 ×
ΔsrtA
ΔsrtA
+ srtA
Compound 5 IC50

Inhibitory effects of compound 5 on biofilm formation

Bacterial adherence and aggregation are initial steps in the biofilm formation process (Scharnow et al., 2019). The disruption of biofilm formation of *S. mutans* could also be causedby interruption of SrtA enzyme activity (Lévesque et al., 2005). To investigate the effect of compound **5** on biofilm formation of *S. mutans*, the biomasses of biofilm produced by NG8 and *srtA* mutants formed over 24 h on 96-well plates and resin teeth were assessed through staining with 0.1% safranin. As shown in Figure 2.5A, *S. mutans* adhered to and aggregated on the surface of 96-well polystyrene plates, and biofilm formation was significantly reduced in the presence of compound **5** at a concentration of 4× the IC_{50} (64.4 μM), like the properties of the *srtA*-deletion mutant. The biofilm formation on the surface of resin teeth was also examined, and compound **5** successfully inhibited biofilm formation at concentrations higher than 32.2 μM (Figure 2.5B). The results of these analyses suggest that compound **5**, a small-molecule inhibitor of SrtA, has potential for application to prevent dental plaque.

Figure 2.5 Inhibition of *S. mutans* biofilm formation by compound 5.

Biofilm formation assays were performed using a polystyrene 96-well plate **(A)** and artificial resin teeth **(B)** at 37°C for 24 h. The concentration of compound **5** ranged from 1× the IC_{50} (16.1 μM) to 4× the IC_{50} (64.4 μM) and biomass of the biofilm was measured via 0.1% safranin staining. 0.1% NaF was used as a positive control. Data are presented as the mean ± SD of three independent experiments (* $p < 0.05$, ** $p < 0.01$, and *** $p < 0.001$ based on Student's *t*-test).

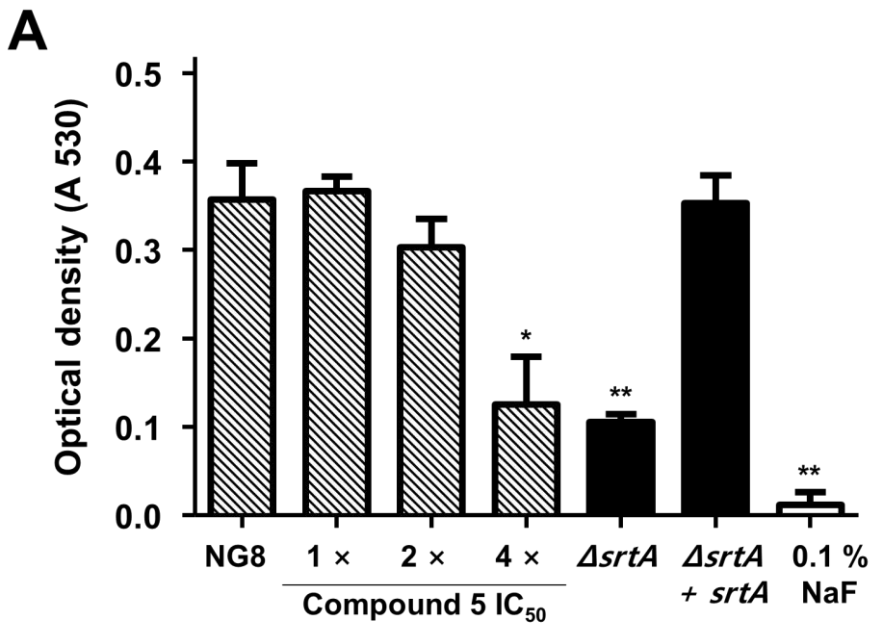
A
Optical density (A 530)
0.5
0.4
0.3
0.2
0.1
0.0
*
**
**
NG8
1 ×
2 ×
4 ×
ΔsrtA
ΔsrtA + srtA
0.1 % NaF
Compound 5 IC50

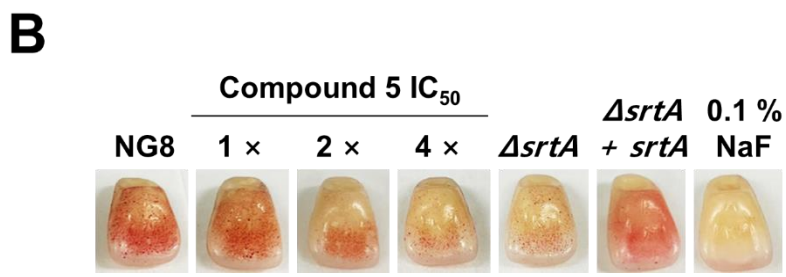
B
Compound 5 IC50
NG8
1 ×
2 ×
4 ×
ΔsrtA
ΔsrtA + srtA
0.1 % NaF

Discussion

SrtA is a membrane-associated transpeptidase that contributes to covalent attachment of numerous infection-associated surface proteins to host tissues (Hendrickx et al., 2011). Because this protein occurs widely in gram-positive pathogens, anti-infection therapies based on SrtA inhibitors may be broadly useful for preventing bacterial infections (Cossart and Jonquières, 2000). *S. mutans* uses SrtA as a tool attaching surface proteins to the peptidoglycan cell wall, thereby supporting development of a biofilm and attachment to the tooth surface (Loesche, 1986; Scharnow et al., 2019). In this study, to identify novel potential inhibitors of *S. mutans* SrtA, chemical assessment of *J. chinensis* was performed using crude extract, which markedly inhibited *S. mutans*-derived SrtA. Bioassay-guided fractionation of the extract using various chromatographic methods following combined spectroscopic analysis yielded six compounds (**5–10**) of various skeletal classes. The structure of compound **5** was designated as 3',3"-dihydroxy-(−)-matairesinol, representing a novel 2,3-dibenzyl-4-butanolide lignan. This compound displayed significant inhibitory activity against *S. mutans* derived-SrtA (IC_{50} = 16.1 μM) without affecting microbial viability, whereas compounds **7–10** displayed moderate to weak SrtA inhibition (Table 2.2). The results of subsequent bioassays with 3',3"-dihydroxy-(−)-matairesinol (**5**) indicated that its bioactivity is related to the inhibition of SrtA-mediated *S. mutans* aggregation, adhesion, and biofilm formation on solid surfaces by inhibiting SrtA activity. The magnitudes of inhibition of adherence and biofilm formation in *S. mutans* treated with compound **1** at 4× the SrtA IC_{50} are comparable to the behaviors of the untreated *srtA*-deletion mutant (Figures 2.4 and 2.5)

Early studies demonstrated that a few compounds from Chinese traditional medicine can inhibit *S. mutans* biofilm formation by inhibiting SrtA activity

(Güvenalp and Demirezer, 2005; Akiyama et al., 2007; Liu and Tu, 2013). For example, curcumin (Hu et al., 2013a; Hu et al., 2013b) and morin (Huang et al., 2014) show inhibitory activities against SrtA derived from *S. mutans* UA159 (IC_{50} = 10.2 μM and 27.2 μM, respectively) and interrupt biofilm formation by reducing the release of surface protein antigen I/II. Astillbin (Wang et al., 2019), a flavonoid compound isolated from *Rhizoma smilacis glabrae*, inhibits SrtA (from strain ATCC25175), with an IC_{50} of 7.5 μg/mL (16.7 μM), as well as biofilm formation. Some lignans have been reported as SrtA inhibitors against *S. mutans* OMZ65, with (−)-rosmarinic acid and caffeic acid having IC_{50} values of 20.1 μM and 20.2 μM, respectively (Lee et al., 2014). 3',3"-Dihydroxy-(−)-matairesinol (**5**), first reported in this study, showed inhibitory activity against *S. mutans* SrtA at a similar concentration (IC_{50} = 16.1 μM) to the substances described above, without inhibition of bacterial growth (Table 2.2, MIC > 300 μM).

The active form of the sortase enzyme is required for *S. mutans* attachment to solid surfaces and it has been verified as a virulence factor for caries (Lee and Boran, 2003; Lévesque et al., 2005). *S. mutans* mutant strains lacking functional sortase cannot adhere to solid surfaces. Inhibitors of SrtA might block SrtA-mediated protein anchoring, preventing the aggregation ability of *S. mutans* cells. Based on these findings, an assay in which saliva-induced cell aggregation was quantified through measurement of turbidity was conducted. The cell aggregation capacities of *S. mutans* strain NG8 (WT) and isogenic knockout mutants were investigated. As shown in Figure 2.3A, the cell aggregation capacity of the *srtA*-deletion mutant was markedly reduced relative to the WT strain. In addition, treatment of NG8 of 3',3"-dihydroxy-(−)-matairesinol (**5**) markedly reduced the aggregation capacity of the bacterial cells in a dose-dependent manner (Figure 2.3B). These assay data suggest that the active form of SrtA is important for controlling *S. mutans* cell aggregation ability.

S. mutans adheres to the oral surface via two mechanisms—sucrose-independent and sucrose-dependent (Krzyściak et al., 2014). Sucrose-independent adhesion is mainly mediated by antigens I/II (Munro et al., 1993; Jenkinson and Demuth, 1997; Love et al., 1997), while sucrose-dependent adhesion is mainly mediated by glucosyltransferases (Gtfs, including GtfB, GtfC, and GtfD) (Bramstedt, 1968), which also mediate interspecies coaggregation and play a critical role in the development and maturation of oral biofilms (Bowen and Koo, 2011; Kim et al., 2020). In addition, glucan-binding protein C (GbpC) is involved in both sucrose-dependent and sucrose-independent adherence and biofilm formation (Mieher et al., 2018). Antigens I/II and GbpC have been reported to harbor the LPXTG motif, the site of recognition and cleavage of SrtA (Igarashi et al., 2003; Igarashi et al., 2004). In this study, saliva-induced cell aggregation and adherence assays on s-HAs were performed without sucrose. When *S. mutans* was incubated with 4× the IC_{50} of compound **5**, cell aggregation (Figure 2.3) and adherence (Figure 2.4) were significantly repressed. By contrast, the inhibitory effects of compound **5** on *S. mutans* biofilm formation on the surface of 96-well polystyrene plates and resin teeth were assessed under sucrose-supplemented conditions. Interestingly, *S. mutans* biofilm formation on polystyrene dishes and resin teeth was also significantly reduced following treatment with compound **5** at a concentration of 4× the IC_{50} (Figure 2.5). These results indicate that SrtA can bind surface proteins containing the LPXTG motif and thus initiates both sucrose-dependent and sucrose-independent adherence and biofilm formation by *S. mutans*. In addition, compound **5** blocks *S. mutans* adhesion and biofilm formation by inhibiting SrtA without being affected by sucrose.

The results from this study suggest that small-molecule inhibitors of *S. mutans* SrtA can be useful prophylactic agents for the prevention of dental plaque. However, several issues have yet to be solved. The ability of compound **5** to inhibit

SrtA activity outside of *S. mutans* cells was demonstrated, but the exact effect *in vivo* remains unknown. Further study is required to clarify the relationship between the inhibition of SrtA activity and the reduction in *S. mutans* adhesion and biofilm formation and to identify the main cellular target of 3',3''-dihydroxy-(−)-matairesinol (**5**). In addition, for SrtA inhibitors to be realized as effective drugs, direct assessment of the inactivation of SrtA and attenuation of virulence in animal models must be demonstrated. Nevertheless, small-molecule inhibitors of SrtA represent a promising approach to the effective inhibition of *S. mutans* and will benefit the management of dental caries.

References

Ahn Sug-Joon, Ahn Sang-Joon, Wen ZT, Brady LJ and Burne RA (2008). Characteristics of biofilm formation by *Streptococcus mutans* in the presence of saliva. *Infect Immun* 76(9), 4259-4268.

Ajdić D, McShan WM, McLaughlin RE, Savić G, Chang J, Carson MB, Primeaux C, Tian R, Kenton S, Jia H, Lin S, Qian Y, Li S, Zhu H, Najar F, Lai H, White J, Roe BA and Ferretti JJ (2002). Genome sequence of *Streptococcus mutans* UA159, a cariogenic dental pathogen. *Proc Natl Acad Sci USA* 99(22), 14434-14439.

Akiyama K, Maruyama M, Yamauchi S, Nakashima Y, Nakato T, Tago R, Sugahara T, Kishida T and Koba Y (2007). Antimicrobiological activity of lignan: Effect of benzylic oxygen and stereochemistry of 2,3-dibenzyl-4-butanolide and 3,4-dibenzyltetrahydrofuran lignans on activity. *Biosci Biotechnol Biochem* 71(7), 1745-1751.

Balsa-Canto E, Henriques D, Gábor A and Banga JR (2016). AMIGO2, a toolbox for dynamic modeling, optimization and control in systems biology. *Bioinformatics* 32(21), 3357-3359.

Barceló F, Ortiz-Lombardía M, Martorell M, Oliver M, Méndez C, Salas JA and Portugal J (2010). DNA binding characteristics of mithramycin and chromomycin analogues obtained by combinatorial biosynthesis. *Biochemistry* 49(49), 10543-10552.

Basabe P, de Román M, Marcos IS, Diez D, Blanco A, Bodero O, Mollinedo F, Sierra BG and Urones JG (2010). Prenylflavonoids and prenyl/alkyl-phloroacetophenones: Synthesis and antitumour biological evaluation. *Eur J Med Chem* 45(9), 4258-4269.

Bérdy J (2012). Thoughts and facts about antibiotics: Where we are now and where we are heading. *J Antibiot (Tokyo)* 65(8), 385-395.

Bianchi N, Osti F, Rutigliano C, Corradini FG, Borsetti E, Tomassetti M, Mischiati C, Feriotto G and Gambari R (1999). The DNA-binding drugs mithramycin and chromomycin are powerful inducers of erythroid differentiation of human K562 cells. *Br J Haematol* 104(2), 258-265.

Bianchi N, Rutigliano C, Passadore M, Tomassetti M, Pippo L, Mischiati C, Feriotto G and Gambari R (1997). Targeting of the HIV-1 long terminal repeat with chromomycin potentiates the inhibitory effects of a triplex-forming oligonucleotide on Sp1-DNA interactions and in vitro transcription. *Biochem J* 326(Pt 3), 919-927.

Bowen WH and Koo H (2011). Biology of Streptococcus mutans-derived glucosyltransferases: Role in extracellular matrix formation of cariogenic biofilms. *Caries Res* 45(1), 69-86.

Bramstedt F (1968). Polysaccharide synthesis through plaque streptococci as an important factor in the etiology of caries. *Ddz* 22(11), 563-564 passim.

Brazhnikova MG, Krugliak EB, Kovsharova IN, Konstantinova NV and Proshliakova VV (1962). Isolation, purification and study on some physico-chemical properties of a new antibiotic olivomycin. *Antibiotiki* 7, 39-44.

But PPHK, T., Guo JX and Sung CK (1997). International Collation of Traditional and Folk Medicine. *World Scientific.* (2nd ed.), 16-17.

Carroll AR, Copp BR, Davis RA, Keyzers RA and Prinsep MR (2019). Marine natural products. *Nat Prod Rep* 36(1), 122-173.

Chakrabarti S, Bhattacharyya D and Dasgupta D (2000). Structural basis of DNA recognition by anticancer antibiotics, chromomycin A(3), and mithramycin: Roles of minor groove width and ligand flexibility. *Biopolymers* 56(2), 85-95.

Chatterjee S, Zaman K, Ryu H, Conforto A and Ratan RR (2001). Sequence-selective DNA

binding drugs mithramycin A and chromomycin A3 are potent inhibitors of neuronal apoptosis induced by oxidative stress and DNA damage in cortical neurons. *Ann Neurol* 49(3), 345-354.

Cho E, Kwon OS, Chung B, Lee J, Sun J, Shin J and Oh KB (2020). Antibacterial activity of chromomycins from a marine-derived *Streptomyces microflavus*. *Mar Drugs* 18(10), 522.

Cho H, Chung B, Kim CK, Oh DC, Oh KB and Shin J (2017). *Spatholobus suberectus* Dunn. constituents inhibit sortase A and *Staphylococcus aureus* cell clumping to fibrinogen. *Arch Pharm Res* 40(4), 518-523.

Clark C, Kosowska-Shick K, McGhee P, Dewasse B, Beachel L and Appelbaum PC (2009). Resistance selection studies comparing the activity of razupenem (PTZ601) to vancomycin and linezolid against eight methicillin-resistant and two methicillin-susceptible *Staphylococcus aureus* strains. *Antimicrob Agents Chemother* 53(7), 3118-3121.

CLSI (2017). *Reference Methods for Broth Dilution Antifungal Susceptibility Testing of Filamentous Fungi*, (3rd ed.). CLSI standard M38; Clinical and Laboratory Standards Institute, USA.

CLSI (2018) *Methods for Dilution Antimicrobial Susceptibility Tests for Bacteria That Grow Aerobically*, (11th ed.). CLSI standard M07; Clinical and Laboratory Standards Institute, USA.

CDC (2019). *Antibiotic resistance threats in the United States, 2019.* US Department of Health and Human Services, Centers for Disease Control and Prevention, USA

Corrie J, Green G, Ritchie E and Taylor W (1970). The chemical constituents of Australian *Zanthoxylum* species. V. The constituents of *Z. pluviatile* Hartley; the structures of two new lignans. *Aust J Chem* 23(1), 133-145.

Cossart P and Jonquières R (2000). Sortase, a universal target for therapeutic agents against gram-positive bacteria? *Proc Natl Acad Sci USA* 97(10), 5013-5015.

Dixon WT and Murphy D (1974). Electron spin resonance spectra of radicals derived from tropolones and benztropolones. *J Chem Soc Perk T 2*(12), 1430-1433.

Dramsi S, Trieu-Cuot P and Bierne H (2005). Sorting sortases: A nomenclature proposal for the various sortases of gram-positive bacteria. *Res Micobiol* 156(3), 289-297.

Fang JM, Chen YC, Wang BW and Cheng YS (1996). Terpenes from heartwood of *Juniperus chinensis*. *Phytochemistry* 41(5), 1361-1365.

Fang JM, Lee CK and Cheng YS (1992). Lignans from leaves of *Juniperus chinensis*. *Phytochemistry* 31(10), 3659-3661.

Fang JM, Lee CK and Cheng YS (1993). Diterpenes from leaves of *Juniperus chinensis*. *Phytochemistry* 33(5), 1169-1172.

Farrell DJ, Robbins M, Rhys-Williams W and Love WG (2011). Investigation of the potential for mutational resistance to XF-73, retapamulin, mupirocin, fusidic acid, daptomycin, and vancomycin in methicillin-resistant *Staphylococcus aureus* isolates during a 55-passage study. *Antimicrob Agents Chemother* 55(3), 1177-1181.

Ferrero L, Cameron B and Crouzet J (1995). Analysis of *gyrA* and *grlA* mutations in stepwise-selected ciprofloxacin-resistant mutants of *Staphylococcus aureus*. *Antimicrob Agents Chemother* 39(7), 1554-1558.

Forsyth RA, Haselbeck RJ, Ohlsen KL, Yamamoto RT, Xu H, Trawick JD, Wall D, Wang L, Brown-Driver V, Froelich JM, C KG, King P, McCarthy M, Malone C, Misiner B, Robbins D, Tan Z, Zhu Zy ZY, Carr G, Mosca DA, Zamudio C, Foulkes JG and Zyskind JW (2002). A genome-wide strategy for the identification of essential genes in *Staphylococcus aureus*. *Mol Microbiol* 43(6), 1387-1400.

Grundy WE, Goldstein AW, Rickher CJ, Hanes ME, Varren HB, Jr. and Sylvester JC (1953). Aureolic acid, a new antibiotic. I. Microbiologic studies. *Antibiot Chemother*

(Northfield) 3(12), 1215-1217.
Güvenalp Z and Demirezer LÖ (2005). Flavonol glycosides from *Asperula arvensis* L. *Turk J Chem* 29(2), 163-169.
Hendrickx AP, Budzik JM, Oh SY and Schneewind O (2011). Architects at the bacterial surface - sortases and the assembly of pili with isopeptide bonds. *Nat Rev Microbiol* 9(3), 166-176.
Holmes AH, Moore LS, Sundsfjord A, Steinbakk M, Regmi S, Karkey A, Guerin PJ and Piddock LJ (2016). Understanding the mechanisms and drivers of antimicrobial resistance. *Lancet* 387(10014), 176-187.
Hu P, Huang P and Chen MW (2013a). Curcumin reduces *Streptococcus mutans* biofilm formation by inhibiting sortase A activity. *Arch Oral Biol* 58(10), 1343-1348.
Hu P, Huang P and Chen WM (2013b). Curcumin inhibits the Sortase A activity of the *Streptococcus mutans* UA159. *Appl Biochem Biotechnol* 171(2), 396-402.
Hu Y, Espindola AP, Stewart NA, Wei S, Posner BA and MacMillan JB (2011). Chromomycin SA analogs from a marine-derived *Streptomyces* sp. *Bioorg Med Chem* 19(17), 5183-5189.
Huang P, Hu P, Zhou SY, Li Q and Chen WM (2014). Morin inhibits sortase A and subsequent biofilm formation in *Streptococcus mutans*. *Curr Microbiol* 68(1), 47-52.
Hutchings MI, Truman AW and Wilkinson B (2019). Antibiotics: Past, present and future. *Curr Opin Microbiol* 51, 72-80.
Igarashi T, Asaga E and Goto N (2003). The sortase of *Streptococcus mutans* mediates cell wall anchoring of a surface protein antigen. *Oral Microbiol Immunol* 18(4), 266-269.
Igarashi T, Asaga E, Sato Y and Goto N (2004). Inactivation of srtA gene of *Streptococcus mutans* inhibits dextran-dependent aggregation by glucan-binding protein C. *Oral Microbiol Immunol* 19(1), 57-60.
Imai T, Sato M, Takaku N, Kawai S, Ohashi H, Nomura M and Kushi M (2005). Characterization of physiological functions of sapwood IV: Formation and accumulation of lignans in sapwood of *Cryptomeria japonica* (L.f.) D. Don after felling. *Holzforschung* 59(4), 418-421.
Jayasuriya H, Lingham RB, Graham P, Quamina D, Herranz L, Genilloud O, Gagliardi M, Danzeisen R, Tomassini JE, Zink DL, Guan Z and Singh SB (2002). Durhamycin A, a potent inhibitor of HIV Tat transactivation. *J Nat Prod* 65(8), 1091-1095.
Jenkinson HF and Demuth DR (1997). Structure, function and immunogenicity of streptococcal antigen I/II polypeptides. *Mol Microbiol* 23(2), 183-190.
Jung HJ, Jung HA, Min BS and Choi JS (2015). Anticholinesterase and β-Site Amyloid Precursor Protein Cleaving Enzyme 1 Inhibitory Compounds from the Heartwood of *Juniperus chinensis*. *Chem Pharm Bull (Tokyo)* 63(11), 955-960.
Kamjam M, Sivalingam P, Deng Z and Hong K (2017). Deep sea actinomycetes and their secondary metabolites. *Front Microbiol* 8, 760.
Kanehisa M, Furumichi M, Tanabe M, Sato Y and Morishima K (2017). KEGG: New perspectives on genomes, pathways, diseases and drugs. *Nucleic Acids Res* 45(D1), D353-D361.
Kanehisa M and Goto S (2000). KEGG: Kyoto encyclopedia of genes and genomes. *Nucleic Acids Res* 28(1), 27-30.
Katayama Y, Ito T and Hiramatsu K (2000). A new class of genetic element, staphylococcus cassette chromosome *mec*, encodes methicillin resistance in *Staphylococcus aureus*. *Antimicrob Agents Chemother* 44(6), 1549-1555.
Katayama Y, Sekine M, Hishinuma T, Aiba Y and Hiramatsu K (2016). Complete reconstitution of the vancomycin-intermediate *Staphylococcus aureus* phenotype of strain Mu50 in vancomycin-susceptible *S. aureus*. *Antimicrob Agents Chemother* 60(6), 3730-3742.

Kim CY, Ahn MJ and Kim J (2006). A preparative isolation and purification of arctigenin and matairesinol from *Forsythia koreana* by centrifugal partition chromatography. *J Sep Sci* 29(5), 656-659.

Kim D, Barraza JP, Arthur RA, Hara A, Lewis K, Liu Y, Scisci EL, Hajishengallis E, Whiteley M and Koo H (2020). Spatial mapping of polymicrobial communities reveals a precise biogeography associated with human dental caries. *Proc Natl Acad Sci USA* 117(22), 12375-12386.

Kosowska-Shick K, Clark C, Pankuch GA, McGhee P, Dewasse B, Beachel L and Appelbaum PC (2009). Activity of telavancin against staphylococci and enterococci determined by MIC and resistance selection studies. *Antimicrob Agents Chemother* 53(10), 4217-4224.

Krzyściak W, Jurczak A, Kościelniak D, Bystrowska B and Skalniak A (2014). The virulence of *Streptococcus mutans* and the ability to form biofilms. *Eur J Clin Microbiol Infect Dis* 33(4), 499-515.

Kumar S, Stecher G, Li M, Knyaz C and Tamura K (2018). MEGA X: Molecular evolutionary genetics analysis across computing platforms. *Mol Biol Evol* 35(6), 1547-1549.

Kupferschmidt K (2016). Resistance fighters. *Science* 352(6287), 758-761.

Laxminarayan R (2014). Antibiotic effectiveness: Balancing conservation against innovation. *Science* 345(6202), 1299-1301.

Lee CH, Park JM, Song HY, Jeong EY and Lee HS (2009). Acaricidal activities of major constituents of essential oil of *Juniperus chinensis* leaves against house dust and stored food mites. *J Food Prot* 72(8), 1686-1691.

Lee CK, Fang JM and Cheng YS (1995). Norditerpenes from *Juniperus chinensis*. *Phytochemistry* 39(2), 391-394.

Lee DH, Seo BR, Kim HY, Gum GC, Yu HH, You HK, Kang TH and You YO (2011). Inhibitory effect of Aralia continentalis on the cariogenic properties of *Streptococcus mutans*. *J Ethnopharmacol* 137(2), 979-984.

Lee S, Song IH, Lee JH, Yang WY, Oh KB and Shin J (2014). Sortase A inhibitory metabolites from the roots of *Pulsatilla koreana*. *Bioorg Med Chem Lett* 24(1), 44-48.

Lee SF and Boran TL (2003). Roles of sortase in surface expression of the major protein adhesin P1, saliva-induced aggregation and adherence, and cariogenicity of *Streptococcus mutans*. *Infect Immun* 71(2), 676-681.

Lemos JA, Quivey RG, Koo H and Abranches J (2013). *Streptococcus mutans*: A new g ram-positive paradigm? *Microbiology (Reading)* 159(Pt 3), 436-445.

Lévesque CM, Voronejskaia E, Huang YC, Mair RW, Ellen RP and Cvitkovitch DG (2005). Involvement of sortase anchoring of cell wall proteins in biofilm formation by *Streptococcus mutans*. *Infect Immun* 73(6), 3773-3777.

Levy SB (1982). Microbial resistance to antibiotics. An evolving and persistent problem. *Lancet* 2(8289), 83-88.

Lim JP, Song YC, Kim JW, Ku CH, Eun JS, Leem KH and Kim DK (2002). Free radical scavengers from the heartwood of *Juniperus chinensis*. *Arch Pharm Res* 25(4), 449-452.

Liu Q and Tu P (2013). Chemical constituents from Qianliang tea. *J Chin Pharm Sci* 22(5), 427.

Loesche WJ (1986). Role of *Streptococcus mutans* in human dental decay. *Microbiol Rev* 50(4), 353-380.

Lombó F, Menéndez N, Salas JA and Méndez C (2006). The aureolic acid family of antitumor compounds: Structure, mode of action, biosynthesis, and novel derivatives. *Appl Microbiol Biotechnol* 73(1), 1-14.

Lopes LMX, Yoshida M and Gottlieb OR (1983). Dibenzylbutyrolactone lignans from *Virola sebifera*. *Phytochemistry* 22(6), 1516-1518.

Love RM, McMillan MD and Jenkinson HF (1997). Invasion of dentinal tubules by oral streptococci is associated with collagen recognition mediated by the antigen I/II family of polypeptides. *Infect Immun* 65(12), 5157-5164.

Magiorakos AP, Srinivasan A, Carey RB, Carmeli Y, Falagas ME, Giske CG, Harbarth S, Hindler JF, Kahlmeter G, Olsson-Liljequist B, Paterson DL, Rice LB, Stelling J, Struelens MJ, Vatopoulos A, Weber JT and Monnet DL (2012). Multidrug-resistant, extensively drug-resistant and pandrug-resistant bacteria: An international expert proposal for interim standard definitions for acquired resistance. *Clin Microbiol Infect* 18(3), 268-281.

Maura D, Ballok AE and Rahme LG (2016). Considerations and caveats in anti-virulence drug development. *Curr Opin Microbiol* 33, 41-46.

Mazmanian SK, Liu G, Jensen ER, Lenoy E and Schneewind O (2000). *Staphylococcus aureus* sortase mutants defective in the display of surface proteins and in the pathogenesis of animal infections. *Proc Natl Acad Sci* 97(10), 5510-5515.

Menéndez N, Nur-e-Alam M, Braña AF, Rohr J, Salas JA and Méndez C (2004). Biosynthesis of the antitumor chromomycin A3 in *Streptomyces griseus*: Analysis of the gene cluster and rational design of novel chromomycin analogs. *Chem Biol* 11(1), 21-32.

Mieher JL, Larson MR, Schormann N, Purushotham S, Wu R, Rajashankar KR, Wu H and Deivanayagam C (2018). Glucan binding protein C of *Streptococcus mutans* mediates both sucrose-independent and sucrose-dependent adherence. *Infect Immun* 86(7), e00146-00118.

Mir MA, Majee S, Das S and Dasgupta D (2003). Association of chromatin with anticancer antibiotics, mithramycin and chromomycin A3. *Bioorg Med Chem* 11(13), 2791-2801.

Miyamoto M, Kawamatsu Y, Kawashima K, Shinohara M, Tanaka K, Tatsuoka S and Nakanishi K (1967). Chromomycin A2, A3 and A4. *Tetrahedron* 23(1), 421-437.

Miyata M, Itoh K and Tachibana S (1998). Extractives of *Juniperus chinensis* L. I: Isolation of podophyllotoxin and yatein from the leaves of *J. chinensis*. *J wood sci* 44(5), 397-400.

Munro GH, Evans P, Todryk S, Buckett P, Kelly CG and Lehner T (1993). A protein fragment of streptococcal cell surface antigen I/II which prevents adhesion of *Streptococcus mutans*. *Infect Immun* 61(11), 4590-4598.

Murase H, Noguchi T and Sasaki S (2018). Evaluation of simultaneous binding of chromomycin A(3) to the multiple sites of DNA by the new restriction enzyme assay. *Bioorg Med Chem Lett* 28(10), 1832-1835.

Newman DJ and Cragg GM (2020). Natural products as sources of new drugs over the nearly four decades from 01/1981 to 09/2019. *J Nat Prod* 83(3), 770-803.

Ng EY, Trucksis M and Hooper DC (1996). Quinolone resistance mutations in topoisomerase IV: Relationship to the *flqA* locus and genetic evidence that topoisomerase IV is the primary target and DNA gyrase is the secondary target of fluoroquinolones in *Staphylococcus aureus*. *Antimicrob Agents Chemother* 40(8), 1881-1888.

Norio S EH, Takashi S, Mitsuko A and Kimiaki M (1976). Chromomycin Ap. JP 52102202.

Ogawa H, Yamashita Y, Katahira R, Chiba S, Iwasaki T, Ashizawa T and Nakano H (1998). UCH9, a new antitumor antibiotic produced by *Streptomyces*: I. Producing organism, fermentation, isolation and biological activities. *J Antibiot (Tokyo)* 51(3), 261-266.

Oh I, Yang WY, Chung SC, Kim TY, Oh KB and Shin J (2011). In vitro sortase A inhibitory and antimicrobial activity of flavonoids isolated from the roots of *Sophora flavescens*. *Arch Pharm Res* 34(2), 217-222.

Oh KB, Oh MN, Kim JG, Shin DS and Shin J (2006). Inhibition of sortase-mediated *Staphylococcus aureus* adhesion to fibronectin via fibronectin-binding protein by sortase inhibitors. *Appl Microbiol Biotechnol* 70(1), 102-106.

Ohashi H, Asai T and Kawai S (1994). Screening of main Japanese conifers for antifungal

leaf components, sesquiterpenes of *Juniperus chinensis* var. pyramidalis. *Holzforschung* 48, 193-198.

Otero LH, Rojas-Altuve A, Llarrull LI, Carrasco-López C, Kumarasiri M, Lastochkin E, Fishovitz J, Dawley M, Hesek D, Lee M, Johnson JW, Fisher JF, Chang M, Mobashery S and Hermoso JA (2013). How allosteric control of *Staphylococcus aureus* penicillin binding protein 2a enables methicillin resistance and physiological function. *Proc Natl Acad Sci USA* 110(42), 16808-16813.

Park BS, Kim JG, Kim MR, Lee SE, Takeoka GR, Oh KB and Kim JH (2005). *Curcuma longa* L. constituents inhibit sortase A and *Staphylococcus aureus* cell adhesion to fibronectin. *J Agric Food Chem* 53(23), 9005-9009.

Park JS, Chung B, Lee WH, Lee J, Suh Y, Oh DC, Oh KB and Shin J (2020). Sortase A-inhibitory coumarins from the folk medicinal plant *Poncirus trifoliata*. *J Nat Prod* 83(10), 3004-3011.

Park JS, Ko K, Kim SH, Lee JK, Park JS, Park K, Kim MR, Kang K, Oh DC, Kim SY, Yumnam S, Kwon HC and Shin J (2021). Tropolone-bearing sesquiterpenes from *Juniperus chinensis*: Structures, photochemistry and bioactivity. *J Nat Prod* 84(7), 2020-2027.

Park SA, Jegal J, Chung KW, Jung HJ, Noh SG, Chung HY, Ahn J, Kim J and Yang MH (2018). Isolation of tyrosinase and melanogenesis inhibitory flavonoids from *Juniperus chinensis* fruits. *Biosci Biotechnol Biochem* 82(12), 2041-2048.

Park W, Ahn CH, Cho H, Kim CK, Shin J and Oh KB (2017). Inhibitory effects of flavonoids from *Spatholobus suberectus* on sortase A and sortase A-sediated aggregation of *Streptococcus mutans*. *J Microbiol Biotechnol* 27(8), 1457-1460.

Petersen FC, Pecharki D and Scheie AA (2004). Biofilm mode of growth of *Streptococcus intermedius* favored by a competence-stimulating signaling peptide. *J Bacteriol* 186(18), 6327-6331.

Pettit GR, Tan R, Pettit RK, Doubek DL, Chapuis JC and Weber CA (2015). Antineoplastic agents 596. Isolation and structure of chromomycin A 5 from a Beaufort Sea microorganism. *RSC Adv* 5(12), 9116-9122.

Pinto F, Silveira E, Vasconcelos A, Florêncio K, Oliveira F, Del Bianco Sahm B, Costa-Lotufo L, Bauermeister A, Lopes N, Wilke D and Pessoa O (2019). Dextrorotatory chromomycins from the marine *Streptomyces* sp. associated to *Palythoa caribaeorum*. *J Braz Chem Soc* 31(1), 143-152.

Procópio RE, Silva IR, Martins MK, Azevedo JL and Araújo JM (2012). Antibiotics produced by *Streptomyces*. *Braz J Infect Dis* 16(5), 466-471.

Ramesh S and Mathivanan N (2009). Screening of marine actinomycetes isolated from the Bay of Bengal, India for antimicrobial activity and industrial enzymes. *World J Microbiol Biotechnol* 25(12), 2103-2111.

Rao KV, Cullen WP and Sobin BA (1962). A new antibiotic with antitumor properties. *Antibiot Chemother (Northfield)* 12, 182-186.

Rasko DA and Sperandio V (2010). Anti-virulence strategies to combat bacteria-mediated disease. *Nat Rev Drug Discov* 9(2), 117-128.

Remsing LL, Bahadori HR, Carbone GM, McGuffie EM, Catapano CV and Rohr J (2003). Inhibition of c-*src* transcription by mithramycin: Structure-activity relationships of biosynthetically produced mithramycin analogues using the c-src promoter as target. *Biochemistry* 42(27), 8313-8324.

Saitou N and Nei M (1987). The neighbor-joining method: A new method for reconstructing phylogenetic trees. *Mol Biol Evol* 4(4), 406-425.

Sato K, Okamura N, Utagawa K, Ito Y and Watanabe M (1960). Studies on the antitumor activity of chromomycin A3. *Sci Rep Res Inst Tohoku Univ Med* 9, 224-232.

Scharnow AM, Solinski AE and Wuest WM (2019). Targeting *S. mutans* biofilms: A

perspective on preventing dental caries. *Medchemcomm* 10(7), 1057-1067.
Sensi P, Greco AM and Pagani H (1958). Isolation and properties of a new antibiotic, L.A. 7017. *Antibiot Chemother (Northfield)* 8(5), 241-244.
Simon H, Wittig B and Zimmer C (1994). Effect of netropsin, distamycin A and chromomycin A3 on the binding and cleavage reaction of DNA gyrase. *FEBS Lett* 353(1), 79-83.
Stapleton PD and Taylor PW (2002). Methicillin resistance in *Staphylococcus aureus*: Mechanisms and modulation. *Sci Prog* 85(Pt 1), 57-72.
Subramani R and Aalbersberg W (2012). Marine actinomycetes: An ongoing source of novel bioactive metabolites. *Microbiol Res* 167(10), 571-580.
Toume K, Tsukahara K, Ito H, Arai MA and Ishibashi M (2014). Chromomycins A2 and A3 from marine actinomycetes with TRAIL resistance-overcoming and Wnt signal inhibitory activities. *Mar Drugs* 12(6), 3466-3476.
Trapnell C, Hendrickson DG, Sauvageau M, Goff L, Rinn JL and Pachter L (2013). Differential analysis of gene regulation at transcript resolution with RNA-seq. *Nat Biotechnol* 31(1), 46-53.
Trapnell C, Pachter L and Salzberg SL (2009). TopHat: Discovering splice junctions with RNA-Seq. *Bioinformatics* 25(9), 1105-1111.
Wang CM, Hsu YM, Jhan YL, Tsai SJ, Lin SX, Su CH and Chou CH (2015). Structure elucidation of procyanidins Isolated from *Rhododendron formosanum* and their anti-oxidative and anti-bacterial activities. *Molecules* 20(7), 12787-12803.
Wang J, Shi Y, Jing S, Dong H, Wang D and Wang T (2019). Astilbin inhibits the activity of sortase A from *Streptococcus mutans*. *Molecules* 24(3), 465.
Won TH, Song IH, Kim KH, Yang WY, Lee SK, Oh DC, Oh WK, Oh KB and Shin J (2015). Bioactive metabolites from the fruits of *Psoralea corylifolia*. *J Nat Prod* 78(4), 666-673.
Yang WY, Kim CK, Ahn CH, Kim H, Shin J and Oh KB (2016). Flavonoid glycosides inhibit sortase A and sortase A-mediated aggregation of *Streptococcus mutans*, an oral bacterium responsible for human dental caries. *J Microbiol Biotechnol* 26(9), 1566-1569.
Yang WY, Won TH, Ahn CH, Lee SH, Yang HC, Shin J and Oh KB (2015). *Streptococcus mutans* sortase A inhibitory metabolites from the flowers of *Sophora japonica*. *Bioorg Med Chem Lett* 25(7), 1394-1397.
Yoshimura Y, Koenuma M, Matsumoto K, Tori K and Terui Y (1988). NMR studies of chromomycins, olivomycins, and their derivatives. *J Antibiot (Tokyo)* 41(1), 53-67.
Zaman SB, Hussain MA, Nye R, Mehta V, Mamun KT and Hossain N (2017). A review on antibiotic resistance: Alarm bells are ringing. *Cureus* 9(6), e1403-e1403.
Zihlif M, Catchpoole DR, Stewart BW and Wakelin LP (2010). Effects of DNA minor groove binding agents on global gene expression. *Cancer Genom Proteom* 7(6), 323-330.

Supplementary Materials

Table S1. Differentially expressed genes of chromomycin-treated groups

ID	gene	DMSO	CHR	log_2 (FC)*	name
SAOUHSC_01017	purH	4351.02	94.1421	-5.53	bifunctional phosphoribosylaminoimidazolecarboxamide formyltransferase/IMP cyclohydrolase
SAOUHSC_01018	*purD*	4554.64	115.131	-5.31	phosphoribosylamine--glycine ligase
SAOUHSC_01016	*purN*	3827.15	107.842	-5.15	phosphoribosylglycinamide formyltransferase
SAOUHSC_01015	*purM*	5339.09	205.262	-4.70	phosphoribosylaminoimidazole synthetase
SAOUHSC_01171	*pyrF*	428.334	19.4489	-4.46	orotidine 5'-phosphate decarboxylase
SAOUHSC_01014	purF	5525.68	313.143	-4.14	amidophosphoribosyltransferase
SAOUHSC_01172	pyrE	288.734	16.4122	-4.14	orotate phosphoribosyltransferase
SAOUHSC_01170	carB	574.372	33.638	-4.09	carbamoyl phosphate synthase large subunit
SAOUHSC_01169	*carA*	621.144	47.3663	-3.71	carbamoyl phosphate synthase small subunit
SAOUHSC_01013	*purL*	4387.95	442.541	-3.31	phosphoribosylformylglycinamidine synthase II
SAOUHSC_01168	pyrC	627.258	63.9082	-3.29	dihydroorotase
SAOUHSC_00629	*mnhE*	233.582	26.6023	-3.13	monovalent cation/H+ antiporter subunit E
SAOUHSC_00632	*mnhG*	861.679	104.629	-3.04	monovalent cation/H+ antiporter subunit G
SAOUHSC_01166	pyrB	496.28	64.9617	-2.93	aspartate carbamoyltransferase catalytic subunit
SAOUHSC_00120	*capG*	46.1254	6.54837	-2.82	UDP-N-acetylglucosamine 2-epimerase
SAOUHSC_00124	*capK*	37.2421	5.42866	-2.78	capsular polysaccharide biosynthesis protein Cap5K
SAOUHSC_00628	*mnhD*	536.004	83.5362	-2.68	monovalent cation/H+ antiporter subunit D
SAOUHSC_00195	*fadA*	44.5387	7.1168	-2.65	acetyl-CoA acetyltransferase
SAOUHSC_00927	*oppA*	296.443	47.9116	-2.63	oligopeptide ABC transporter substrate-binding protein
SAOUHSC_00125	*capL*	46.3576	7.86414	-2.56	cap5L protein/glycosyltransferase
SAOUHSC_01012	*purQ*	4563.74	774.697	-2.56	phosphoribosylformylglycinamidine synthase I
SAOUHSC_00128	*capO*	68.5547	12.3174	-2.48	cap5O protein/UDP-N-acetyl-D-mannosaminuronic acid dehydrogenase
SAOUHSC_02541	*mobB*	180.472	32.7751	-2.46	molybdopterin-guanine dinucleotide biosynthesis protein MobB
SAOUHSC_02877	*crtN*	312.085	57.4296	-2.44	squalene synthase
SAOUHSC_00127	*capN*	62.5191	12.0201	-2.38	cap5N protein/UDP-glucose 4-epimerase
SAOUHSC_01011	*purS*	4886.25	945.946	-2.37	phosphoribosylformylglycinamidine synthase PurS
SAOUHSC_00119	*capF*	36.2761	7.14459	-2.34	capsular polysaccharide biosynthesis protein Cap8F
SAOUHSC_00170	*rlp*	38.4134	7.8758	-2.29	RGD-containing lipoprotein
SAOUHSC_01010	*purC*	1367.79	280.979	-2.28	phosphoribosylaminoimidazole-succinocarboxamide synthase
SAOUHSC_01165	*pyrP*	328.73	68.8351	-2.26	uracil permease
SAOUHSC_02988	*asp1*	20.1972	4.25075	-2.25	accessory Sec system protein Asp1
SAOUHSC_01950	*epiD*	9.65198	2.11276	-2.19	flavoprotein EpiD
SAOUHSC_00926	*oppF*	411.204	90.2654	-2.19	oligopeptide ABC transporter ATP-binding protein
SAOUHSC_02879	*crtM*	436.465	95.8768	-2.19	squalene desaturase
SAOUHSC_00626	*mnhB*	704.247	155.746	-2.18	monovalent cation/H+ antiporter subunit B
SAOUHSC_02542	*moeA*	222.684	49.9582	-2.16	molybdopterin biosynthesis protein MoeA
SAOUHSC_02986	*asp3*	18.2197	4.12153	-2.14	accessory Sec system protein Asp3
SAOUHSC_01009	*purK*	1347.48	308.385	-2.13	5-(carboxyamino)imidazole ribonucleotide synthase
SAOUHSC_02764	*cntD*	80.5152	18.7872	-2.10	peptide ABC transporter ATP-binding protein

SAOUHSC_00121	*capH*	39.7775	9.3562	-2.09	capsular polysaccharide biosynthesis protein O-acetyl transferase Cap5H
SAOUHSC_00627	*mnhC2*	561.646	132.422	-2.08	monovalent cation/H+ antiporter subunit C
SAOUHSC_00178	---	159.212	37.7659	-2.08	maltose ABC transporter permease
SAOUHSC_00798	*pgm*	897.214	213.638	-2.07	2,3-bisphosphoglycerate-independent phosphoglycerate mutase
SAOUHSC_02538	*moaD*	231.097	55.4725	-2.06	molybdopterin converting factor subunit 1
SAOUHSC_02763	*opp1F*	70.817	17.0051	-2.06	peptide ABC transporter ATP-binding protein
SAOUHSC_00126	*capM*	62.6575	15.1447	-2.05	capsular polysaccharide biosynthesis protein Cap8M
SAOUHSC_01400	*alr2*	57.493	13.9275	-2.05	alanine racemase
SAOUHSC_00118	*capE*	33.3821	8.11873	-2.04	capsular polysaccharide biosynthesis protein Cap5E
SAOUHSC_02987	*asp2*	22.6835	5.51982	-2.04	accessory Sec system protein Asp2
SAOUHSC_00905	*rexA*	228.443	56.0813	-2.03	ATP-dependent nuclease subunit A
SAOUHSC_00883	*mnhG*	1565.48	386.482	-2.02	monovalent cation/H+ antiporter subunit G
SAOUHSC_01008	*purE*	355.416	91.2217	-1.96	5-(carboxyamino)imidazole ribonucleotide mutase
SAOUHSC_00123	*capJ*	49.3869	12.7598	-1.95	capsular polysaccharide biosynthesis protein Cap5J
SAOUHSC_02284	*ilvC*	15.9087	4.14651	-1.94	ketol-acid reductoisomerase
SAOUHSC_02488	rpmJ	174375	45528.6	-1.94	50S ribosomal protein L36
SAOUHSC_00310	ulaA	149.539	39.4012	-1.92	PTS system ascorbate-specific transporter subunit IIC
SAOUHSC_02742	*opuCC*	192.465	52.8119	-1.87	amino acid transporter
SAOUHSC_00117	*capD*	47.7039	13.1208	-1.86	capsular polysaccharide biosynthesis protein Cap5D
SAOUHSC_00885	*mnhE*	1598.33	441.771	-1.86	monovalent cation/H+ antiporter subunit E
SAOUHSC_00320	---	115.732	32.2533	-1.84	NADPH-dependent FMN reductase
SAOUHSC_01611	*bmfBB*	480.784	135.307	-1.83	2-oxoisovalerate dehydrogenase, E2 component, dihydrolipoamide acetyltransferase
SAOUHSC_00797	tpiA	904.917	254.869	-1.83	triosephosphate isomerase
SAOUHSC_02403	*mtlD*	391.95	110.562	-1.83	mannitol-1-phosphate 5-dehydrogenase
SAOUHSC_02741	*opuCD*	319.009	92.0475	-1.79	amino acid ABC transporter permease
SAOUHSC_02983	*gtfB*	259.276	75.6157	-1.78	accessory Sec system glycosylation chaperone GtfB
SAOUHSC_01708	*pxpA*	236.776	69.4799	-1.77	LamB/YcsF family protein
SAOUHSC_00019	*purA*	336.394	100.124	-1.75	adenylosuccinate synthetase
SAOUHSC_00884	*mnhF*	700.247	210.144	-1.74	monovalent cation/H+ antiporter subunit F
SAOUHSC_02182	---	2.36621	0.723548	-1.71	tail length tape measure protein
SAOUHSC_02540	*moaE*	180.186	55.2974	-1.70	molybdopterin converting factor moa
SAOUHSC_02287	*leuC*	19.7088	6.13268	-1.68	isopropylmalate isomerase large subunit
SAOUHSC_02682	*nasF*	565.364	177.517	-1.67	uroporphyrin-III C-methyltransferase
SAOUHSC_02874	*copZ*	2006.26	630.866	-1.67	cation transporter E1-E2 family ATPase
SAOUHSC_00177	*malF*	147.947	46.5898	-1.67	maltose ABC transporter permease
SAOUHSC_00122	*capI*	40.8085	12.882	-1.66	capsular polysaccharide biosynthesis protein Cap5I
SAOUHSC_02285	*leuA*	18.5275	6.05298	-1.61	2-isopropylmalate synthase
SAOUHSC_02181	---	2.92649	0.959948	-1.61	phi PVL orfs 18-19-like protein
SAOUHSC_02683	*nasE*	448.186	148.26	-1.60	assimilatory nitrite reductase [NAD(P)H] small subunit
SAOUHSC_01709	*accC*	237.888	78.8044	-1.59	acetyl-CoA carboxylase biotin carboxylase
SAOUHSC_01205	*ftsY*	201.828	67.6506	-1.58	signal recognition particle-docking protein FtsY
SAOUHSC_02984	*gtfA*	313.159	105.425	-1.57	accessory Sec system glycosyltransferase GtfA

SAOUHSC_01206	---	188.625	63.695	-1.57	DNA-binding protein
SAOUHSC_02493	rpmD	4250.81	1435.75	-1.57	50S ribosomal protein L30
SAOUHSC_02606	*hutI*	161.718	54.8392	-1.56	imidazolonepropionase
SAOUHSC_00338	*metE*	41.1655	13.9994	-1.56	5-methyltetrahydropteroyltriglutamate--homocysteine S-methyltransferase
SAOUHSC_02536	*moaA*	442.245	150.733	-1.55	molybdenum cofactor biosynthesis protein A
SAOUHSC_01811	*dnaE*	274.02	93.5251	-1.55	DNA polymerase III subunit alpha superfamily protein
SAOUHSC_01397	*dapB*	59.8468	20.6204	-1.54	4-hydroxy-tetrahydrodipicolinate reductase
SAOUHSC_00147	*argB*	34.8037	12.1153	-1.52	acetylglutamate kinase
SAOUHSC_02849	*cidC*	714.993	249.891	-1.52	pyruvate oxidase
SAOUHSC_03051	gidB	199.885	71.0323	-1.49	16S rRNA methyltransferase GidB
SAOUHSC_00148	argJ	23.189	8.38297	-1.47	bifunctional ornithine acetyltransferase/N-acetylglutamate synthase
SAOUHSC_00129	*capP*	94.2432	34.3572	-1.46	UDP-N-acetylglucosamine 2-epimerase
SAOUHSC_00435	---	8.93919	3.26109	-1.45	glutamate synthase large subunit
SAOUHSC_02679	*narJ*	640.224	234.008	-1.45	respiratory nitrate reductase subunit delta
SAOUHSC_01612	*bfmBAB*	655.757	241.073	-1.44	2-oxoisovalerate dehydrogenase, E1 component subunit beta
SAOUHSC_02286	*leuB*	26.5562	9.78339	-1.44	3-isopropylmalate dehydrogenase
SAOUHSC_01749	queA	492.771	182.874	-1.43	S-adenosylmethionine:tRNA ribosyltransferase-isomerase
SAOUHSC_00699	*phrB*	251.63	93.5014	-1.43	deoxyribodipyrimidine photolyase
SAOUHSC_02122	*ligA*	263.884	98.4654	-1.42	NAD-dependent DNA ligase
SAOUHSC_02489	infA	4251.4	1589.59	-1.42	translation initiation factor IF-1
SAOUHSC_01398	*dapD*	97.8811	36.7065	-1.41	2,3,4,5-tetrahydropyridine-2,6-dicarboxylate N-acetyltransferase
SAOUHSC_00513	*yacO*	395.851	149.262	-1.41	23S rRNA (guanosine(2251)-2'-O)-methyltransferase RlmB
SAOUHSC_02743	*opuCB*	157.527	59.6111	-1.40	amino acid ABC transporter permease
SAOUHSC_02490	adk	2320.92	879.748	-1.40	adenylate kinase
SAOUHSC_02051	*rinA*	56.3593	21.4092	-1.40	int gene activator RinA
SAOUHSC_02487	rpsM	4012.69	1525.92	-1.39	30S ribosomal protein S13
SAOUHSC_00103	*phnE2*	18.7987	7.16322	-1.39	phosphonates ABC transporter permease
SAOUHSC_03012	---	4.14858	1.60331	-1.37	histidinol-phosphate aminotransferase
SAOUHSC_00860	---	241.823	93.4747	-1.37	5-nucleotidase family protein
SAOUHSC_00886	*mnhD*	1086.44	423.122	-1.36	monovalent cation/H+ antiporter subunit D
SAOUHSC_02989	secY	19.5709	7.65544	-1.35	accessory Sec system protein translocase subunit SecY2
SAOUHSC_00625	*mnhA*	544.581	216.018	-1.33	monovalent cation/H+ antiporter subunit A
SAOUHSC_02765	*cnzC*	73.4629	29.2009	-1.33	nickel ABC transporter permease
SAOUHSC_02932	*betA*	21.75	8.64695	-1.33	choline dehydrogenase
SAOUHSC_02340	atpC	9623.81	3826.5	-1.33	F0F1 ATP synthase subunit epsilon
SAOUHSC_01369	trpC	8.14894	3.25505	-1.32	indole-3-glycerol-phosphate synthase
SAOUHSC_01396	*dapA*	63.0426	25.2703	-1.32	4-hydroxy-tetrahydrodipicolinate synthase
SAOUHSC_02485	*rpoA*	1626.38	661.38	-1.30	DNA-directed RNA polymerase subunit alpha
SAOUHSC_02537	mobA	289.573	117.889	-1.30	molybdopterin-guanine dinucleotide biosynthesis protein MobA
SAOUHSC_01089	*isdG*	100.889	41.6509	-1.28	heme-degrading monooxygenase IsdG
SAOUHSC_00116	*capC*	63.6363	26.4534	-1.27	capsular polysaccharide biosynthesis protein Cap8C

SAOUHSC_02942	*nrdD*	71.3382	29.8046	-1.26	anaerobic ribonucleoside triphosphate reductase
SAOUHSC_01766	*folC*	498.034	210.247	-1.24	folylpolyglutamate synthase/dihydrofolate synthase
SAOUHSC_02305	*alr*	480.385	203.129	-1.24	alanine racemase
SAOUHSC_02315	*kdpE*	50.2043	21.2457	-1.24	DNA-binding response regulator
SAOUHSC_01274	*glpP*	166.978	70.8285	-1.24	glycerol uptake operon antiterminator regulatory protein
SAOUHSC_00780	uvrA	301.855	129.096	-1.23	excinuclease ABC subunit A
SAOUHSC_00287	---	684.09	293.379	-1.22	ABC transporter ATP-binding protein
SAOUHSC_02053	---	239.014	102.969	-1.21	transcriptional activator rinb-like protein
SAOUHSC_02873	*cop*	132.092	57.2962	-1.21	cation transporter E1-E2 family ATPase
SAOUHSC_02486	*rpsK*	3148.53	1368.13	-1.20	30S ribosomal protein S11
SAOUHSC_00436	gltD	14.312	6.22605	-1.20	glutamate synthase subunit beta
SAOUHSC_02744	*opuCA*	101.524	44.3294	-1.20	amino acid ABC transporter ATP-binding protein
SAOUHSC_02341	*atpD*	6341.64	2771.18	-1.19	F0F1 ATP synthase subunit beta
SAOUHSC_00188	*pflA*	1577.08	690.761	-1.19	pyruvate formate-lyase 1 activating enzyme
SAOUHSC_00291	---	31.4601	13.8076	-1.19	PfkB family carbohydrate kinase
SAOUHSC_01951	*rinA*	12.0523	5.30212	-1.18	epidermin biosynthesis protein EpiC
SAOUHSC_00171	ggt	73.7736	32.479	-1.18	gamma-glutamyltranspeptidase
SAOUHSC_02402	*mtlA*	314.438	138.72	-1.18	PTS system mannitol-specific transporter subunit IIA
SAOUHSC_02343	*atpG*	4185.87	1847.75	-1.18	F0F1 ATP synthase subunit gamma
SAOUHSC_02484	rplQ	3089.89	1375.44	-1.17	50S ribosomal protein L17
SAOUHSC_02875	---	289.944	129.068	-1.17	D-lactate dehydrogenase
SAOUHSC_02306	acpS	438.424	195.599	-1.16	4'-phosphopantetheinyl transferase
SAOUHSC_00239	*rbsK*	56.8023	25.6125	-1.15	ribokinase
SAOUHSC_03008	*hisF*	12.1335	5.47327	-1.15	multifunctional imidazole glycerol phosphate synthase subunit/phosphoribosyl-AMP cyclo-hydrolase/phosphoribosyl-ATP pyrophosphatase
SAOUHSC_01273	mutL	101.659	46.2291	-1.14	DNA mismatch repair protein
SAOUHSC_03009	*hisA*	13.2627	6.1058	-1.12	1-(5-phosphoribosyl)-5-[(5-phosphoribosylamino)methylidene-zamino] imidazole-4-carboxamide isomerase
SAOUHSC_02491	secY	3187.04	1472.9	-1.11	preprotein translocase subunit SecY
SAOUHSC_00340	*metC*	16.3153	7.57104	-1.11	trans-sulfuration enzyme family protein
SAOUHSC_02496	rplF	1852.94	861.853	-1.10	50S ribosomal protein L6
SAOUHSC_01385	*pstB*	8.28282	3.86244	-1.10	phosphate transporter ATP-binding protein
SAOUHSC_02328	thiE	241.861	112.982	-1.10	thiamine-phosphate pyrophosphorylase
SAOUHSC_02544	*moaB*	120.318	56.2123	-1.10	molybdopterin precursor biosynthesis MoaB
SAOUHSC_01322	*thrB*	104.426	48.814	-1.10	homoserine kinase
SAOUHSC_02352	*mnaA*	2211.82	1039.55	-1.09	UDP-GlcNAc 2-epimerase
SAOUHSC_01932	*hsdS*	68.847	32.5382	-1.08	type I restriction-modification system subunit S
SAOUHSC_01613	*bfmBAA*	513.664	243.308	-1.08	2-oxoisovalerate dehydrogenase, E1 component subunit alpha
SAOUHSC_00169	---	48.7755	23.123	-1.08	peptide ABC transporter permease
SAOUHSC_00887	*mnhC*	2051.65	976.883	-1.07	monovalent cation/H+ antiporter subunit C
SAOUHSC_00339	*metF*	23.2634	11.0818	-1.07	bifunctional homocysteine S-methyltransferase /5,10-methylenetetrahydrofolate reductase
SAOUHSC_00464	ksgA	160.807	76.6337	-1.07	dimethyladenosine transferase
SAOUHSC_02495	rplR	2666.9	1272.25	-1.07	50S ribosomal protein L18

SAOUHSC_01472	*dinG*	176.63	85.0005	-1.06	DnaQ family exonuclease/DinG family helicase
SAOUHSC_02678	*narI*	618.24	298.127	-1.05	respiratory nitrate reductase subunit gamma
SAOUHSC_00176	*malE*	46.5867	22.4937	-1.05	extracellular solute-binding protein
SAOUHSC_02329	*thiM*	313.003	151.221	-1.05	hydroxyethylthiazole kinase
SAOUHSC_02452	*lacD*	9.5276	4.60719	-1.05	tagatose 1,6-diphosphate aldolase
SAOUHSC_00888	*mnhB*	1073.61	520.092	-1.05	monovalent cation/H+ antiporter subunit B
SAOUHSC_01710	*accB*	115.471	56.0262	-1.04	acetyl-CoA carboxylase biotin carboxyl carrier protein subunit
SAOUHSC_02976	*pmi manA*	169.209	82.5581	-1.04	mannose-6-phosphate isomerase
SAOUHSC_00102	*phnE1*	27.1109	13.2682	-1.03	phosphonates ABC transporter permease
SAOUHSC_02864	*feoB*	67.4949	33.1443	-1.03	ferrous iron transport protein B
SAOUHSC_00104	*phnC*	21.7816	10.7075	-1.02	amino acid ABC transporter ATP-binding protein
SAOUHSC_00804	smpB	654.025	321.618	-1.02	SsrA-binding protein
SAOUHSC_01148	*ftsQ*	323.092	159.131	-1.02	cell division protein
SAOUHSC_01099	*mutS2*	147.968	73.0908	-1.02	recombination and DNA strand exchange inhibitor protein
SAOUHSC_03052	*gidA*	131.244	65.2362	-1.01	tRNA uridine 5-carboxymethylaminomethyl modification protein GidA
SAOUHSC_00624	---	687.469	342.34	-1.01	integrase/recombinase
SAOUHSC_02680	*narH*	518.412	258.947	-1.00	nitrate reductase subunit beta
SAOUHSC_02400	*mtlF*	47.2945	23.6427	-1.00	PTS system mannitol-specific protein
SAOUHSC_00317	*glpT*	752.074	1504.93	1.00	glycerol-3-phosphate transporter
SAOUHSC_02108	*ftnA*	713.055	1448.11	1.02	ferritin
SAOUHSC_00324	---	89.8528	187.028	1.06	50S ribosomal protein L7 serine acetyltransferase
SAOUHSC_03045	*cspB*	75333.1	157975	1.07	cold shock protein
SAOUHSC_00524	rpoB	2366.63	5012.78	1.08	DNA-directed RNA polymerase subunit beta
SAOUHSC_01201	acpP	10790.9	23283.1	1.11	acyl carrier protein
SAOUHSC_00069	*spa*	3448.78	7576.8	1.14	protein A
SAOUHSC_01079	*isdB*	42.5294	93.668	1.14	neurofilament protein
SAOUHSC_01362	dmpI	500.87	1123.38	1.17	4-oxalocrotonate tautomerase
SAOUHSC_02803	*fnbA*	117.399	274.954	1.23	fibronectin-binding protein
SAOUHSC_00192	*coa*	84.7677	202.807	1.26	staphylocoagulase
SAOUHSC_02802	*fnbB*	164.607	398.993	1.28	fibronectin binding protein B
SAOUHSC_01651	rpmG	14145.4	34805.2	1.30	50S ribosomal protein L33
SAOUHSC_00818	*nuc*	1085.28	2727.88	1.33	thermonuclease
SAOUHSC_02171	*sak*	260.495	661.661	1.34	staphylokinase
SAOUHSC_01570	---	554.397	1447.05	1.38	PVL orf 37-like protein
SAOUHSC_02170	---	1707.99	4587.53	1.43	peptidoglycan hydrolase
SAOUHSC_02173	*ami*	11.6847	34.8526	1.58	amidase
SAOUHSC_01953	*epiA*	144.865	508.125	1.81	gallidermin superfamily epiA protein

* $\log_2$(fold_change)

** Hypothetical proteins were excluded.

Table S2. Significantly related KEGG pathways of DEGs.

ID	KEGG pathway	DEG count
sao01100	Metabolic pathways	88
sao01110	Biosynthesis of secondary metabolites	45
sao01230	Biosynthesis of amino acids	21
sao01120	Microbial metabolism in diverse environments	18
sao01240	Biosynthesis of cofactors	17
sao02010	ABC transporters	16
sao00230	Purine metabolism	14
sao02024	Quorum sensing	11
sao02020	Two-component system	9
sao00541	O-Antigen nucleotide sugar biosynthesis	8
sao01250	Biosynthesis of nucleotide sugars	8
sao00250	Alanine, aspartate and glutamate metabolism	8
sao03010	Ribosome	8
sao00240	Pyrimidine metabolism	7
sao01210	2-Oxocarboxylic acid metabolism	6
sao00790	Folate biosynthesis	6
sao00520	Amino sugar and nucleotide sugar metabolism	5
sao00910	Nitrogen metabolism	5
sao00051	Fructose and mannose metabolism	5
sao00620	Pyruvate metabolism	5
sao00640	Propanoate metabolism	5

Figure S1. The ^{1}H NMR (400 MHz, chloroform-*d*) spectrum of 1

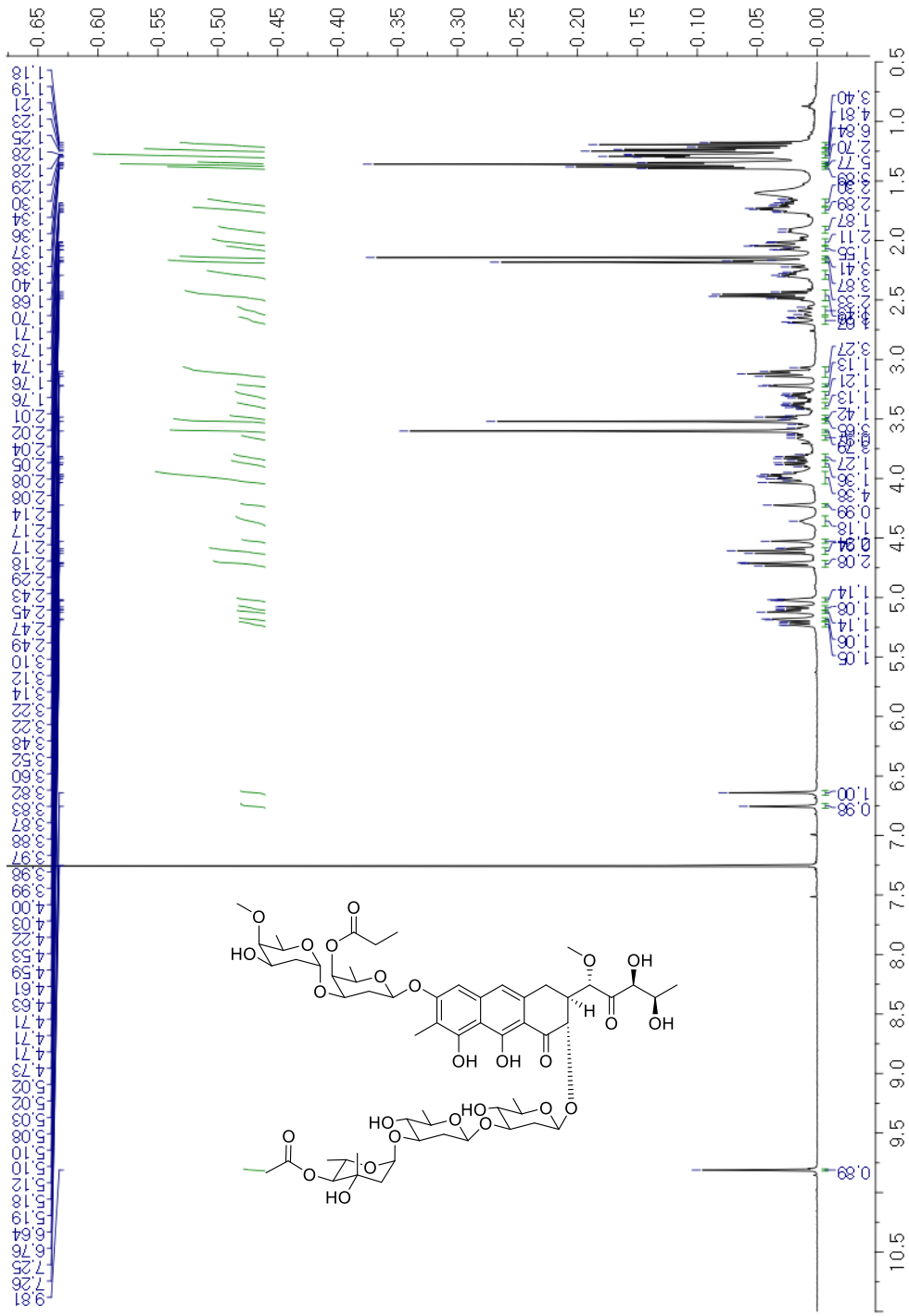

Figure S2. The ^{13}C NMR (100 MHz, chloroform-*d*) spectrum of 1

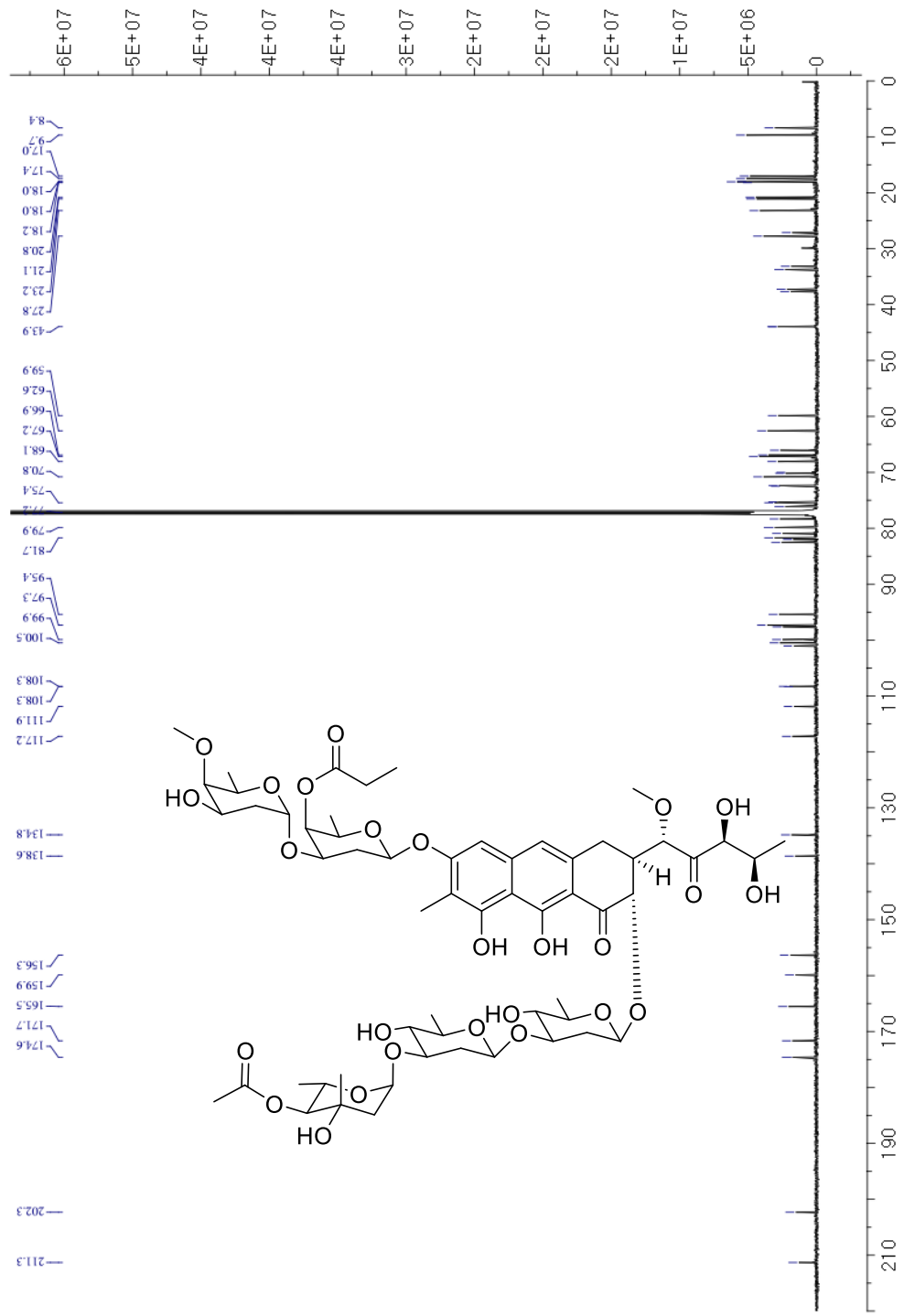

Figure S3. The COSY (400 MHz, $CDCl_3$) spectrum of 1

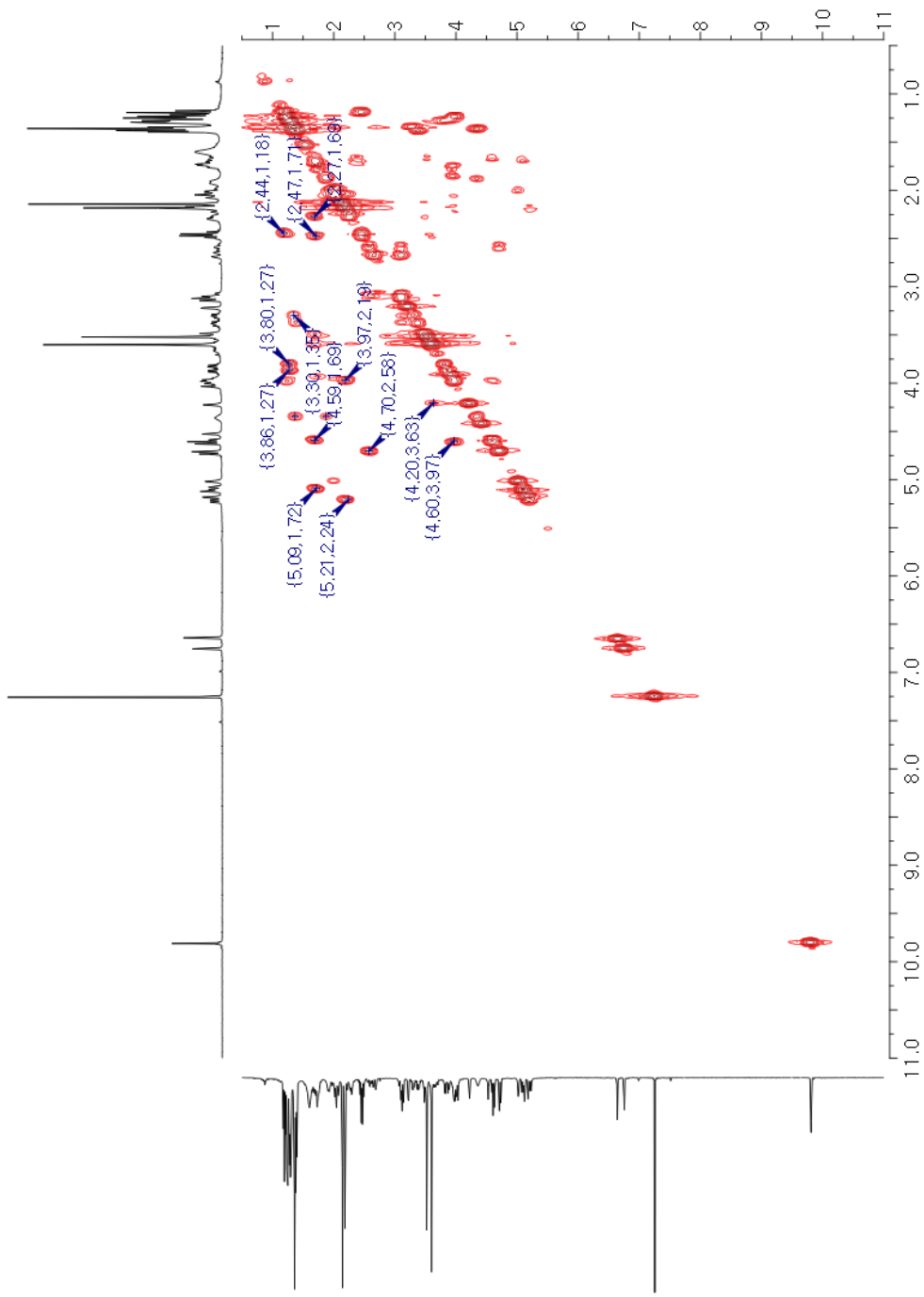

Figure S4. The TOCSY (400 MHz, $CDCl_3$) spectrum of 1

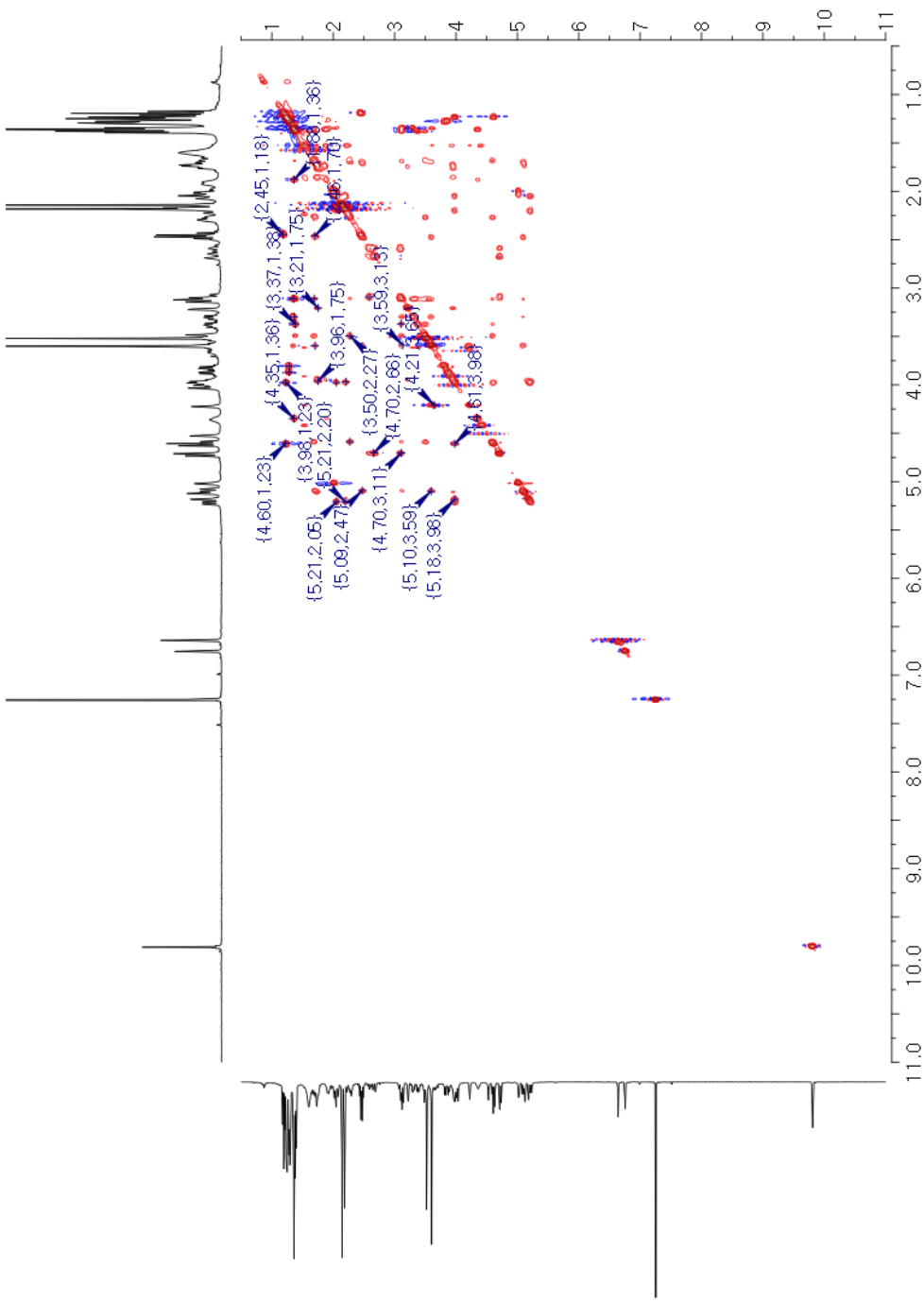

Figure S5. The eHSQC (400 MHz, chloroform-*d*) spectrum of 1

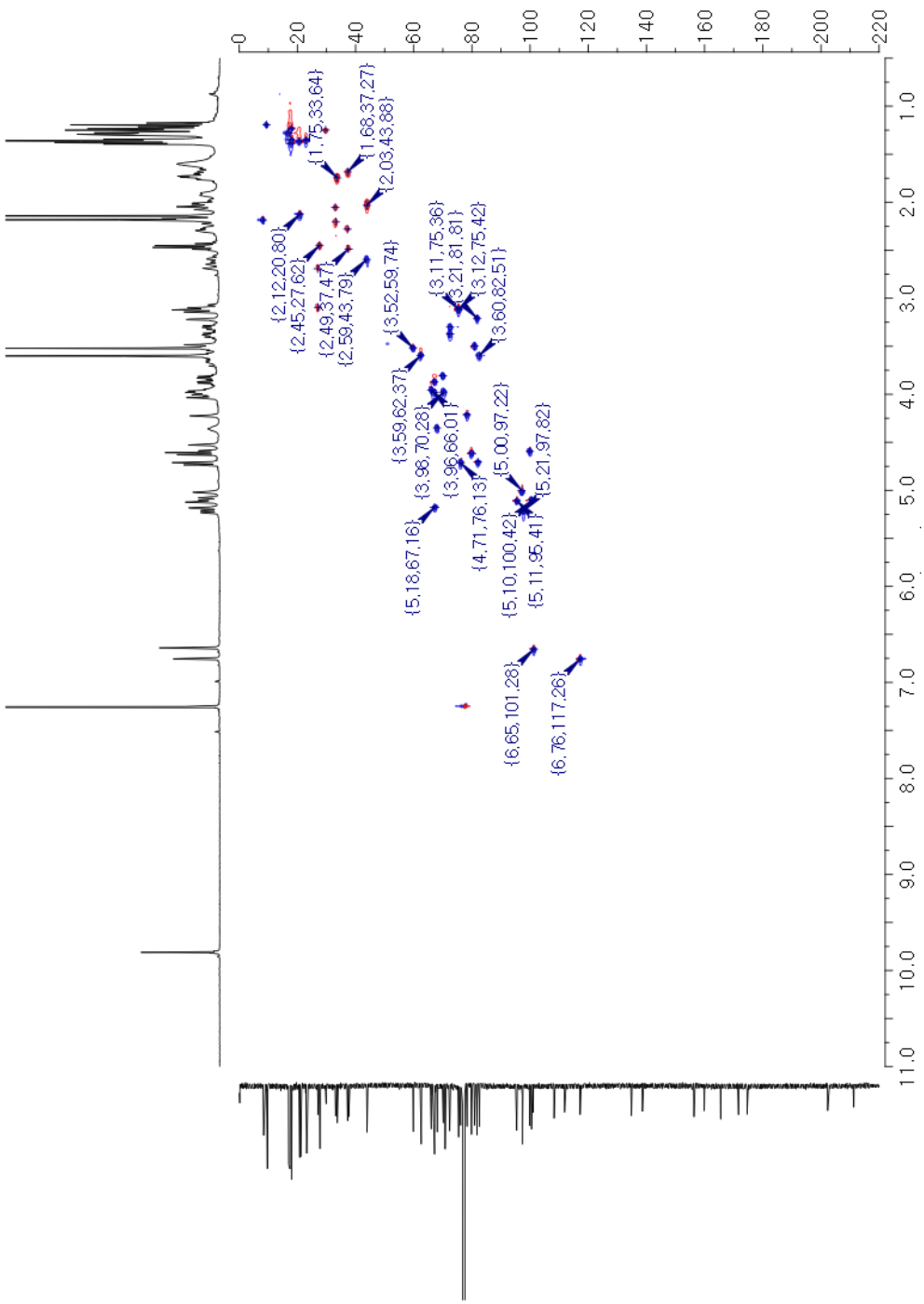

Figure S6. The HMBC (400 MHz, chloroform-*d*) spectrum of 1

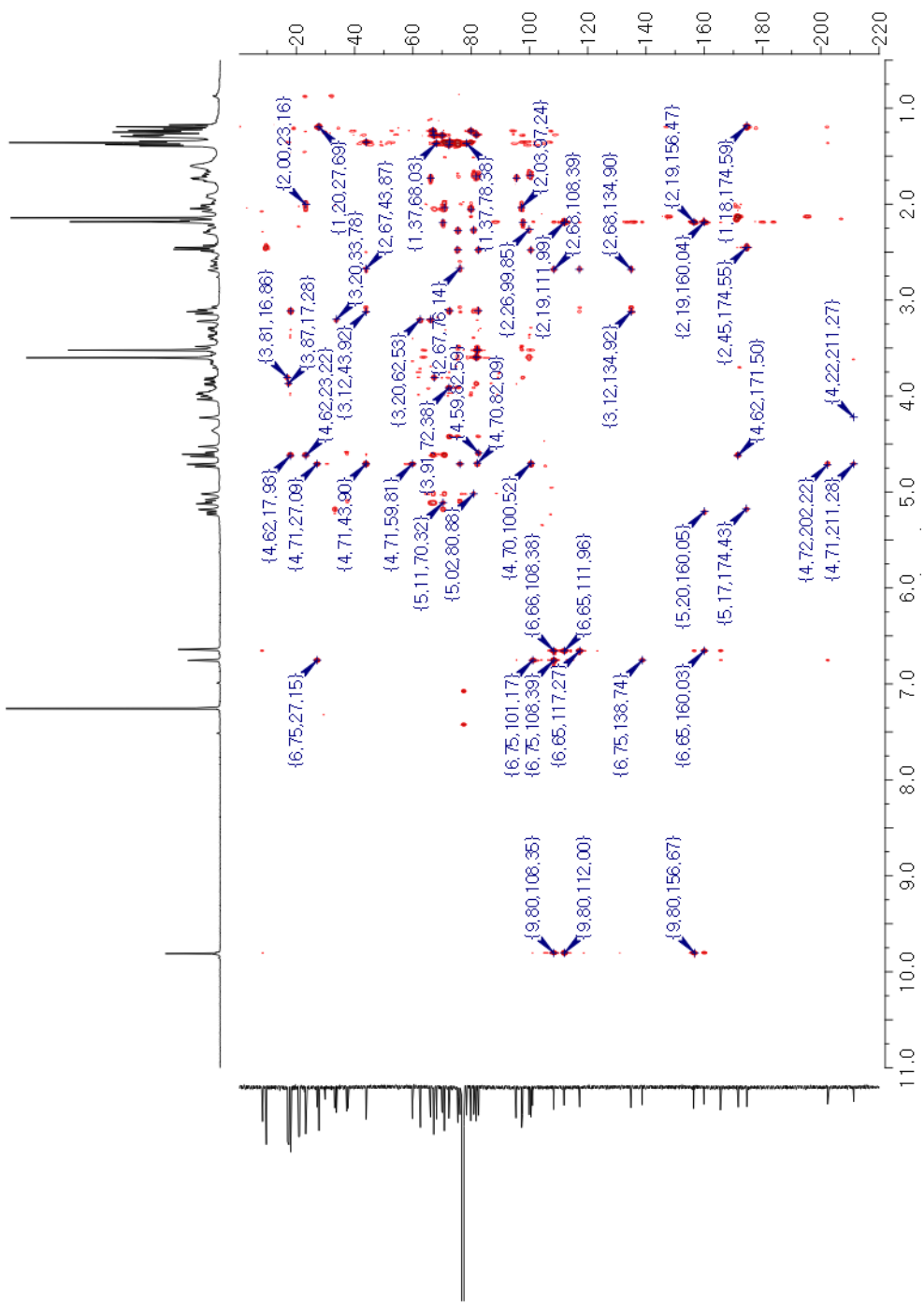

Figure S7. The ^{1}H NMR spectrum of 3',3''-dihydroxy-(-)-matairesinol (5) (600 MHz, DMSO-d_6)

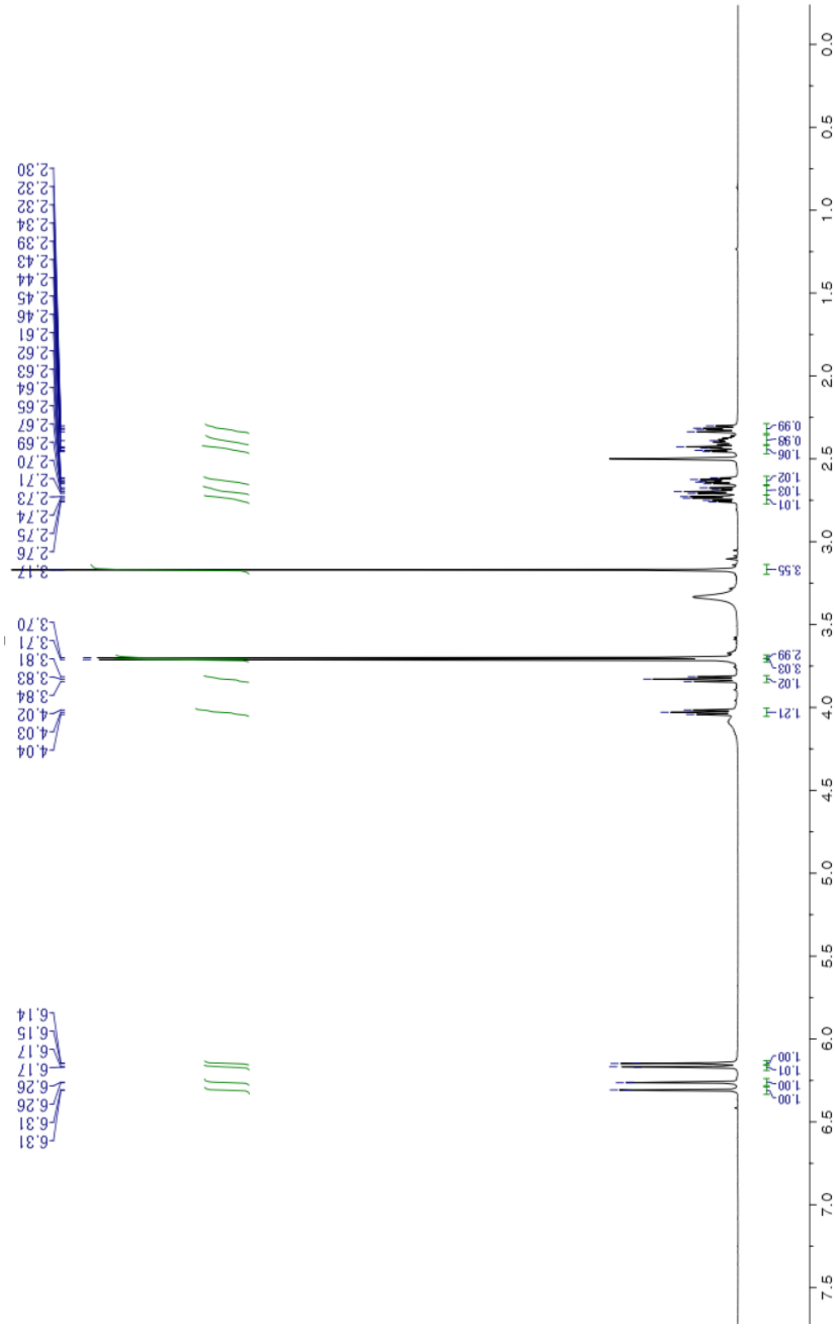

Figure S8. The ^{13}C NMR spectrum of 3',3''-dihydroxy-(-)-matairesinol (5) (150 MHz, DMSO-d_6)

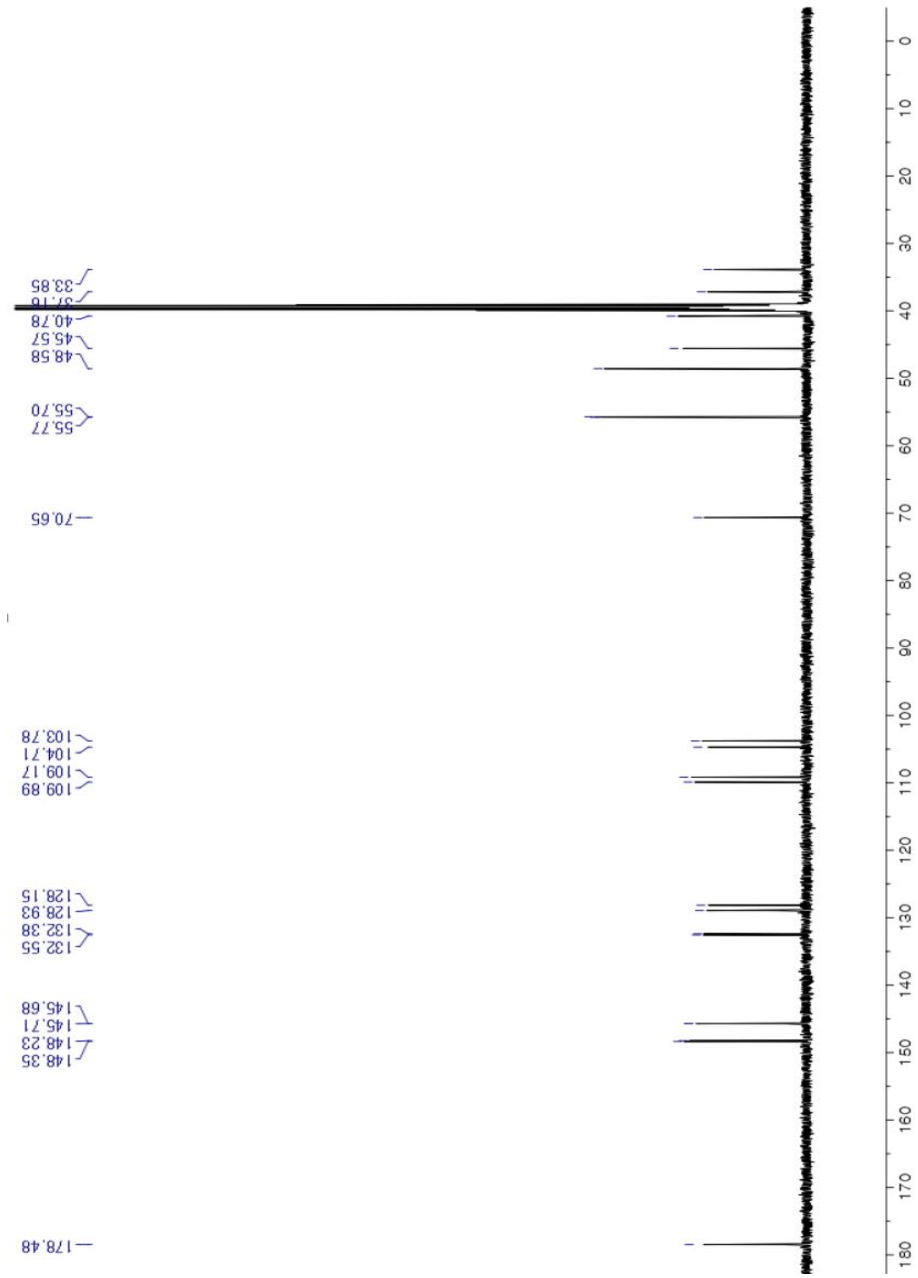

Figure S9. The HSQC spectrum of 3',3''-dihydroxy-(-)-matairesinol (5) (600 MHz, DMSO-d_6)

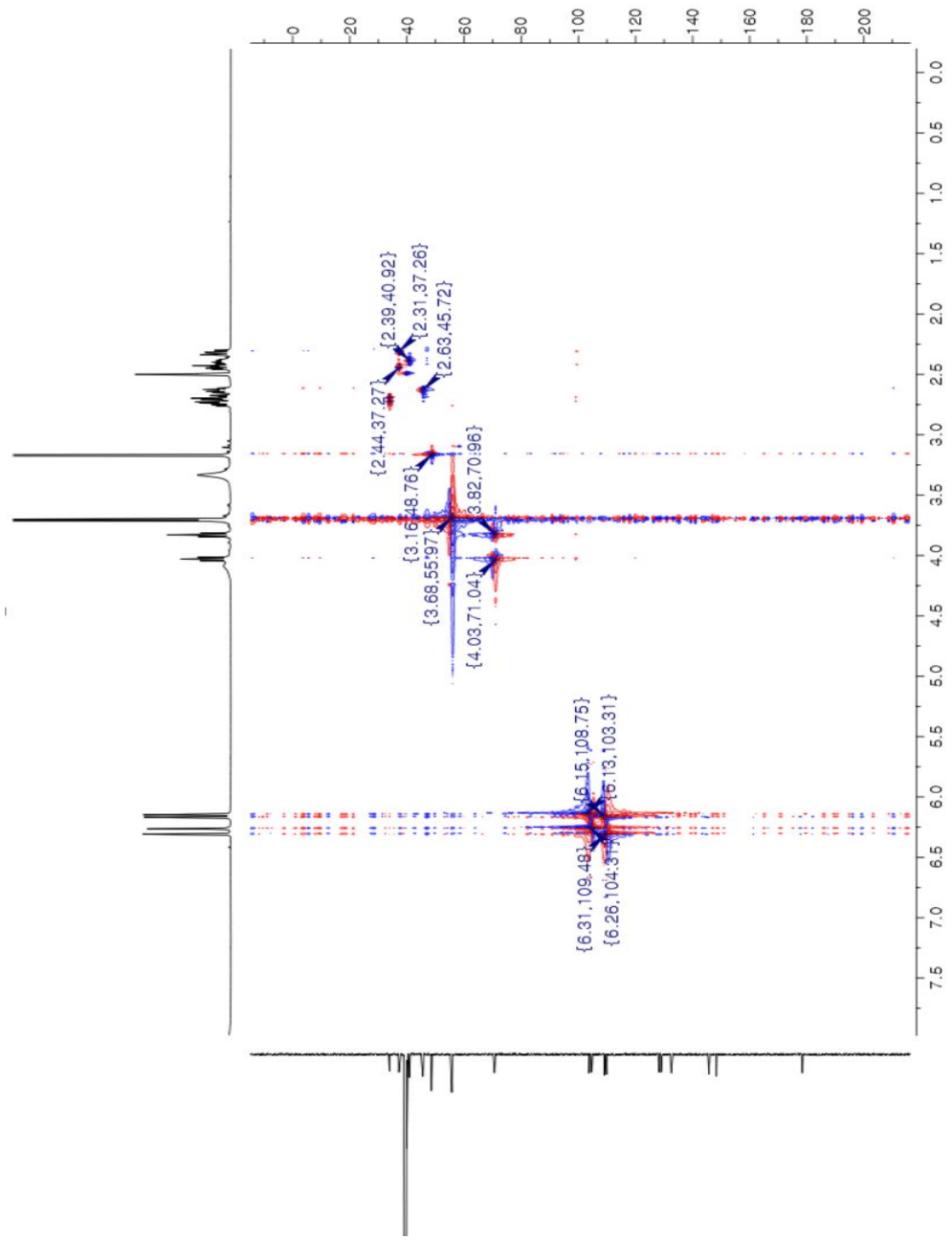

Figure S10. The COSY spectrum of 3',3''-dihydroxy-(-)-matairesinol (5) (600 MHz, DMSO-d_6)

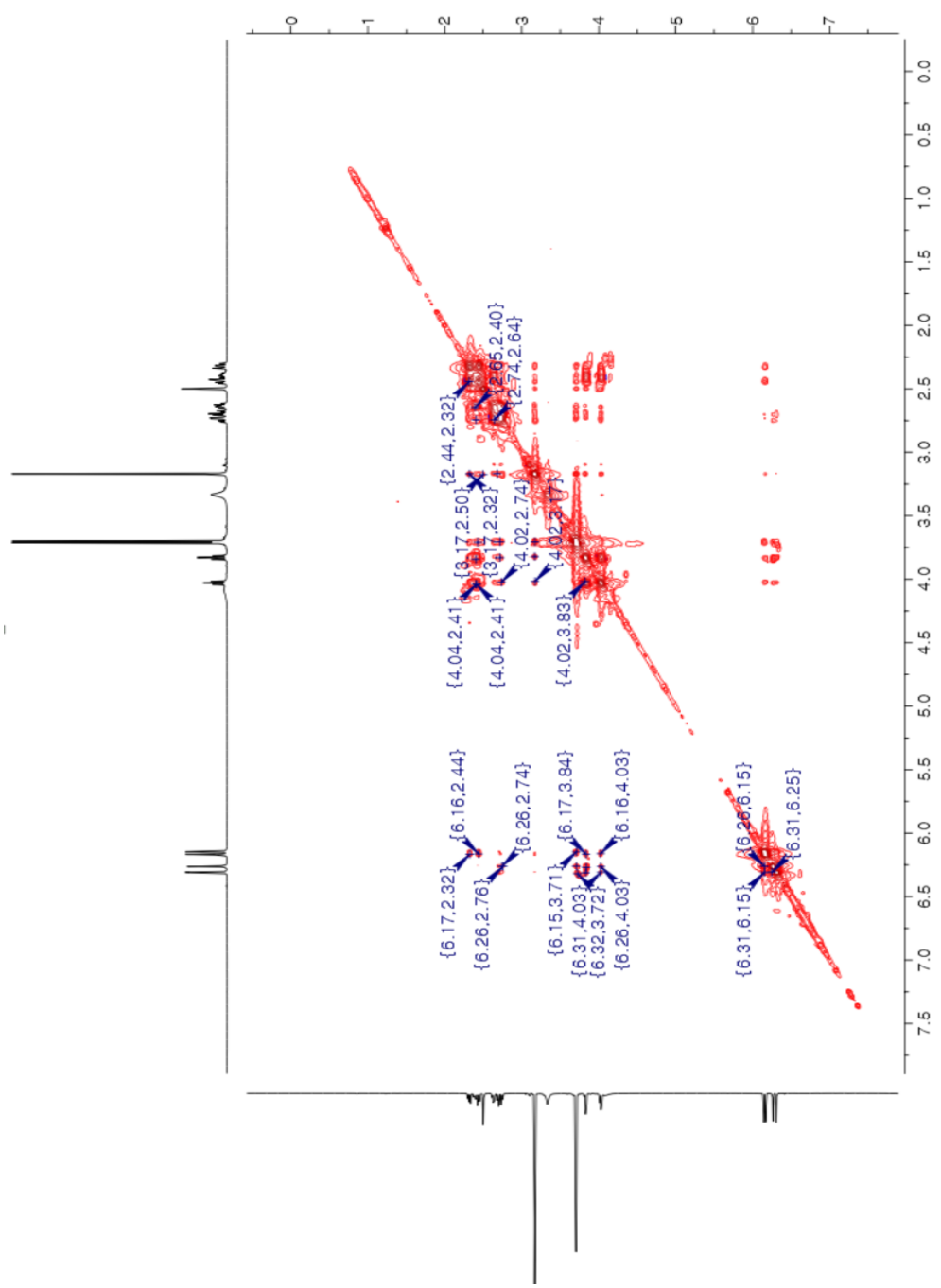

Figure S11. The HMBC spectrum of 3',3''-dihydroxy-(-)-matairesinol (5) (600 MHz, DMSO-d_6)

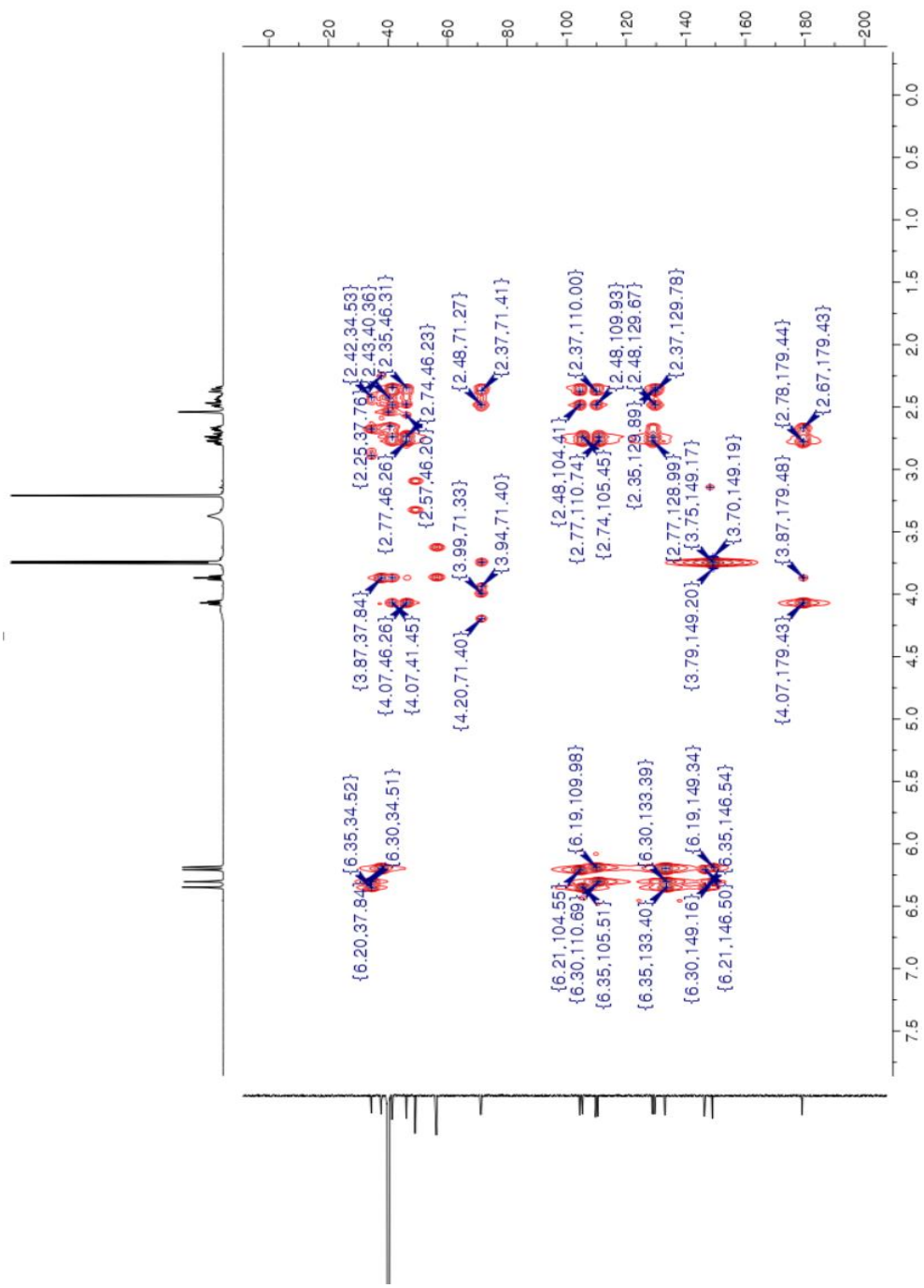

Figure S12. The NOESY spectrum of 3',3''-dihydroxy-(-)-matairesinol (5) (500 MHz, DMSO-d_6)

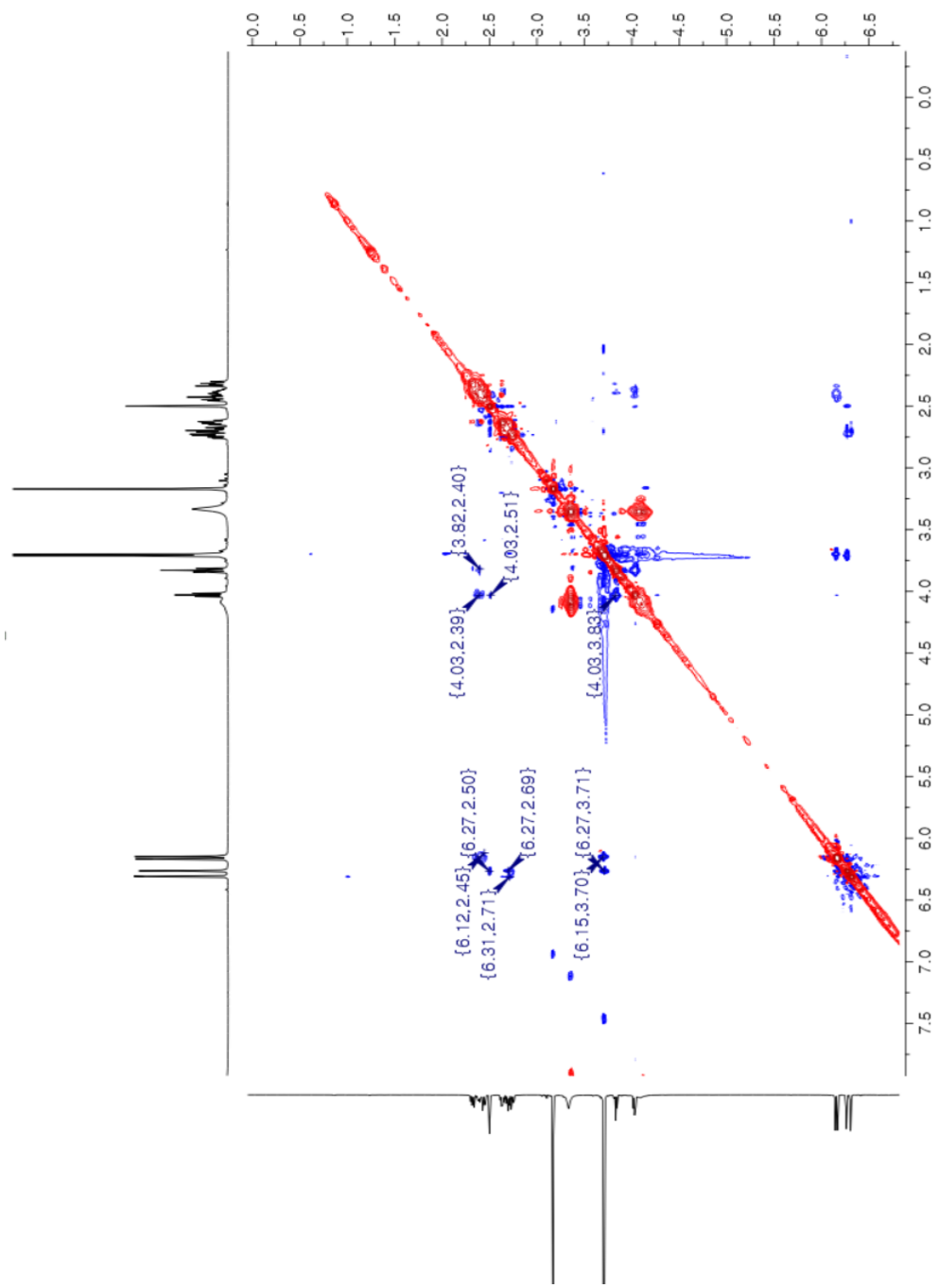

Figure S13. The HR-ESI-MS data of 3',3''-dihydroxy-(-)-matairesinol (5)

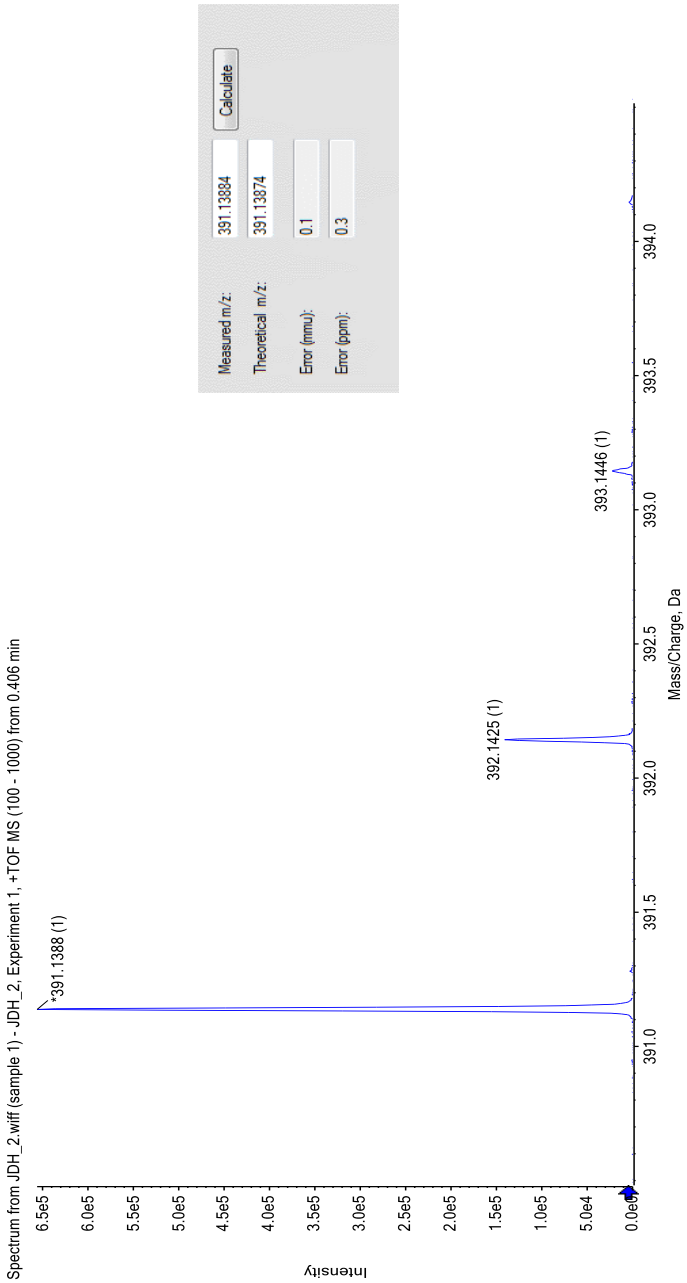

Abstract in Korean

서울대학교 대학원
농생명공학부 응용생명화학전공
조은지

해양미생물 및 육상식물 유래의 천연물은 그 구조적 다양성과 넓은 생리활성 스펙트럼으로 인해 매우 높은 연구 가치를 갖는다. 이 연구에서는 해양방선균 *Streptomyces microflavus*와 전통 생약 향나무 *Juniperus chinensis* 유래 대사산물의 항균활성을 평가하고 그 활성이 나타나는 작용기전을 탐구하였다.

첫번째 파트는 해양 유래 방선균으로부터 유래한 항생 물질에 대해 연구한 내용을 다룬다. 스크리닝에서 항세균 활성을 가지고 있는 것으로 나타난 해양 유래 방선균 *Streptomyces* sp. MBTI36를 연구에 사용하였고, 해당 균주는 16S rDNA 염기서열 분석을 통해 *S. microflavus*라 동정되었다. 실험균주의 배양액으로부터 4개의 항균활성물질 **1**–**4**을 분리하였으며, 물질의 구조는 핵자기공명법을 포함하는 분광학적 방법들과 선행연구와의 비교분석을 통해 규명한 결과 기지물질 크로모마이신 Ap, A_2, A_3 (**2**-**4**)와 함께 새로운 크로모마이신 A_9 (**1**)인 것으로 확인되었다. 물질 **1**–**4**는 MRSA를 포함하는 그람 양성 세균에 대해 뛰어난 항균 활성을 보이는 것으로 나타났으며, 21일 간의 계대배양 실험을 통해 이 물질들이 병원균의 항생제 내성을 유발하는 경향이 매우 낮음을 증명하였다.

두번째 파트에서는 활성 추적 분획법을 통해 전통 한약재인 향나무 *Jniperus chinensis*로부터 SrtA 저해 물질 **5**–**10**을 분리하고 분광학적 분석을 통해 구조를 규명하였다. 그 중 물질 **5**는 신규 물질 3',3"-dihydroxy-(−)-matairesinol 인 것으로 규명되었다 . 이 물질은 치아 우식균 *Streptococcus mutans*의 성장을 저해하지 않으면서 (MIC > 300 μM) 해당 균 유래 SrtA에 대해 강한 저해 활성을 보였다 (IC_{50} = 16.1 μM). 반면, (−)-matairesinol (**6**)은 은 해당 단백질을 전혀 저해하지 못하였으며, 물질 **7**–**10**은 SrtA에 대해 미약한 활성을 나타내었다. 부가적인 실험을 통해 물질 **5**가 *S. mutans*의 응집, 부착, 생물막 형성 또한 효과적으로 억제할 수

있는 것이 확인되었으며, 특히 SrtA IC_{50} 값의 4배에 달하는 농도의 물질 **5**를 처리한 경우 생물막 형성의 저해 수준은 *srtA* 결손 균주의 양상에 비견하는 것으로 나타났다.

위와 같은 결과를 통해, 이 연구는 병원성 세균을 효과적으로 저해할 수 있는 천연물과 그 작용 기전을 제시하였다.

주요어 : 크로모마이신, 항생제, 항생제 내성, 항병원성 약제, 해양 유래 방선균, sortase A 저해제, *Juniperus chinensis*, *Streptomyces microflavus*

학 번 : 2015-21798

Publications

Cho E, Kwon OS, Chung B, Lee J, Sun J, Shin J, Oh KB (2020) Antibacterial activity of chromomycins from a marine-derived *Streptomyces microflavus*. *Mar Drugs* 18(10):522

Cho E, Hwang JY, Park JS, Oh D, Oh DC, Park HG, Shin J, Oh KB (2022) Inhibition of *Streptococcus mutans* adhesion and biofilm formation with small-molecule inhibitors of sortase A from *Juniperus chinensis*. *J Oral Microbiol* 14(1):2088937

Chung B, Hwang JY, Park SC, Kwon OS, **Cho E**, Lee J, Lee HS, Oh DC, Shin J, Oh KB (2022) Inhibitory effects of nitrogenous metabolites from a marine-derived *Streptomyces bacillaris* on isocitrate lyase of *Candida albicans*. *Mar Drugs* 20(2):138.

Lim HJ, An JS, Bae ES, **Cho E**, Hwang S, Nam SJ, Oh KB, Lee SK, Oh DC (2022) Ligiamycins A and B, decalin-amino-maleimides from the co-culture of *Streptomyces* sp. and *Achromobacter* sp. isolated from the marine wharf roach, *Ligia exotica*. *Mar Drugs* 20(2):83

Hwang JY, Chung B, Kwon OS, Park SC, **Cho E**, Oh DC, Shin J, Oh KB (2021) Inhibitory effects of epipolythiodioxopiperazine fungal metabolites on isocitrate lyase in the glyoxylate cycle of *Candida albicans*. *Mar Drugs* 19(6):295.

Park JS, **Cho E**, Hwang JY, Park SC, Chung B, Kwon OS, Sim CJ, Oh DC, Oh KB, Shin J (2020) Bioactive bis(indole) alkaloids from a *Spongosorites* sp. sponge. *Mar Drugs* 19(1):3

Park SC, Chung B, Lee J, **Cho E**, Hwang JY, Oh DC, Shin J, Oh KB (2020) Sortase A-inhibitory metabolites from a marine-derived fungus *Aspergillus* sp. *Mar Drugs* 18(7):359.

Bae J, **Cho E**, Park JS, Won TH, Seo SY, Oh DC, Oh KB, Shin J (2020) Isocadiolides A-H: Polybrominated aromatics from a *Synoicum* sp. ascidian. *J Nat Prod* 83(2):429-437

Kim H, Hwang JY, Chung B, **Cho E**, Bae S, Shin J, Oh KB (2019) 2-Alkyl-4-hydroxyquinolines from a marine-derived *Streptomyces* sp. inhibit hyphal growth induction in *Candida albicans*. *Mar Drugs* 17(2):133

Ma CT, Eom T, **Cho E**, Wu B, Kim TR, Oh KB, Han SB, Kwon SW, Park JH (2017) Aquilanols A and B, macrocyclic humulene-type sesquiterpenoids from the

agarwood of *Aquilaria malaccensis*. *J Nat Prod* 80(11):3043-3048.

Ahn CH, Lee S, **Cho E**, Kim H, Chung B, Park W, Shin J, Oh KB (2017) A farnesoic acid-responsive transcription factor, Hot1, regulates yeast-hypha morphogenesis in *Candida albicans*. *FEBS Lett* 591(9):1225-1235.

Shin B, Kim BY, **Cho E**, Oh KB, Shin J, Goodfellow M, Oh DC (2016) Actinomadurol, an antibacterial norditerpenoid from a rare actinomycete, *Actinomadura* sp. KC 191. *J Nat Prod* 79(7):1886-1890.

Kim CK, Woo JK, Kim SH, **Cho E**, Lee YJ, Lee HS, Sim CJ, Oh DC, Oh KB, Shin J (2015) Meroterpenoids from a tropical *Dysidea* sp. sponge. *J Nat Prod* 78(11):2814-2821.

Acknowledgement

처음 이 학교에 입학할 때만 해도 이렇게 오랜 시간을 머무를 줄은 몰랐던 것 같습니다. 항상 농담처럼 관악산에 너무 오래 있었다고 말하고는 했는데, 드디어 하산할 때가 다가왔나 봅니다. 아주 많은 일이 있었던 것도 같고, 또 별 일 없었던 것도 같지만 학위를 하는 기간이 제 인생에 있어서 아주 귀하고 중요한 시간이었다는 사실은 분명합니다. 너무 호들갑 떨지 않고 담백한 감사의 글을 적고자 하지만 그간 여기저기서 받은 것들이 너무 많아 과연 얼마나 성공적일지는 모르겠습니다.

가장 먼저 오랜 기간동안 저를 지도해 주신 오기봉 교수님, 이 기회를 빌어 진심으로 감사의 말씀을 드립니다. 부족한 점 많은 학생을 믿고 기다려 주시고 힘껏 끌어 주셔서 제가 그래도 여기까지 올 수 있었습니다. 학문적으로도, 인간적으로도 이렇게까지 본받고 존경할 수 있는 지도교수님을 만난 것이 저에게 정말 큰 행운입니다. 교수님 앞으로의 삶에도 건강과 평안만 가득하셨으면 좋겠습니다.

늘 저희 연구실과 교류하며 물질 구조 동정과 여러 연구에 많은 도움 주신 약학대학 신종헌 교수님 감사드립니다. 덕택에 제 연구의 가치를 더욱 끌어올릴 수 있었던 것 같습니다. 해양 방선균 균주를 흔쾌히 제공하여 연구의 시작에 큰 도움을 주신 KIOST 이희승 박사님께도 깊은 감사의 말씀을 드립니다. 심사를 위해 먼 데서부터 고생스럽게 왕래해 주신 것도 감사합니다. 두 분께서 써 주신 시간과 수고가 정말 많은 것 같습니다. 또 저의 박사 학위 심사에 힘써 주신 이상기 교수님, 권용훈 교수님 정말 감사드립니다. 숙고하여 검토해 주신 질문과 코멘트들 덕분에 많이 배우고 보다 더 좋은 논문을 완성할 수 있었습니다. 붙임성도 별로 없는 학생에게 오며 가며 매번 많은 격려 주신 것도 잊지 않겠습니다. 오랜 기간 많은 가르침을 주신 응용생명화학 전공 교수님들께도 감사의 말씀을 올립니다. 제가 응화였기 때문에 배울 수 있던 것이 아주 많았다고 생각합니다. 물질 구조를 결정하는데 많은 도움을 주셨던 약학대학 권오석 박사님, 황지연 박사님께도 감사드립니다.

가족보다도 더 오랜 시간을 함께 있었던 미생물생물공학 연구실 선후배님들께도 고맙다는 말을 하고 싶습니다. 함께 하며 주고받은 학문적인 논의들, 삶의 고민들, 작은 대화들 속에서 많이 배우고 위로 받았습니다. 운이 좋아 너무나 훌륭한 연구의 동료들을 만난 것 같습니다.

긴 시간동안 교류하며 도움 주고 응원해 준 응용생명화학부 대학원생 친구들도 너무 고맙습니다. 한 명 한 명 빼놓지 않고 꼭 연락하겠습니다.

누구보다 많은 응원과 기도를 쏟아 주신 나의 부모님, 저보다도 제 학위를 마치는 날을 기다려 오셨을 것 같아요. 제가 너무 싫은 내색을 많이 해서 저에게는 물어 보지도 않고 궁금해만 하셨던 것 알고 있어요. 그래도 믿고 기다려줘서 감사합니다. 많이 사랑해요! 그 외에도 정말 넘치는 위로와 도움의 손길이 있었는데 일일이 언급할 수 없을 만큼 많습니다. 하나같이 모두 감사드리며, 언젠가 빼놓지 않고 전부 갚을 수 있는 날이 오기를 기대합니다.